UNIVERSITY MICROFILMS, ANN ARBOR, MICH.

L. C. Card no. Mic 58-3713

MITRA, Shashanka Shekhar. THE INFRARED AND RAMAN SPECTRA OF BRUCITE, $Mg(OH)_2$.

University of Michigan, Ph. D., 1958
Physics, general

Negative Microfilm Received from University

THE INFRARED AND RAMAN SPECTRA OF BRUCITE, $Mg(OH)_2$

by
Shashanka Shekhar Mitra

A dissertation submitted in partial fulfillment
of the requirements for the degree of
Doctor of Philosophy in the
University of Michigan
1957

Doctoral Committee:

Assistant Professor C. Wilbur Peters, Chairman
Professor David M. Dennison
Assistant Professor Karl T. Hecht
Assistant Professor Samuel Krimm
Assistant Professor Robert C. Taylor

THE INFRARED AND RAMAN SPECTRA OF BRUCITE, $Mg(OH)_2$

Abstract

by Shashanka Shekhar Mitra

The infrared spectrum of brucite observed by Mara and Sutherland showed surprising complexity in the OH stretching region and seemed to defy explanation on the basis of simple structure for the crystal deduced from early x-ray diffraction measurements.This led Mara and Sutherland to suggest the existence of a larger unit cell containing several $Mg(OH)_2$ groups.However,subsequent studies by refined x-ray diffraction techniques,proton magnetic resonance,and neutron diffraction have confirmed,beyond doubt,the previously reported structure of brucite.

The objectives of the present research are: (1) to determine the symmetry classification and selection rules for the different modes of oscillation from a factor group analysis of the known structure of brucite for the purpose of assigning the observed infrared and Raman fundamentals, (2) to investigate quantitatively the model proposed by Hexter and Dows to explain the complex structure in the near infrared spectra of brucite.

The spectrum of brucite has been studied in the region from 350 cm^{-1} to 11000 cm^{-1}, chiefly using Perkin Elmer single beam model 12c and double beam model 21 spectrometers equipped with KBr,NaCl,LiF and CaF_2 prisms. By far the richest region of spectra is from 3000 cm^{-1} to 5000 cm^{-1}. In addition to careful reinvestigation of the spectra in the previously studied regions,the present research includes polarized reflectivity measurements in the highly opaque lattice region (350 cm^{-1} to 1000 cm^{-1}), and around 3700 cm^{-1} to determine the optical constants and to decide about the strongest band in this highly absorbing region,extensive low temperature (at liquid nitrogen point) spectra in the near infrared

region,detailed powder spectra of chemically prepared $Mg(OH)_2$ and $Mg(OD)_2$, and transmission measurements in the second overtone region.The Raman spectrum of the crystal has been investigated for the first time.

The only Raman band observed in the hydroxyl stretching region at 3655 cm^{-1} has been assigned to the symmetric A_{1g} mode,whereas the strongest of the infrared bands in this region at 3700 cm^{-1} ,polarized parallel to the c-axis,has been assigned to the antisymmetric A_{2u} mode.Among the translatory lattice vibrations,both A_{2u} and E_u modes have been assigned to the strong infrared reststrahlen band at 515 cm^{-1} observed in both the polarizations.The OH librational modes have been tentatively assigned.Assignments for the overtones of the OH stretching fundamentals have also been proposed. Thus the intense bands of the infrared and Raman spectra are in accord with the known unit cell of the crystal.

The possibility of explaining the complex spectra in the near infrared region as combinations of the stretching and librational modes has been explored.The model proposed by Hexter and Dows,which assumes a simple harmonic librational potential energy,is found to be completely inadequate. Two modifications have been proposed: an interaction term involving the two non-equivalent OH ions in the unit cell of the crystal,and a potential energy expression dependent upon 3-fold and 6-fold symmetry to incorporate the special features of the brucite space group.The results of perturbation calculations showed only a few features in common with the observed spectra. It appears that for a complete explanation one has to assume additional combinations with lattice modes which become active only in combination.

মা ও বোনটির জন্য

PREFACE

The author is deeply indebted to Professor G.B.B.M Sutherland for making possible the author's stay in the United States and for suggesting the problem of the present investigation. He would like to express his appreciation for the constant guidance he received from Professor C.W. Peters and Professor K.T. Hecht throughout the progress of the work. He would also like to thank the following for their aid:

Professor R.C. Taylor, for his many helpful suggestions and his assistance in obtaining the Raman spectra.

Professor D.L. Wood, for his suggestions regarding sample preparations.

Professor S. Krimm, Dr. N. Ockman, Dr. A.G. De Rocco and Dr. E. Palik for offering miscellaneous help.

Financial support in the form of a pre-doctoral fellowship (1955-1957) from the Corning Glass Works Foundation is gratefully acknowledged.

TABLE OF CONTENTS

	Page
PREFACE	iii
LIST OF TABLES	vi
LIST OF ILLUSTRATIONS	vii
INTRODUCTION	1
CHAPTER 1. REVIEW OF PREVIOUS WORK	3
1.1 Occurrence and External Appearance	3
1.2 X-ray Diffraction Studies	4
1.3 Position of the Hydrogens	6
1.4 Infrared Studies	10
CHAPTER 2. FACTOR GROUP ANALYSIS	16
2.1 Introduction	16
2.2 Classification of Crystal Fundamentals	17
2.3 Application of Group Theory	18
2.4 Normal Modes of Oscillation in Brucite	23
2.5 The OH Vibrations	24
2.6 The Lattice Vibrations	27
2.7 Summary	29
CHAPTER 3. EXPERIMENTAL METHODS	30
3.1 Preparation of Samples	30
3.2 Infrared Instrumentation	33
3.3 Raman Measurements	36
CHAPTER 4. EXPERIMENTAL RESULTS OF THE PRESENT STUDY	37
4.1 Introduction	37
4.2 Raman Spectrum	38
4.3 Reflection Spectra	38
4.3a Reflection Spectra ($350cm^{-1}$ to $1000cm^{-1}$)	39
4.3b Reflection Spectra ($3450cm^{-1}$ to 3900 cm^{-1})	43
4.4 Powder Spectra of $Mg(OH)_2$ and $Mg(OD)_2$	47
4.4a Powder Spectrum of $Mg(OH)_2$ at 3700 cm^{-1})	47
4.4b Comparison of $Mg(OH)_2$ and $Mg(OD)_2$ Powder Spectra	52
4.5 Single Crystal Transmission Spectra	56
4.5a Transmission Spectra of Samples Cut Parallel to the Cleavage Plane at Room and Liquid Nitrogen Temperatures	56
4.5b Polarized Transmission Spectra (2650 cm^{-1} to 5200 cm^{-1})	67

		Page
4.5c	Transmission Spectra of Tilted Samples (3400 cm^{-1} to 3950 cm^{-1})	74
4.5d	Overtone Regions (6000 cm^{-1} to 11000 cm^{-1})	78
4.6	Summary	81
CHAPTER 5.	ASSIGNMENTS AND DISCUSSION	89
5.1	OH Stretching Modes	89
5.2	Overtones of the OH Fundamentals	93
5.3	External (Lattice) Fundamentals	94
5.4	Complex Structure of the Absorption Spectra in the OH Stretching Region	98
5.4a	Introduction	98
5.4b	The Model of Hexter and Dows	102
5.4c	Two Weakly Interacting Coupled Librators	108
5.4d	Single Librator with 3-fold and 6-fold Restricting Potential	115
5.4e	Discussion	123
5.5	Summary	125
BIBLIOGRAPHY		128

LIST OF TABLES

		Page
1.	List of Infrared Absorption Bands of Brucite (Mara)	12
2.	$Mg(OH)_2$ and $Mg(OD)_2$ Powder Bands (Mara)	13
3.	Character Table and Distribution of Modes	25
4.	Comparison of $Mg(OH)_2$ and $Mg(OD)_2$ Bands (Powder)	57
5.	List of Infrared and Raman Bands of Brucite	85
6.	Correspondence of the Sum and Difference Bands	101
7.	Multiplication Table for the Infrared Active Stretching Libration Combinations	109
8.	Degeneracies and Quantum Numbers for Two Coupled Librators	110
9.	Perturbation Corrections for a Single Librator with 3-fold and 6-fold Restricting Potential	119
10.	Perturbation Correction for Two Sets of Parameters (3-fold and 6-fold Restricting Potential)	121
11.	Assignments of Fundamentals and OH Overtones	125

LIST OF ILLUSTRATIONS

Figure		Page
1.	Structure of Brucite	5
2.	Normal Modes of Vibrations in Brucite	28
3.	The Modified Source Optics for the P-E. 12C Spectrometer	34
4.	Reflection Spectra of Brucite for Two Crystal Orientations, from 350 cm^{-1} to 1000 cm^{-1} (NaCl and KBr)	41
5.	Polarized Reflection Spectra of Brucite, from 350 cm^{-1} to 1000 cm^{-1} (NaCl and KBr)	42
6.	Reflection Spectra of Brucite for two Crystal Orientations, from 3450 cm^{-1} to 3850 cm^{-1}	44
7.	Polarized Reflection Spectra of Brucite, from 3450 cm^{-1} to 3850 cm^{-1}	45
8.	Optical Constants of Brucite ($\vec{E}$ $\parallel$ to c-axis), from 3400 cm^{-1} to 3950 cm^{-1}	48
9.	Transmission Spectrum of Brucite Powder, from 3500 cm^{-1} to 3850 cm^{-1}	49
10.	Transmission Spectrum of Brucite Powder, from 3600 cm^{-1} to 4700 cm^{-1}	50
11.	Transmission Powder Spectrum of Brucite, from 3200 cm^{-1} to 3600 cm^{-1}	51
12.	Transmission Spectrum of $Mg(OD)_2$ Powder, from 2750 cm^{-1} to 3550 cm^{-1}	53
13.	Transmission Spectrum of $Mg(OD)_2$ Powder, from 2400 cm^{-1} to 2800 cm^{-1}	54
14.	$Mg(OD)_2$ Transmission Spectrum (2225 cm^{-1} to 2300 cm^{-1}	55
15.	Transmission Spectra of Brucite at Two Temperatures, from 2700 cm^{-1} to 3100 cm^{-1} (sample $\parallel$ to Cleavage, 750 μ)	59
16.	Transmission Spectra of Brucite at Two Temperatures, from 3125 cm^{-1} to 3450 cm^{-1} (sample $\parallel$ to Cleavage, 300 μ)	60

Figure		Page
17.	Transmission Spectra of Brucite at Two Temperatures, from 3900 cm^{-1} to 4600 cm^{-1} (sample // to Cleavage, 300 μ)	62
18.	Transmission Spectra of Brucite at Two Temperatures, from 3900 cm^{-1} to 4200 cm^{-1} (sample // to Cleavage, 100 μ)	63
19.	Transmission Spectra of Brucite at Two Temperatures, from 4600 cm^{-1} to 5200 cm^{-1} (sample // to Cleavage, 750 μ)	65
20.	Transmission Spectra of Brucite (sample // to Cleavage, 100 μ) at Two Temperatures, from 3450 cm^{-1} to 3950 cm^{-1} (CaF_2)	66
21.	Polarized Transmission Spectra of Brucite, from 2650 cm^{-1} to 3150 cm^{-1} (sample 2 mm)	68
22.	Polarized Transmission Spectra of Brucite, from 3150 cm^{-1} to 3900 cm^{-1} (sample, 300 μ)	70
23.	Polarized Transmission Spectra of Brucite, from 3900 cm^{-1} to 4600 cm^{-1} (sample, 300 μ)	72
24.	Polarized Transmission Spectra of Brucite, from 4600 cm^{-1} to 5200 cm^{-1} (sample, 300 μ)	73
25.	Transmission Spectra of Brucite Crystal with c-axis at 0°, 30° and 45° to Incident Beam, from 3400 cm^{-1} to 3900 cm^{-1} (100 μ thick)	75
26.	Spectra of a Tilted Sample (Parallel to Cleavage, 100 μ thick) at Two Temperatures, from 3400 cm^{-1} to 3900 cm^{-1} (CaF_2)	77
27.	Spectra of Brucite for Two Crystal Orientations, from 6000 cm^{-1} to 11000 cm^{-1}	79
28.	Polarized Transmission Spectra of Brucite, from 6000 cm^{-1} to 11000 cm^{-1} (sample 2.25 mm thick)	80
29.a	Powder Spectra of Brucite and $Mg(OD)_2$	83
b	Polarized Transmission Spectra of Brucite (2600 cm^{-1} to 5000 cm^{-1})	83
30.	Infrared Active Sum and Difference Bands	99
31.	A Single Librator	103
32.	Spectrum of a Single Harmonic Librator	107
33.	Energy Levels of Two Coupled Librators	112

Figure		Page
34.	The Spectrum of Two Coupled Librators	114
35.	Libration Potential with or without the 3-fold Term	116
36.	Energy Levels of a Single Librator in a Restricting Potential with 3-fold and 6-fold Terms	122

INTRODUCTION

In the study of a number of crystals, in this laboratory, Mara and Sutherland examined the infrared spectrum of brucite, $Mg(OH)_2$, and surprisingly found a spectrum whose great complexity in the OH stretching region seemed to defy explanation on the basis of the simple structure for the crystal deduced from early x-ray diffraction measurements. This led Mara and Sutherland to propose that the unit cell contained more than one $Mg(OH)_2$ group, contradictory to the structure determined from x-rays. However, subsequent studies by refined x-ray diffraction techniques, proton magnetic resonance, and neutron diffraction have confirmed, beyond doubt, the previously reported structure of brucite and have also given the precise equilibrium positions of the hydrogen atoms. Subsequently, Hexter and Dows suggested that the peculiar form of the near infrared spectrum could arise from combinations of the OH stretching and libration modes.

Objectives of the present investigation:

By virtue of the precise knowledge of the unit cell and space group now available, a factor group analysis can be carried out; and the symmetry classification and selection rules can be obtained for the different modes of oscillation. This would make possible the assignment of the fundamentals of the infrared and Raman spectra.

Moreover, it was hoped that the proposal made by Hexter and Dows could be qualitatively verified with the aid of more precise and detailed information on the infrared bands in the OH stretching region, and perhaps quantitatively confirmed by an approximate evaluation of the interactions involved.

CHAPTER 1

REVIEW OF PREVIOUS WORK

1.1 Occurrence and External Appearance

Brucite, $Mg(OH)_2$, is a mineral named after its discoverer A. Bruce, who first found it at Hoboken, New Jersey in 1814. It generally occurs in metamorphic calcite-brucite rocks as an alteration of periclease, MgO. Sometimes it is also found in serpentine. Its most common occurrence is in plates or scaly aggregates. It also occurs sometimes in a fibrous variety known as nemalite, which has been shown by x-ray diffraction methods to have the same crystal structure as the commoner form. The samples are generally colorless, although a light bluish-green variety sometimes occurs. The transparency of the crystal in sizeable quantities is rather poor due to internal fractures. The crystal is uniaxial and only moderately birefringent. It can be easily cleaved in planes perpendicular to the optic axis. The indices of refraction as given by Rogers and Kerr[1] are $n_\omega = 1.566$ and $n_\epsilon = 1.585$.

1.2 X-Ray Diffraction Studies

The crystal structure of brucite as determined by the x-ray diffraction study was first reported in 1919 by G. Aminoff[2]. The crystal is hexagonal and belongs to the space group D^3_{3d} ($P\bar{3}$ m). The unique c-axis is perpendicular to the cleavage planes, in which the three equivalent a-axes intersect at 60° angles. This plane is designated as the (0001) plane, where the numbers represent the Miller indices. It has been shown that the unit cell contains only one $Mg(OH)_2$ molecule. The dimensions of the unit cell have been determined by various authors: Aminoff[3], Levi and Ferrari[4], Natti and Passerini[5], Bury and Davies[6], Megaw[7], Trendelenburg and Wieland[8], and Garrido[9]. The last author has also shown that the fibrous variety nemalite has the same crystal structure as the more common brucite. The unit cell dimensions quoted here are those of Trendelenburg and Wieland and are given in Struktur-bericht. They are a=3.12A and c=4.73A.

The structure is shown diagrammatically in Figure 1. The magnesium ions lie in the (0001) planes. Viewing along the c-axis one finds the Mg ions situated at the center of puckered hexagons, whose corners are occupied by hydroxyl ions. The planes containing the hydroxyl ions are parallel to the (0001) plane and are 0.22c and -0.22c apart from it. The OH ions are thus alternately above and below the plane containing the magnesium ions. The three planes containing the Mg and OH ions thus form a layer in the layer lattice structure of brucite. The next layer is formed about a

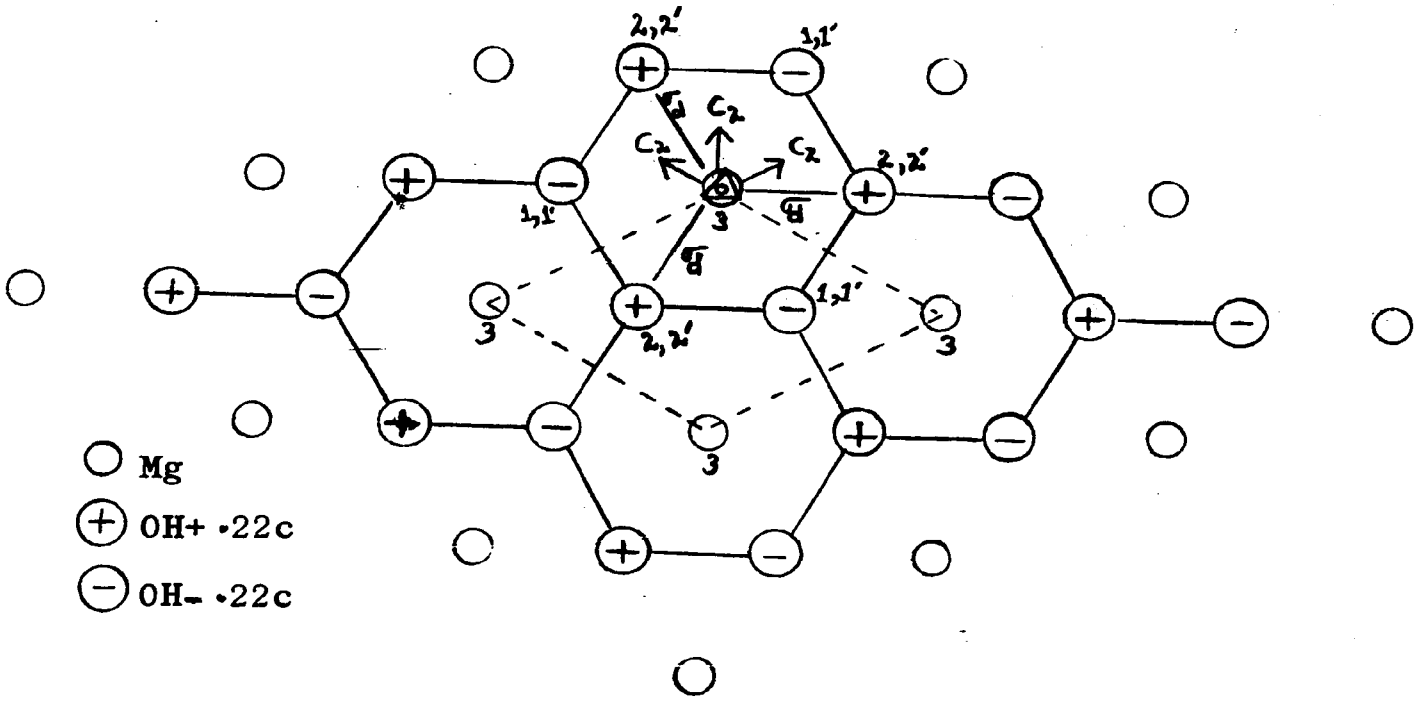


Figure 1a. Structure of Brucite, projection on (0001) plane (c-axis perpendicular to the page) showing the symmetry elements of the space group D^3_{3d}.

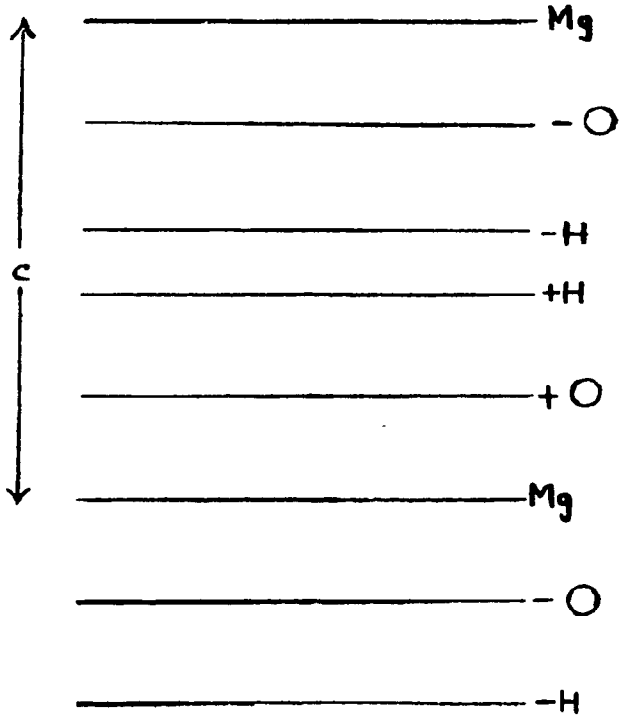


Figure 1b. Layer lattice structure of Brucite

plane of Mg ions which is situated at a distance c from the previous one. The layers are supposed to be held together by weak secondary forces occurring between the neighboring layers of OH ions. These van der Waal's forces are much weaker than ionic forces and thus explain the occurrence of cleavage planes. The lines joining equivalent ions in successive layers are all parallel to the c-axis.

1.3 Positions of the Hydrogens

The positions of the protons are very difficult to locate by x-ray methods and in the structure described above, the hydrogen positions have not been given. Bernal and Megaw[10] were the first to make predictions concerning the location of hydrogen atoms from evidence gathered in an extensive x-ray diffraction study of a large number of crystals containing the hydroxyl ions. One of the aims of their research was to explain the part played by hydrogen in the forces existing between hydroxyl ions. Since the succeeding layers in brucite are separated by relatively large distances and because the hydroxyl ions are arranged in hexagonal close packing, they concluded that there would be negligible hydrogen bonding between the OH ions of neighboring layers. Since the hydrogen is free of any direct influence from the nearby OH ions their reasonable inference was that it should be oriented parallel to the c-axis.

The recent infrared work, using polarized radiation, by Mara and Sutherland (the details of which will be given

in the next section) seemed at first interpretation to cast some doubt on the findings of Bernal and Megaw regarding the location of the hydrogen atoms and also on the size of the unit cell. In the region of the OH stretching fundamental, (3700 cm^{-1}), they have observed a whole complex of bands with various polarizations, instead of only one band polarized parallel to the c-axis as predicted by the Bernal and Megaw model (see Chapter 2). They have also examined the spectrum of powdered $Mg(OD)_2$ and the gross complex pattern of bands is shifted by a constant ratio (nearly $\sqrt{2}$) and so could not explain the complexity as arising from the combination of the OH stretching mode with the low-lying lattice oscillations involving the magnesium ions. They concluded that the unit cell for brucite is much larger than that predicted by the x-ray diffraction studies, containing at least as many hydroxyl ions as there are observed stretching fundamentals. To account for the polarization properties of these bands they suggested that the positions of the hydrogen atoms had been incorrectly assigned from the x-ray data.

In view of these opposing conclusions from the x-ray and infrared work, Petch and Megaw[12] undertook a re-examination of the crystal structure of brucite and the isomorphous portlandite, $Ca(OH)_2$. They could not, however, find any evidence for a larger unit cell in either of the crystals and the space group was also confirmed. They emphasized that these findings can not be regarded as a failure to locate the hydrogen positions by the x-ray method, because if there were

a systematic displacement of the proton positions from their special locations in the small unit cell, there would have been a lowering of the symmetry of the whole structure. If the hydrogen atoms were displaced it seems plausible that the positions of the other atoms would have also been affected. Any consideration of interatomic forces suggests that if the contribution of hydrogen to these is not negligible, at least the oxygen positions should be influenced. It seems quite improbable that the arrangement of the oxygens will indicate a higher symmetry than that of the hydrogens. The reasoning of Petch and Megaw does not rule out the possiblility of statistically disordered displacement of hydrogens. However, x-ray data does not give any positive evidence for it and there is no assurance that it would explain the infrared results in the way Mara and Sutherland proposed. Petch[13] has also reported that a study of portlandite using a Geiger counter x-ray diffractometer gave strong evidence supporting the hydrogen positions predicted by Bernal and Megaw.

Very recently, Elleman and Williams[14] have determined the proton positions in brucite by a comparison of nuclear magnetic resonance spectra with the existing x-ray data. The proton resonance spectra obtained by them showed a sixty degree periodicity as the crystal was rotated around the c-axis. This result suggests that the protons have a hexagonal arrangement. Hence, they accepted the hydrogen arrangement proposed by Bernal and Megaw and used additional magnetic resonance data to determine the spacing between adjacent H

planes as 0.69±0.02A. This value combined with the x-ray value for the separation between adjacent O layers gives the value 0.98±0.02A for the internuclear distance in the OH ion. This value compares well with the spectroscopic values for the OH distances for various gaseous molecules[15]: 0.957A in water vapor, 0.958A in methyl alcohol, 0.971A in the free OH radical and 1.03A in OH^+. Figure 1 (b) gives a diagrammatic representation of the layers of various atoms arranged perpendicular to the c-axis in brucite crystal.

More direct evidence about the hydrogen positions comes from the recent neutron diffraction study of the isomorphous calcium hydroxide crystals by Busing and Levy[16]. Their result confirms the x-ray structure and the hydrogen positions postulated by Bernal and Megaw. They also reported a detailed description of the thermal motions, derived from the refinement of the neutron data by Fourier and least squares procedures. The OH distance reported by them, after allowing for the asymmetric thermal motion, is 0.984A in the $Ca(OH)_2$ crystal, which is in very good agreement with that in $Mg(OH)_2$ determined by the proton resonance method.

From all the evidences presented above, it seems that the proton positions in the brucite crystal are now definitely known, and the Bernal and Megaw structure is the correct one. Mara and Sutherland[17] in a recent communication have also indicated that they no longer rule out the structure postulated by Bernal and Megaw in the light of the infrared spectra of

brucite.

1.4 Infrared Studies

The pioneering work of Coblentz[18] on the infrared spectra of brucite, the early works of Plyler[19] and Keller and Pickett[20] are discussed in detail by Mara[21]. Their region of interest was chiefly around 2.7 μ.

Yeou Ta[22] reported on the overtone region. He used a plate cut parallel to the cleavage plane. With the specimen inclined at an angle of 40° to the incident radiation, an absorption band was discovered at 7142 cm^{-1}. When the cleavage plane was held normal to the beam, this peak was completely absent from the spectrum. Moreover, with polarized radiation it was observed that this band was detectable only with a component of the electric vector oriented parallel to the c-axis of the crystal. He interpreted this band as the first overtone of the OH stretching frequency and hence he concluded that the OH bonds in brucite were parallel to the c-axis of the crystal. Louisfert[23], in addition to discovering a few new bands, confirmed Yeou Ta's result.

Duval and Lecomte[24,25] investigated the region 2000 cm^{-1} to 770 cm^{-1}, using a rock salt prism. They reported on the spectra of chemically prepared $Mg(OH)_2$, finely pulverized brucite and crystalline brucite. A band was located at 1538 cm^{-1} in the chemically prepared $Mg(OH)_2$ and in powdered sample but not in the crystal sample. Mara is of the opinion that this band is probably due to magnesium carbonate, to which finely powdered $Mg(OH)_2$ is easily transformed by the atmospheric carbon dioxide. Moreover, it appears that Duval and

Lecomte's interpretation of this band as an OH deformation fundamental frequency is erroneous because the factor group analysis (see Chapter 2) for the brucite crystal does not predict any such fundamental frequencies other than the OH stretching fundamentals and the low-lying lattice oscillations.

Mara[21] investigated the transmission spectra of brucite in the interval 800 cm^{-1} to 7300 cm^{-1} using a LiF prism in the OH stretching region. He used samples both parallel and perpendicular to the cleavage plane, and polarized radiation. When the c-axis was held parallel to the incident beam, i.e., light incident normally on the cleavage plane, no effect of the direction of the electric vector was noted on the intensity of the bands, as expected. The important features of the spectra reported by him are an overtone band at 7300 cm^{-1}, a group of relatively sharp bands between 3200 cm^{-1} and 5000 cm^{-1}, a shallow diffuse band near 1600 cm^{-1}, two weak bands at 1412 cm^{-1} and 1383 cm^{-1}, and complete opacity beyond 850 cm^{-1}. All the bands reported by Mara are given in Table 1 with their positions in microns and wave numbers, along with the orientations for which they appear and their dichroic properties. Parallel (P) or normal (N) describe the polarization properties with respect to the c-axis, i.e., represent the occurrence of maximum intensity with the electric vector oriented parallel or perpendicular to the c-axis of the crystal. Those which are designated with a (c) in addition, are completely polarized parallel to the c-axis, i.e., missing altogether when the electric vector is perpendicular to the unique axis of the crystal. The richest region of the spec-

Table 1

List of Infrared Absorption Bands of Brucite (Mara)

$\vec{E} \perp$ c-axis	$\vec{E} \parallel$ c-axis		
	1.33μ	P(c)	7520 cm^{-1}
	1.37	P(c)	7300
2.06μ	2.06		4860
2.19	2.19	P	4565
2.24	2.24		4465
2.32	2.32	P	4310
(2.45)	2.45	P	4082
2.47	(2.47)	N	4049
(2.49)	2.49	P	4016
2.53	2.53	P	3952
2.64	(2.64)	N	3788
2.71	2.71	P	3690
	2.74	P(c)	3649
2.83	2.83	P?	3533
2.97	2.97		3367
3.01	3.01		3320
3.06	3.06	N	3268
(3.08)	3.08	P	3247
3.35	3.35		2985
3.45	3.45		2898
	3.73	P(c)	2681
5.00	5.00		2000
6.25	6.25	P	1600
7.08	7.08		1412
7.23	7.23		1383
8.3	8.3		1205
9.9	9.9		1010

trum lies between 3200 cm^{-1} and 5000 cm^{-1}, sixteen bands being reported in this interval. Samples perpendicular to the cleavage planes were almost opaque near 3650 cm^{-1}, because his thinnest samples in this orientation were nearly 300 μ thick. Hence, to record the bands polarized parallel to the c-axis in this region, he used samples parallel to the cleavage planes inclined at different angles to the incident beam.

Mara also studied the powder spectra of brucite and chemically prepared $Mg(OD)_2$ with a NaCl prism. The bands observed by him are given in Table 2.

TABLE 2

$M_g(OH)_2$ AND $M_g(OD)_2$ POWDER BANDS (MARA)

$Mg(OH)_2$	$Mg(OD)_2$	$Mg(OD)_2/Mg(OH)_2$
2.30 μ	3.25 μ	1.41
2.48	3.43	1.38
2.73	3.73	1.37
3.07	4.35	1.42

The ratios between the two sets of frequencies are roughly equal to $\sqrt{2}$, though there were some minor differences in the relative intensities of the bands in $Mg(OH)_2$ and the deuterated product.

Mara could not give a detailed assignment of the observed bands because he lacked any information about the lattice oscillations, and he did not classify the normal modes of vibration according to symmetry type. The band at 7300 cm^{-1} was referred by him as the first overtone of the OH stretching vibration, though he did not attempt to specify any single frequency in the 2.7μ region as the OH stretching fundamental. Instead, his tentative conclusion had been that there existed at least ten OH stretching fundamental frequencies exhibiting different dichroic properties, with at least six of them having components of dipole moment change perpendicular to the c-axis.

It is worthwhile to mention that the infrared spectrum of the isomorphous $Ca(OH)_2$, studied by Petch and Megaw[12] and Sutherland, Mara and Liang (private communication), also shows a similar complex structure in the OH stretching region.

It is one of the objects of the present research to show that there really exists only one infrared active fundamental polarized parallel to the c-axis in the $\sim$3700 cm^{-1} region as predicted by the factor group analysis of the accepted structure of brucite. Another purpose is to investigate the possibility that the complex structure around this fundamental can be explained as combinations of the stretching fundamentals with librational modes of the OH bonds following a suggestion of Hexter and Dows[26].

The only reflectivity measurement on brucite reported so far is that by Hasche[27]. The region scanned by him is

from 2000 cm^{-1} to 10,000 cm^{-1} and he did not report any reflection band. No record of any Raman spectrum of brucite was found in a search of the literature.

CHAPTER 2

FACTOR GROUP ANALYSIS

2.1 Introduction

Theoretically a crystal composed of N atoms has 3N degrees of freedom, distributed among 3N-3 fundamental modes of oscillation and three pure translations. However only a very few of these are actually active in infrared absorption or Raman scattering. The important rule governing these transitions states that all modes of vibration, other than those in which equivalent atoms move identically in phase, are forbidden in their fundamentals both in infrared absorption and the Raman effect; in other words, the effect of a translation of the unit cell on such modes is equivalent to that of the identity operation. If the unit cell of a crystal consists of n atoms, the number of infrared and Raman active fundamental modes will be at most 3n-3. It can be shown that a classification of these modes into internal molecular and lattice vibrations can be accomplished by taking into consideration only the factor group of the

crystal instead of the entire space group. The factor group may be defined as the group formed by the symmetry elements present in the smallest possible unit cell (Bravais cell) where the latter is defined in such a way that one may obtain the entire space group just by pure lattice translations of this unit cell. A factor group is always isomorphous with one or the other of the thirty-two crystallographic point groups.

The derivation of selection rules and the classification of crystal fundamentals can be accomplished by two chief methods of attack. Bhagavantam and Venkatarayudu's[28,29] method of factor group analysis will be followed here, the other method being the site group analysis of Halford[30]. Bhagavantam and Venkatarayudu consider the atoms in the unit cell as a large molecule; and then the usual method for determining the selection rules and classifying the normal modes of a molecule is applied to this unit cell group. It has, however, been pointed out by Hornig[31] that one may obtain equivalent results by either of the methods.

2.2 Classification of Crystal Fundamentals

As has already been pointed out, it is necessary to consider only the group of n non-equivalent points that are contained in the Bravais unit cell. Leaving the three acoustic oscillations one is left with 3n-3 optical modes. The object is now to classify these 3n-3 optical vibrations as either external or internal ones. If the crystal is assumed to be composed of a number of structural groups, it is expected

that the forces holding together the atoms within a group are much stronger than those keeping the various groups together in the crystal. The internal vibrations are those which arise chiefly from the motions of the atoms within a group. The external vibrations (which are commonly known as lattice vibrations) are due to motions of the groups relative to one another. As it has been assumed that the forces between the groups are much weaker than those among the atoms within a group, it is expected that the external oscillations will occur at much lower frequencies than the internal ones. The lattice vibrations are conveniently divided into rotatory and translatory types which, in the limit of vanishing forces among the groups, correspond to pure rotations and translations repectively.

2.3 Application of Group Theory

In this section a brief review of Bhagavantam and Venkatarayudu's method will be given with a slight modification for using it with diatomic groups such as OH. The results will be stated without proof. For details one is referred to their book[32] on the application of group theory.

The space group of a crystal being known, one can easily write down the character table and the irreducible representations of the corresponding isomorphous point group. If N is the order of the group and h_j the number of group operations contained in the j^{th} class, one can find N_k, the number of times a particular irreducible representation Γ_k

is contained in another representation Γ' by

$$N_k = \frac{1}{N} \sum_j h_j \chi_k(R) \chi'_j(R) \qquad (2\text{-}1)$$

where $\chi_k(R)$ and $\chi'_j(R)$ are respectively the characters of the group operation R in the representations Γ_k and Γ'. By a specific choice of the representation, Γ', and its appropriate characters $\chi'_j(R)$ we are now in a position to classify the normal modes. In fact, equation (2-1) can also be used to predict infrared and Raman activity if we use the translation (vector) and symmetric tensor representations, respectively for Γ'.

If our representation is defined by all the 3n cartesian coördinates comprising the total number of degrees of freedom possessed by the n non-equivalent points in the unit cell, we have for the group character $\chi'_j(R)$ of this representation:

$$\chi'_j(n_i) = \omega_R (\pm 1 + 2\cos\phi_R) \qquad (2\text{-}2)$$

where ω_R is the number of atoms invariant under the symmetry operation R; ϕ_R is the angle of rotation; and the plus and minus signs stand, respectively, for proper and improper rotations. Substituting equation (2-2) in (2-1), one readily gets the distribution of the total number of modes, n_i (acoustic, external and internal), among the various species.

In classifying the acoustic series (three in number) one needs to put ω_R equal to unity for all the symmetry operations

because the whole unit cell moves as one entity in these modes. The character for this representaion, defined by three cartesian coördinates only, is given by:

$$\chi'_j\ (T) = \pm 1 + 2\cos\phi_R \qquad (2\text{-}3)$$

Substitution of equation (2-3) in (2-1) yields the number T of acoustic modes distributed among the different species. Equation (2-3) gives also the character for the representation of the electric dipole moment vector, and can thus be used to derive the infrared selection rules for the fundamentals.

If s be the total number of groups present in the unit cell then the character of an operation R in the representation for the external translatory vibrations (T') is given by:

$$\chi'_j\ (T') = [\omega_R\ (s) - 1]\ \ (\pm 1 + 2\cos\phi_R) \qquad (2\text{-}4)$$

where $\omega_R(s)$ is the number of groups that remain invariant under a symmetry operation R. In writing down equation (2-4) due care has been taken to exclude the acoustic modes, which have already been accounted for in equation (2-3).

To obtain the value $\chi'_j\ (R')$ for the rotatory types of external oscillations one has to know the number of polyatomic groups that remain invariant under an operation R. Let this be represented by $\omega_R(s-p)$ where p is the number of monatomic groups, which are excluded because they have no rotational degrees of freedom. Then

$$\chi'_j(R') = [\omega_R(s-p)] \quad (1 \pm 2\cos\phi_R) \qquad (2\text{-}5)$$

$(1 \pm 2\cos\phi_R)$ is the character of the transformation matrix for the angular momentum vector. Plus and minus signs are respectively for proper and improper rotations. It should be borne in mind, however, that the formula given above is not suitable for linear ions or molecules, because these groups have only two degrees of rotational freedom. This is the case for the OH ions in brucite, whose axis is chosen as the z-axis. The transformation matrices for angular momentum in the case of two degrees of freedom are given[33] by

$$\begin{pmatrix} P_{x'} \\ P_{y'} \end{pmatrix} = \begin{pmatrix} \pm\cos\phi_R & \pm\sin\phi_R \\ \mp\sin\phi_R & \pm\cos\phi_R \end{pmatrix} \begin{pmatrix} P_x \\ P_y \end{pmatrix}$$

for the operations $C(\phi_R)$ and $S(\phi_R)$, and

$$\begin{pmatrix} P_{x'} \\ P_{y'} \end{pmatrix} = \begin{pmatrix} \cos 2\theta & \sin 2\theta \\ \sin 2\theta & -\cos 2\theta \end{pmatrix} \begin{pmatrix} P_x \\ P_y \end{pmatrix}$$

for the operations $C_2(\theta)$ and σ_v. Therefore the characters are $\pm 2\cos\phi_R$ for proper and improper rotations around the z-axis, whereas they are zero for rotations around axes perpendicular to z, and reflections in planes containing z. Symbolically the character for the representation of the rotatory modes in the case of linear molecules can be written

as

$$\chi'_j(R') = [\omega_R(s-p)]\,\chi'_j(P) \qquad (2\text{-}5')$$

where $\chi'_j(P)$ $\begin{cases} = \pm 2\cos\phi_R & \text{for } C(\phi_R) \text{ and } S(\phi_R) \\ = 0 & \text{for } C_2(\theta) \text{ and } \sigma_v. \end{cases}$

R', the number of rotatory external oscillations present in a particular irreducible representation, may now be obtained from equation (2-1) after substituting for χ'_j from equation (2-5').

Finally, we are now in a position to obtain the number of internal vibrations, n'_i in different irreducible representations by subtracting T, T' and R' from n_i.

We have already indicated the method of obtaining the irreducible representations of the infrared active fundamentals while discussing the acoustic modes. For Raman scattering one needs to consider the character for the polarizability or symmetric tensor representation:

$$\chi'_j(\alpha) = (\pm 1 + 2\cos\phi)\,2\cos\phi \qquad (2\text{-}6)$$

plus and minus signs, as usual are for pure rotation and rotation-reflection, respectively. The selection rules can be summed up as:

$$\frac{1}{N}\sum_j h_j\,\chi'_j(T)\,\chi_i(R) \begin{cases} = 0 & \text{IR forbidden} \\ \neq 0 & \text{IR permitted} \end{cases} \qquad (2\text{-}7)$$

and

$$\frac{1}{N} \sum_j h_j \chi'_j(\alpha)\chi_i(R) \begin{cases} = 0 \text{ Raman forbidden} \\ \qquad (2\text{-}8) \\ \neq 0 \text{ Raman permitted} \end{cases}$$

2.4 Normal Modes of Oscillations in Brucite

The brucite crystal belongs to the space group D^3_{3d}. The projection on the (0001) plane showing the symmetry elements and the unit cell containing one molecule (surrounded by dotted lines) are shown in Figure 1. The detailed description of the structure was given in Chapter 1. In the figure the two oxygens are represented by 1 and 2, the two hydrogens by 1' and 2' and the magnesium ion by 3. In our notation n=5, s=3 (two hydroxyl groups and one Mg atom), p=1 (one Mg atom).

The symmetry operations of this group and the number of atoms invariant under them are given below. To explain the notation one example is given. Under the operation of reflection at the center, the atom 1 goes to 2,1' to 2', whereas the atom 3 remains invariant, hence ω_R=1.

Operation		ω_R
E(identity)	(1)(2)(1')(2')(3)	5
$2S_6$	(1,2)(1',2')(3)	1
$2C_3$	(1)(2)(1')(2')(3)	5
i	(1,2)(1',2')(3)	1
$3C'_2$	(1,2)(1',2')(3)	1
$3\sigma_d$	(1)(2)(1')(2')(3)	5

The character table with the activities and the classification of the normal modes is given on the next page.

2.5 The OH Vibrations

Since the hydroxyl ions are the only molecular groups present in the crystal, all the internal modes n_i' belong to them. The OH free radical, a diatomic molecule, possesses only one mode of internal vibration; but since the unit cell of brucite contains two OH ions it is expected that this mode should split into two in the crystal. This is borne out by the table. Of the two internal modes one (A_{1g}) is completely symmetric and is Raman active and forbidden in the infrared. While the A_{2u} mode, which is antisymmetric with respect to the center of symmetry is infrared active and inactive in Raman scattering. As is seen from the table, this band should be polarized parallel to the c-axis of the crystal.

For the Raman active band the depolarization ratio will now be calculated. The absolute value of this ratio is very difficult to measure, especially in the case of brucite, whose transparency is rather poor; but if it comes out to be equal to zero for an appropriate choice of directions, it may be subject to a reliable experimental test. Let light be incident perpendicular to the c-axis (which coincides with z) and the observation be made along the z direction. For the polarization of the incident beam parallel to the c-axis we have only E_z for the incident electric vector.

TABLE 3

CHARACTER TABLE AND DISTRIBUTION OF MODES

D^3_{3d}	E	$2S_6$	$2C_3$	i	$3C_2'$	$3\sigma_d$	n_i	T	T'	R'	n_i'	Raman	IR
A_{1g}	1	1	1	1	1	1	2	0	1	0	1	$p(\alpha_{xx}, \alpha_{yy}, \alpha_{zz})$	f
A_{1u}	1	-1	1	-1	1	-1	0	0	0	0	0	f	f
A_{2g}	1	1	1	1	-1	-1	0	0	0	0	0	f	f
A_{2u}	1	-1	1	-1	-1	1	3	1	1	0	1	f	p M_z
E_g	2	-1	-1	2	0	0	2	0	1	1	0	$p\begin{Bmatrix}\alpha_{xx},\alpha_{yy},\\ \alpha_{xy},\alpha_{xz},\\ \alpha_{yz}\end{Bmatrix}$	f
E_u	2	1	-1	-2	0	0	3	1	1	1	0	f	p M_x, M_y
Φ_R	0°	60°	120°	180°	180°	0°							
$\chi'_j(T)$	3	0	0	-3	-1	1							
$\chi'_j(P)$	2	-1	-1	0	0	0							
$\chi'_j(\alpha)$	6	0	0	6	2	2							

TABLE 3 (con't)

D^3_{3d}	E	$2S_6$	$2C_3$	i	$3C_2'$	$3\sigma_d$	n_i	T	T'	R'	n_i'	Raman	IR
ω_R	5	1	5	1	1	5							
$\omega_R(S)$	3	1	3	1	1	3							
$\omega_R(s\text{-}p)$	2	0	2	0	0	2							
$h_j \chi^{i}_j(n_i)$	15	0	0	-3	-3	15							
$h_j \chi'_j(T)$	3	0	0	-3	-3	3							
$h_j \chi'_j(T')$	6	0	0	0	0	6							
$h_j \chi'_j(R')$	4	0	-4	0	0	0							

Hence,

$$P_x = \alpha_{xz} E_z \; ; \qquad P_y = \alpha_{yz} E_z$$

For the polarization perpendicular to the c-axis we have both E_x and E_y. Hence,

$$P_x = \alpha_{xx} E_x + \alpha_{xy} E_y$$

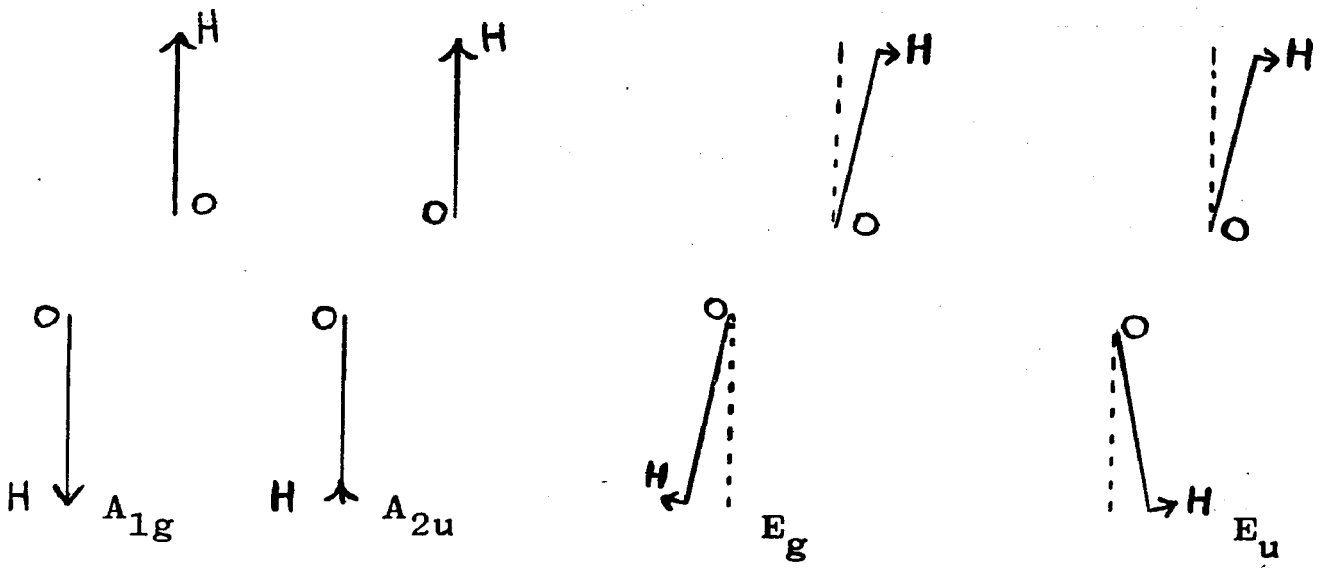
$$P_y = \alpha_{xy} E_x + \alpha_{yy} E_y$$

And we have also $E_x = E_y = 1/2 E_z$.

But for the A_{1g} mode only α_{xx}, α_{yy} and α_{zz} are the non-vanishing elements of the polarizability tensor, hence with the electric vector parallel to c-axis both P_x and P_y are zero, whereas they are not so for the perpendicular polarization. Therefore A_{1g} mode should not be observed when the electric field is polarized parallel to the c-axis.

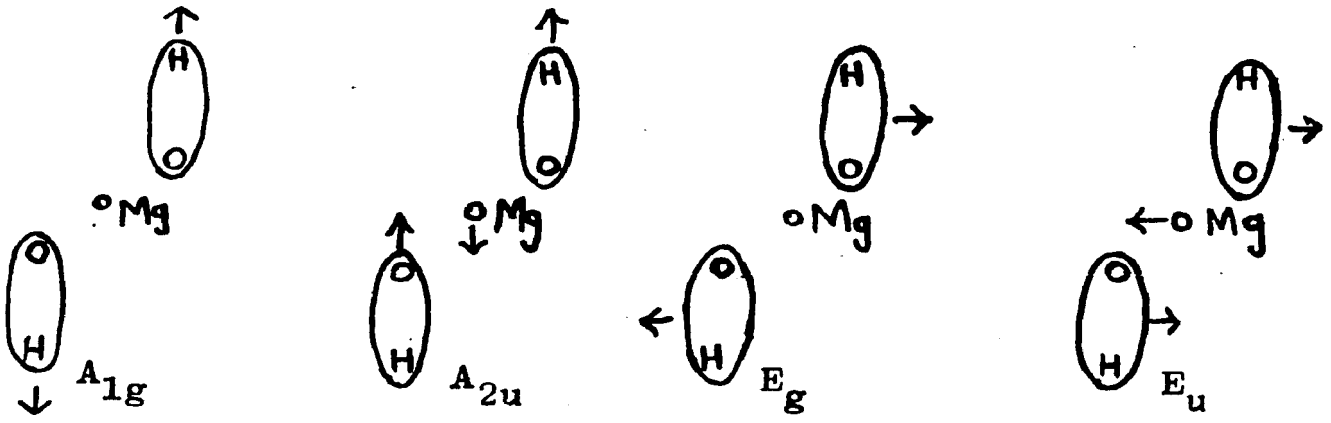
2.6 The Lattice Vibrations

Exclusive of the acoustic modes (T) there are ten external modes distributed among two doubly degenerate vibrations of the rotatory type (R') and two non-degenerate and two doubly degenerate oscillations of the translatory type (T'), which are listed in the table and are shown in Figure 2. The antisymmetric rotatory mode E_u is the only infrared active rotatory mode, and it is polarized perpendicular to the c-axis, whereas the E_g mode is the only rotatory mode permitted in The Raman effect. Among the translatory modes, which represent the vibrations of the hydroxyl groups as a whole relative to the magnesium ion, one non-degenerate A_{2u} and one



Internal Modes

Rotatory external Modes



Translatory external Modes

Figure 2. Normal Modes of vibrations in Brucite

doubly degenerate E_u mode are permitted in infrared absorption. The A_{2u} mode should be polarized parallel to the c-axis, whereas the E_u mode should be polarized perpendicular to it. In Raman scattering only the symmetric modes A_{1g} and E_g are allowed.

2.7 Summary

Following the method of Bhagavantam and Venkatarayudu a factor group analysis giving the distribution of normal modes in the brucite crystal has been presented along with a brief summary of the method. The vibrations have been suitably classified as internal and external modes depending on the relative magnitude of the forces acting between the oscillatory units. The internal modes arising from the vibrations within the OH groups are two in number. One of them (A_{1g}) is Raman active and has a depolarization ratio equal to zero for light incident normal to the c-axis, and the other one (A_{2u}) is infrared active and is polarized parallel to the c-axis. Among the rotatory lattice modes, which are doubly degenerate, one (E_u) is active in the infrared and is polarized perpendicular to the c-axis, and the other (E_g) is permitted only in the Raman effect. The translatory lattice vibrations are six in number, of which, three are active in the infrared and three in the Raman effect. The infrared active mode A_{2u} is polarized parallel to the c-axis, whereas the doubly degenerate E_u mode is polarized perpendicular to the c-axis. The Raman modes have symmetry A_{1g} and E_g.

CHAPTER 3

EXPERIMENTAL METHODS

3.1 Preparation of Samples

Samples parallel to the (0001) plane for the transmission spectra were relatively easy to prepare because, as has already been pointed out, brucite has very easy cleavage planes normal to the c-axis. Since the crystal is very soft (2 on Moh's scale), a tilt by a razor blade was sufficient to separate thin samples parallel to the cleavage plane. Thinnest samples obtained in this way were around twenty-five microns thick. But the softness of the crystal was also a hindrance in obtaining samples of uniform thickness, because sometimes the sharp edge cut through neighboring layers. Only samples of comparatively small surface area (usable with micro-cells), which had fairly uniform thickness throughout, could be obtained by this method. To prepare samples of large surface area (2 cm $\times$ 1 cm or larger) for using with the low temperature cell, a different technique had to be employed. A piece of the material with the desired surface area and thickness of about 2 mm was cleaved by a razor blade. One of the faces was ground on a flat glass plate with emery powder and was

then polished on a rotating disc by rouge. This face was next cemented on an optical quality plane quartz window by a very thin film of a mixture of paraffin and beeswax. The open face was then ground parallel to the polished face by "crystolon" abrasive grain (600B) and water to the desired thickness. Finally, a finer grinding was given by emery powder and a polishing by rouge. The sample could be used in the OH stretching region without removal from the quartz. The brucite adhered none too well to this quartz plate and frequently separated from it. The sample adhered more tightly to a ground glass plate, but the latter had to be removed for transmission measurements. After grinding and polishing, it is separated from the ground glass plate by melting the wax; and the wax was disolved by a mixture of equal parts of carbon tetra-chloride and ethyl alcohol. The thinnest sample obtained by this method was around hundred microns.

Preparation of samples with faces normal to the cleavage plane was a delicate and difficult affair, because of the cleavage property of the crystal. The forces holding the different layers are relatively weak and only a mild shock was sufficient to break the crystal into pieces.

A piece of the crystal, approximately 3 cm thick and with desired face area, was cut in the direction perpendicular to the cleavage plane with a rotating carborundum blade. A relatively smooth surface normal to the cleavage plane was thus obtained. Another similar cut was made about 5 mm away from the first surface. No thinner piece could be obtained

by this way. The same procedure was employed as in the preparation of samples cut parallel to the cleavage plane, the only difference being the great care taken. The grinding direction was parallel to the cleavage plane, i.e., perpendicular to the weak forces holding the layers. The final polishing was accomplished by gently rubbing the crystal on a fine quality emery paper. In spite of all precautions, a sample could be prepared only after quite a number of unsuccessful attempts. Thinnest samples obtained this way were between 250 to 300 microns.

For reflection spectra, samples of quite large surface areas are required. A crystal piece 2 cm × 2 cm and 1/2 cm thick was cut and one of the faces was ground by emery powder and was then highly polished so as to give reflection of distant object by diffused sun light. The rough face was then cemented on a piece of microscope glass slide. Preparation of samples in this way was quite easy for faces both parallel and perpendicular to the c-axis. For Raman spectra samples, in addition to both end faces, some of the side faces had also to be ground and polished.

The spectrum of the powder was obtained from reagent grade $Mg(OH)_2$, which was already in a finely pulverized form. $Mg(OD)_2$ powder was kindly supplied by Professor R.C. Taylor of the Chemistry department. The compound is obtained as a by-product in the process of preparing heavy ammonia as follows:

$$Mg_3N_2+6D_2O \rightarrow 3Mg(OD)_2+2ND_3$$

An excess of D_2O was used and the compound was expected to be approximately 99.6% deuterated, since that was the extent of deuteration in the heavy water, but contamination might decrease this during the course of manipulation and transfer. Finally, all the traces of moisture were removed by vacuum evaporation. This $Mg(OD)_2$ was also in a very finely powdered form. Powders were mulled in hexachlorobutadiene and were pressed between two rock salt plates. Hexachlorobutadiene was the most suitable mulling agent, because its refractive index was very close to those of $Mg(OH)_2$ and $Mg(OD)_2$, and it exhibited no characteristic absorption in the 1 micron to 6 microns interval.

3.2 Infrared Instrumentation

The major portion of the infrared spectrum was recorded on a Perkin-Elmer model 12C single beam spectrometer. A LiF prism was used from 2600 cm^{-1} to 11,000 cm^{-1}, a rock salt prism from 750 cm^{-1} to 2600 cm^{-1}, and for the low frequency region (350 cm^{-1} to 750 cm^{-1}) a KBr prism. The source optics of the spectrometer had been modified by Professor D.L. Wood so as to be useful for reflection measurements as shown in Figure 3. The reflection spectra were obtained by replacing the aluminized mirror M_2, with the sample surface mounted with focussing adjustments. The sample was focussed until maximum energy was recorded. The comparison spectrum was taken with the mirror which was assumed to be 100% reflecting. The spectrometer was calibrated with the known absorption bands of H_2O, CO_2, CH_4, NH_3 [34] and didymium glass[35]. Atmospheric absorption was reduced by blowing extra dry nitrogen through

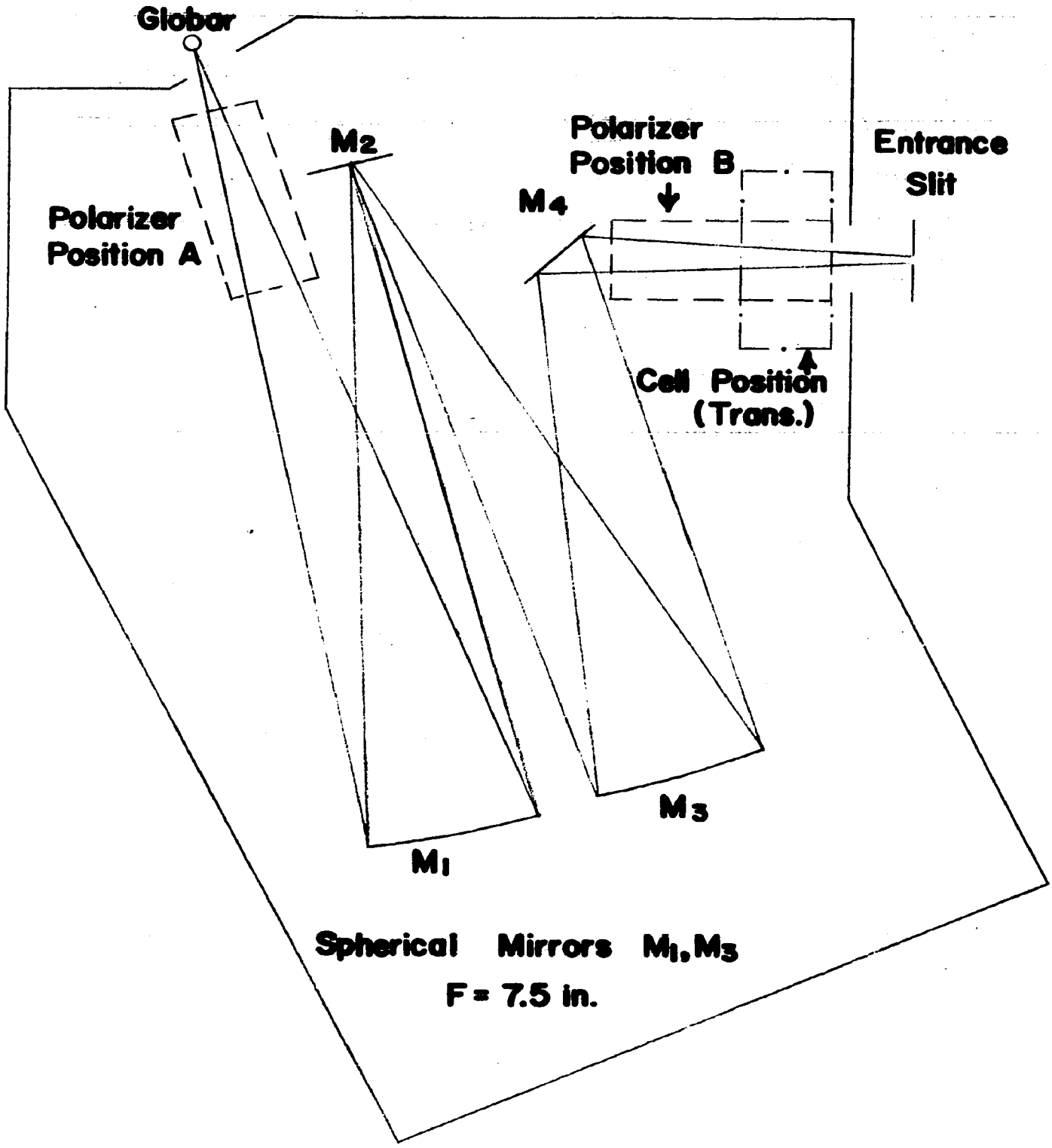


Figure 3. The Modified Source Optics for the P-E. -12C Spectrometer

the source optics and the monochromator chamber. Scattered radiation in the low frequency region was diminished by replacing the 45° mirror behind the exit slit by a frosted aluminized glass surface.

The spectral resolution for frequencies below 5000 cm^{-1} was obtained from the curves in the Perkin-Elmer intruction manual[36], and that for frequencies above 5000 cm^{-1} from the formula of Barnes[37]. The latter result had to be multiplied by a factor of 0.75 in order to bring it into agreement with the Perkin-Elmer values in overlapping regions.

A Perkin-Elmer model 21 double beam spectrometer with a NaCl prism was employed for general scanning of the spectrum, and to obtain transmission data from 800 cm^{-1} to 2600 cm^{-1}. This spectrometer was also used along with a CaF_2 prism for recording some of the low temperature spectra.

The fine structure of the central band of $Mg(OD)_2$ powder was observed with the grating spectrometer built by Hardy[38].

A silver chloride polarizer[39] was used in all measurements of polarized spectra. It consisted of six 0.075 cm thick silver chloride plates placed in a lucite frame at Brewster's angle. In most of the transmission and reflection measurements the polarizer was placed in the B position of Figure 3.

In measuring the polarized reflection spectrum of anisotropic samples (as in the present case) it is always desirable to have the electric vector perpendicular to the plane of incidence so that the convergence of incident beam may not introduce any error. Consequently, whenever possible, the radiation was polarized in such a way as to present the electric vector perpendicular to the plane of incidence; and the

c-axis of the crystal was placed either parallel or perpendicular to the direction of the electric vector.

Transmission spectra at liquid air temperatures were obtained with the low temperature cell designed by Ockman[40]. Samples used with the cell had to be relatively large in area since the position of the cell was away from the focus on the entrance slit.

3.3 Raman Measurements

The Raman spectra were obtained with a Gaertner spectrograph. A helical Toronto arc was used as a source. Sodium nitrite and a mixture made of 20% Cu $(NH_3)_4$ SO_4 solution in water and 4 gms. of NH_4Br per 20 ml of solution were used as filters to isolate the 4358A mercury exciting line and to reduce the background scattering. The dispersion of the spectrometer is 180 cm^{-1} per mm in the spectral region of interest, a 0.1 mm wide slit was used. The details of the experimental arrangement have been described by Vidale and Taylor[41]. The samples were mounted in such a way that all the faces were covered except for the two used for the entrance and exit of radiation. The spectra were photographed on Eastman Kodak 103a-J Bkd. plates. Exposure time ranged from 20 hours to 6 hours. Microphotometer tracings were obtained by a Leeds and Northrup, Korr Alberts instrument. The frequencies were measured by using a calibration chart previously prepared by Professor R.C. Taylor from a comparison with the argon spectrum.

CHAPTER 4

EXPERIMENTAL RESULTS OF THE PRESENT STUDY

4.1 Introduction

The experimental results of the present investigation will be reported in this chapter.

The Raman spectrum of brucite has been observed for the first time in the present research.

The infrared studies included a careful repetition of previous spectra in order to obtain more reliable information as to frequencies, intensities, polarizations etc. and measurements in the new regions, 350 cm^{-1} to 1000 cm^{-1}, and 7500 cm^{-1} to 11,000 cm^{-1}.

The large absorption of the crystal below 1000 cm^{-1} permitted only an indirect determination of absorption maxima from its reflection spectrum. The same technique was used in the vicinity of 3700 cm^{-1}. This region was also investigated with the aid of thin powder samples.

The powder spectra of brucite and $Mg(OD)_2$ were studied only with a NaCl prism by Mara[21]. They have now been repeated using a LiF prism to bring out additional bands and make possible a better comparison of the frequencies of the ab-

sorption maxima of the two substances.

Single crystal transmission data for the balance of the spectrum up to 11,000 cm^{-1} was obtained with a LiF prism. The temperature dependence and polarization properties of the absorption bands were determined wherever feasible.

Most of the spectra reported in this chapter are taken by a LiF prism. A few spectra which have been obtained by a different prism are so marked on the figures.

4.2 Raman Spectrum

It is very difficult to get a sizeable piece of brucite suitable for a Raman scattering experiment because of many internal fractures resulting from its ready cleavage. Probably for this reason no Raman spectrum of the crystal has been reported previously.

Besides the scattering from the crystal imperfections, there was a high background due to fluorescence. With difficulty, two weak but sharp lines have been photographed: one in the OH stretching region and one in the low lying lattice region. Longer exposures and different orientations did not produce any other lines. The separation of these lines from the exciting line (4358A) are 446 cm^{-1} and 3655 cm^{-1} (± 10 cm^{-1} for each). Because the lines were so weak it was not possible to obtain a polarized Raman spectrum.

4.3 Reflection Spectra

The preparation of crystal samples thin enough to give an appreciable percentage transmission in the vicinity of intense absorption bands may be impractical. This situation

exists for brucite at 3700 cm^{-1} and also in the region below 1000 cm^{-1}. Here sample thicknesses of tenths of a micron would be appropriate but as yet it has not been possible to prepare crystal section of brucite thinner than 50 μ. Information on the absorption in such regions is available from the spectral reflectivity which is necessarily large because of the large extinction coefficient. Simon[42] showed that the extinction coefficient can be calculated from the measurement of the reflectivity at two widely separated angles of incidence. Recently, Robinson[43] has modified Simon's method enabling one to evaluate the extinction coefficient and the index of refraction as a function of frequency from reflection measurements at normal incidence, provided that spectral regions away from the peak on both sides, where reflection is constant and small, are included. The method is rigorously applicable only to crystals of orthorombic or higher symmetry; and consequently valid for brucite because of its hexagonal structure. Only very strong bands can be detected this way. Weaker ones generally produce a negligible effect on the reflectivity, but can be observed satisfactorily in transmission.

4.3a Reflection Spectra (350 cm^{-1} to 1000 cm^{-1})

The high opacity of brucite below 1000 cm^{-1} indicates the existence of an extremely intense band in this region. External (lattice) oscillations in an ionic or semi-ionic crystal are generally expected to occur in this low-lying region. Of these modes, usually the translatory ones are

very strong in the infrared.

The reflectivity between 350 cm^{-1} and 1000 cm^{-1} was measured using KBr and NaCl prisms. Two samples with faces parallel and perpendicular to the cleavage plane (i.e., surface perpendicular or parallel to the c-axis) were chosen, and reflection spectra at normal incidence are reproduced in Figure 4. The most notable feature of the spectra from both samples is a very strong and broad band at 515 cm^{-1}. The peak value of reflection is little higher when the c-axis is oriented parallel to the incident beam, but this may not be genuine because a surface parallel to the cleavage can be polished more perfectly than one normal to it. On the low frequency side of the main band there occurs a sharp but relatively weak band at 415 cm^{-1} in both orientations. Both samples also show a broad shoulder at 700 cm^{-1}, and the sample normal to the cleavage plane has an additional weak shoulder at 640 cm^{-1}.

Spectra were also recorded using polarized radiation in order to determine the directions of changing dipole moment vectors in the crystal responsible for these bands. It was observed that the direction of the incident electric field vector does not have any effect on the spectrum when the c-axis is parallel to the incident beam (i.e., sample parallel to the cleavage plane). But for the other case, where the c-axis is normal to the incident beam, the spectrum exhibited dichroic properties. Figure 5 presents the polarized spectra with the electric vector directed parallel and perpendicular to

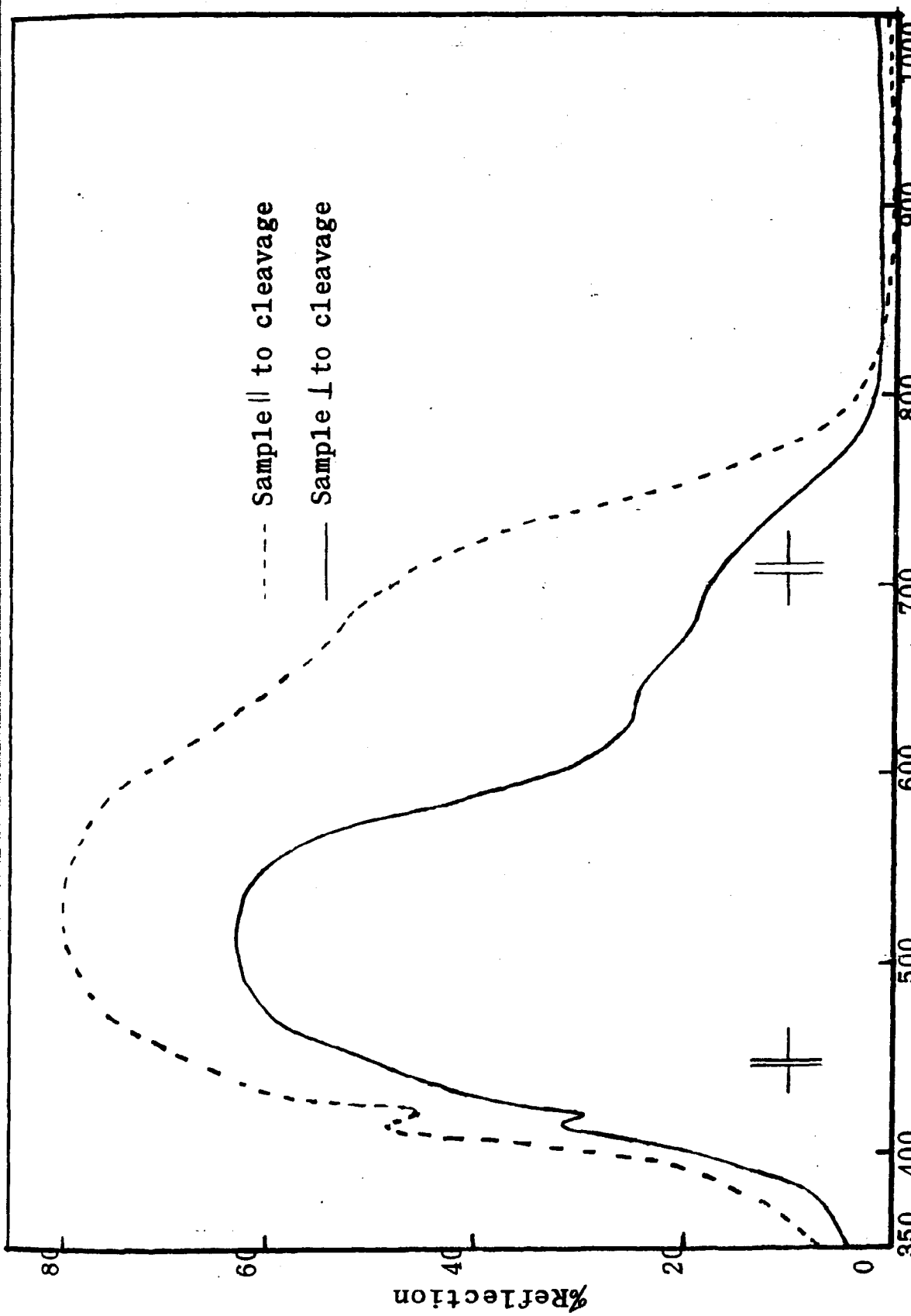


Figure 4. Reflection spectra of Brucite for two crystal orientations, from 350 cm^{-1} to 1000 cm-1 (NaCl and KBr)

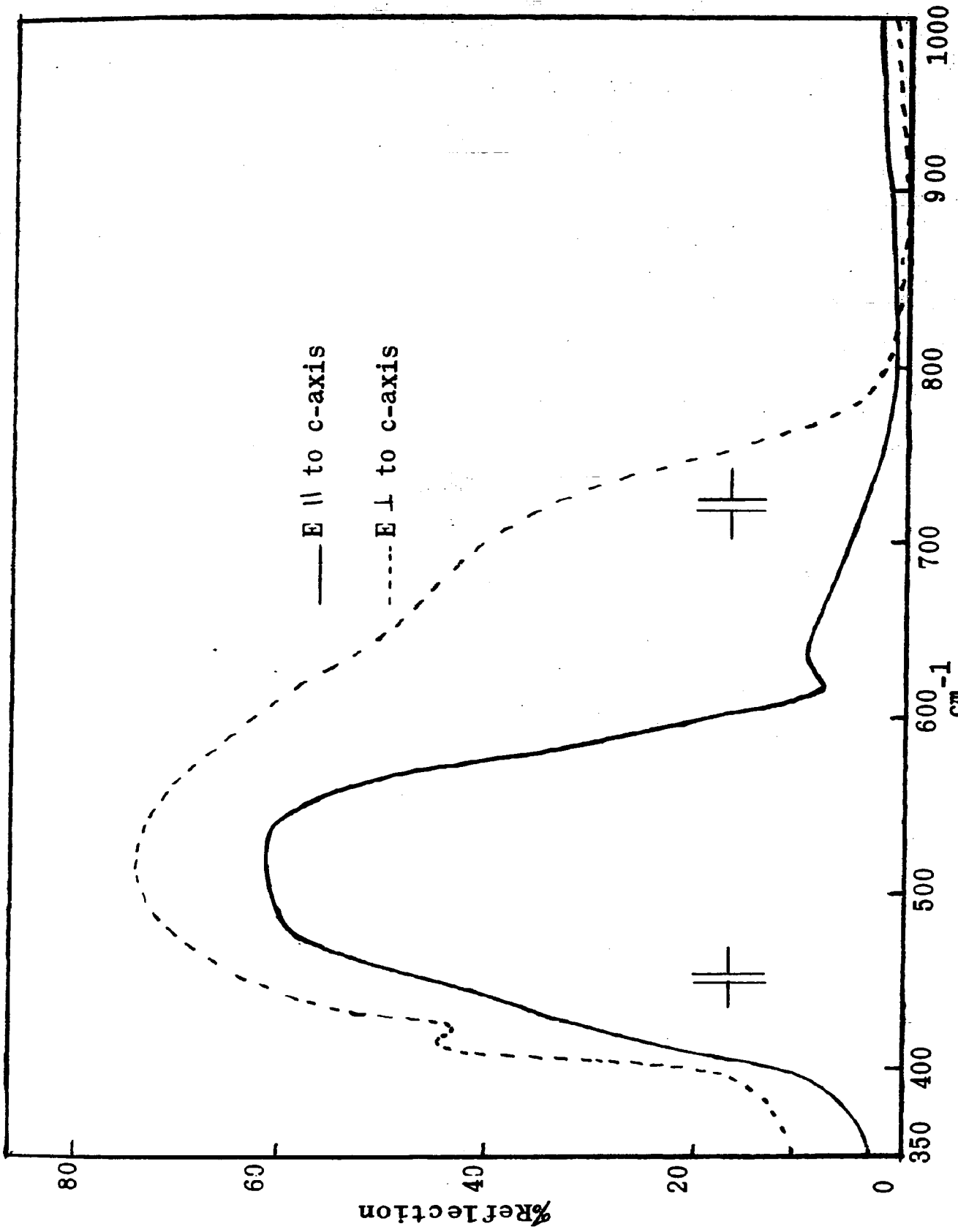


Figure 5. Polarized reflection spectra of Brucite, from 350 cm^{-1} to 1000 cm^{-1} (NaCl and KBr)

the c-axis.

The band at 415 cm^{-1} shows marked dichroic behavior, being completely absent when the electric vector is parallel to the c-axis. The strongest band at 515 cm^{-1} is present in both the polarizations, whereas the band at 640 cm^{-1} is much weaker but better resolved and polarized parallel to the c-axis. The absorption at 700 cm^{-1}, occurring as a shoulder to the main band, is polarized perpendicular to the c-axis and is completely absent in the spectrum of the other polarization.

4.3b Reflection Spectra (3450 cm^{-1} to 3900 cm^{-1})

As already pointed out, the absorption in the OH stretching region is very high around 3700 cm^{-1} for the electric vector parallel to the c-axis. To determine the correct position and intensity of this very strong absorption, and to decide whether this absorption is due to a single strong band, reflection measurements were made in this region also. Figure 6 shows the reflection spectrum from 3400 cm^{-1} to 3900 cm^{-1} of sections cut parallel and perpendicular to the cleavage. Only one strong band is observed in reflection at 3690 cm^{-1}, and that one only in the case of a sample cut perpendicular to the cleavage plane. A polarized spectrum with a sample cut perpendicular to the cleavage plane is reproduced in Figure 7. One observes that the only band, at 3690 cm^{-1}, is completely dichroic, having an infrared transition moment vector parallel to the c-axis. The maximum value of reflec-

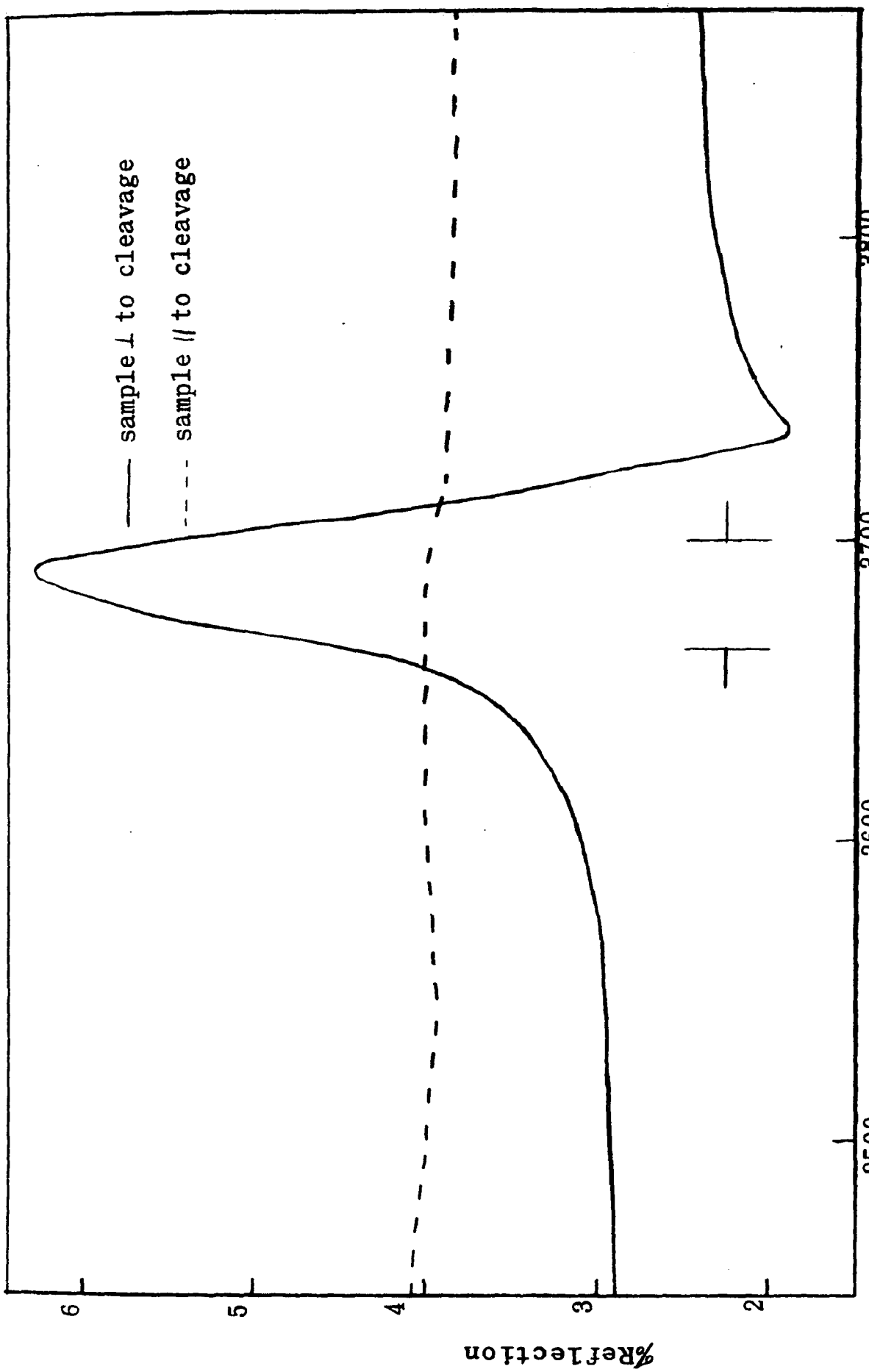


Figure 6. Reflection spectra of Brucite for two crystal orientations, from 3450 cm-1 to 3850 cm-1

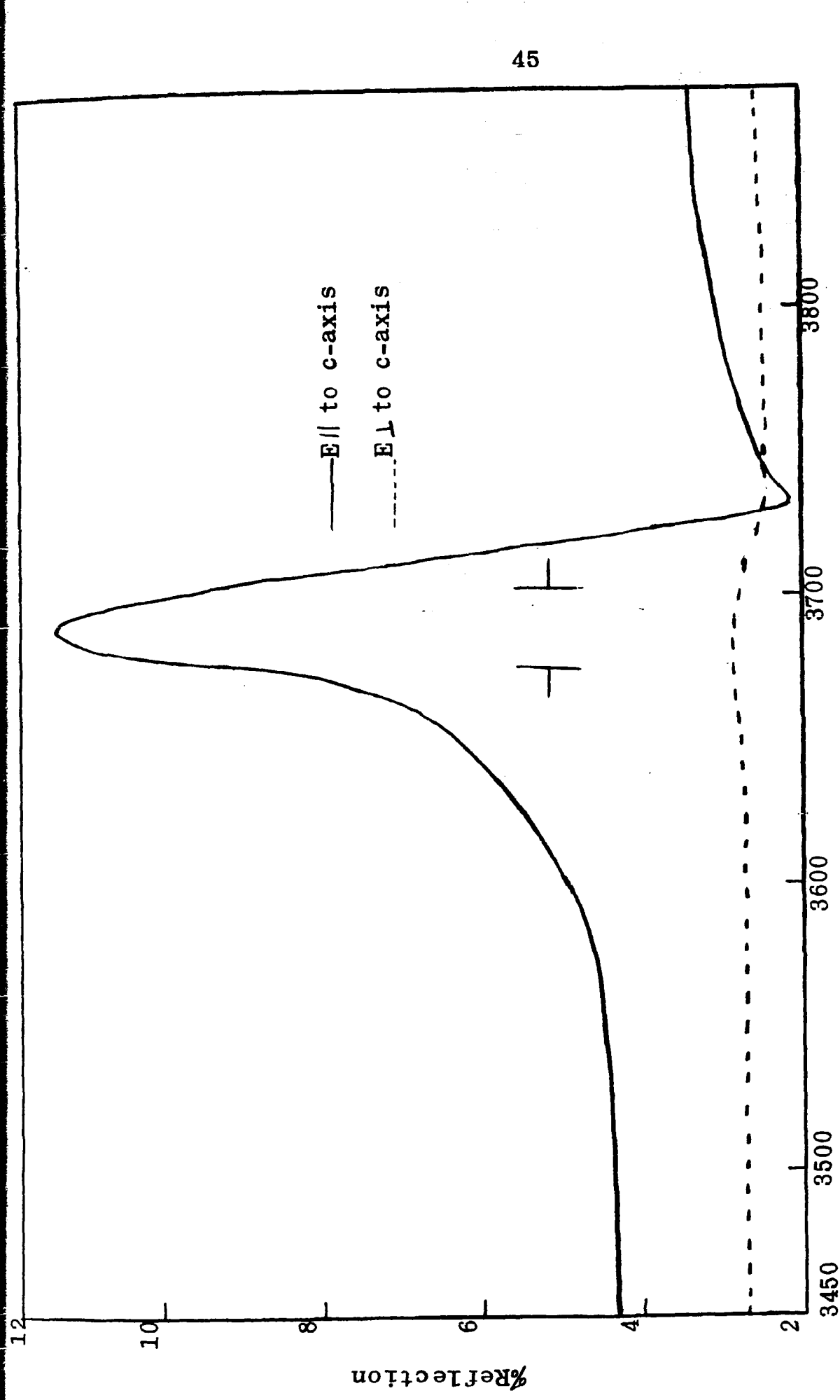


Figure 7. Polarized reflection spectra of Brucite, from 3450 cm^{-1} to 3850 cm^{-1}

tion in the spectrum polarized parallel to the c-axis is greater than that in the unpolarized spectrum of the face perpendicular to the cleavage plane because the latter contains contributions also from the electric vector normal to the c-axis.

In the whole region from 3000 cm^{-1} to 5000 cm^{-1}, in reflection, no additional band could be detected in either of the crystal orientations, though, as will be seen in section 4.5, it is the richest region of absorption bands detected in single crystal transmission.

The extinction coefficient, k, and the refractive index, n, for the reflection band at 3690 cm^{-1} have been evaluated as a function of the frequency by the method indicated by Robinson. They are given by

$$n = \frac{1-r^2}{1+r^2 - 2r\cos\theta} \qquad k = \frac{-2r\sin\theta}{1+r^2 - 2r\cos\theta} \qquad (4\text{-}1)$$

The quantity r^2 is measured directly from observations of the reflection spectrum at normal incidence. The phase difference, θ between the incident and reflected waves is solved by a numerical integration:

$$\theta_c = \frac{1}{\pi} \int_0^{\infty} \frac{d \ln r}{d\omega} \ln\left|\frac{\omega+\omega_c}{\omega-\omega_c}\right| d\omega \qquad (4\text{-}2)$$

where θ_c is the value of θ at frequency ω_c. In practice the limits of integration are the two extremities of the band where the reflection approaches constant values.

Figure 8 shows the n and k curves for the band in question. The peak of the extinction coefficient curve occurs at 3705 cm^{-1} and its value is 0.57. The absorption coefficient, α, is related to k by

$$\alpha = \frac{4\pi k}{\lambda} \qquad (4\text{-}3)$$

where λ is the wave length. The fractional transmission, T, is given by Lambert's law

$$T = e^{-\alpha x} \qquad (4\text{-}4)$$

x being the thickness of the sample. For only a 1μ thick sample the percentage absorption for this band is 94%.

4.4 Powder Spectra of $Mg(OH)_2$ and $Mg(OD)_2$

4.4a Powder Spectrum of $Mg(OH)_2$ at 3700 cm^{-1}

It was pointed out in the last section that the strongest band in the OH stretching region occurs at 3690 cm^{-1} in reflection. The position of this band may also be determined from the transmission of a powder sample whose thickness can be controlled. In powder form, the small crystals present a random orientation to the incident radiation resulting in a spectrum which is an average over all possible orientations. Figure 9 is a reproduction of the powder spectrum. The position of the only band in the vicinity is at 3700 cm^{-1}. This is in good agreement with the value of 3705 cm^{-1} obtained from reflectivity measurements in the previous section. Furthermore, absorption frequencies determined from reflection

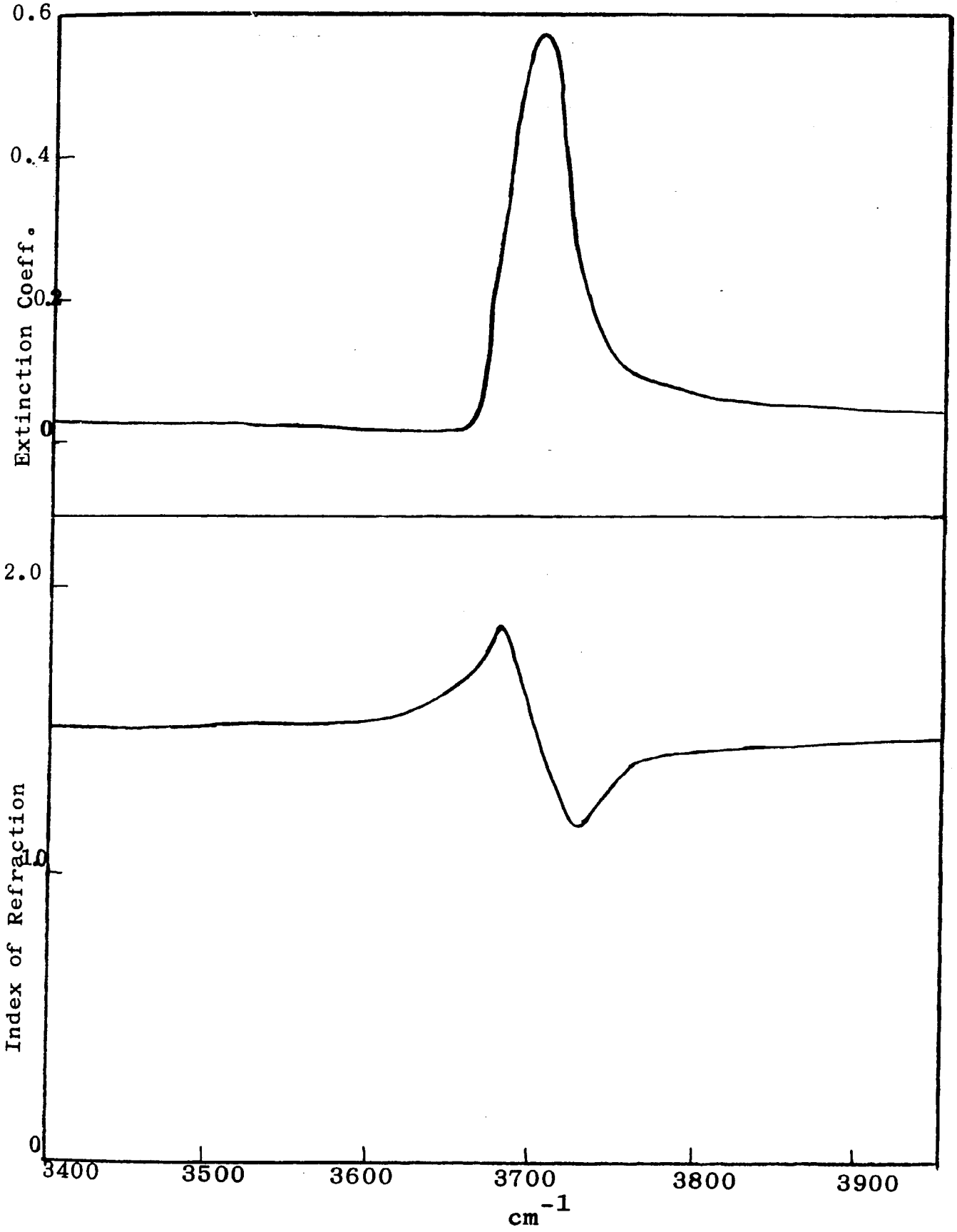


Figure 8. Optical constants of Brucite ($\vec{E} \parallel$ c-axis), from 3400 cm^{-1} to 3950 cm^{-1}

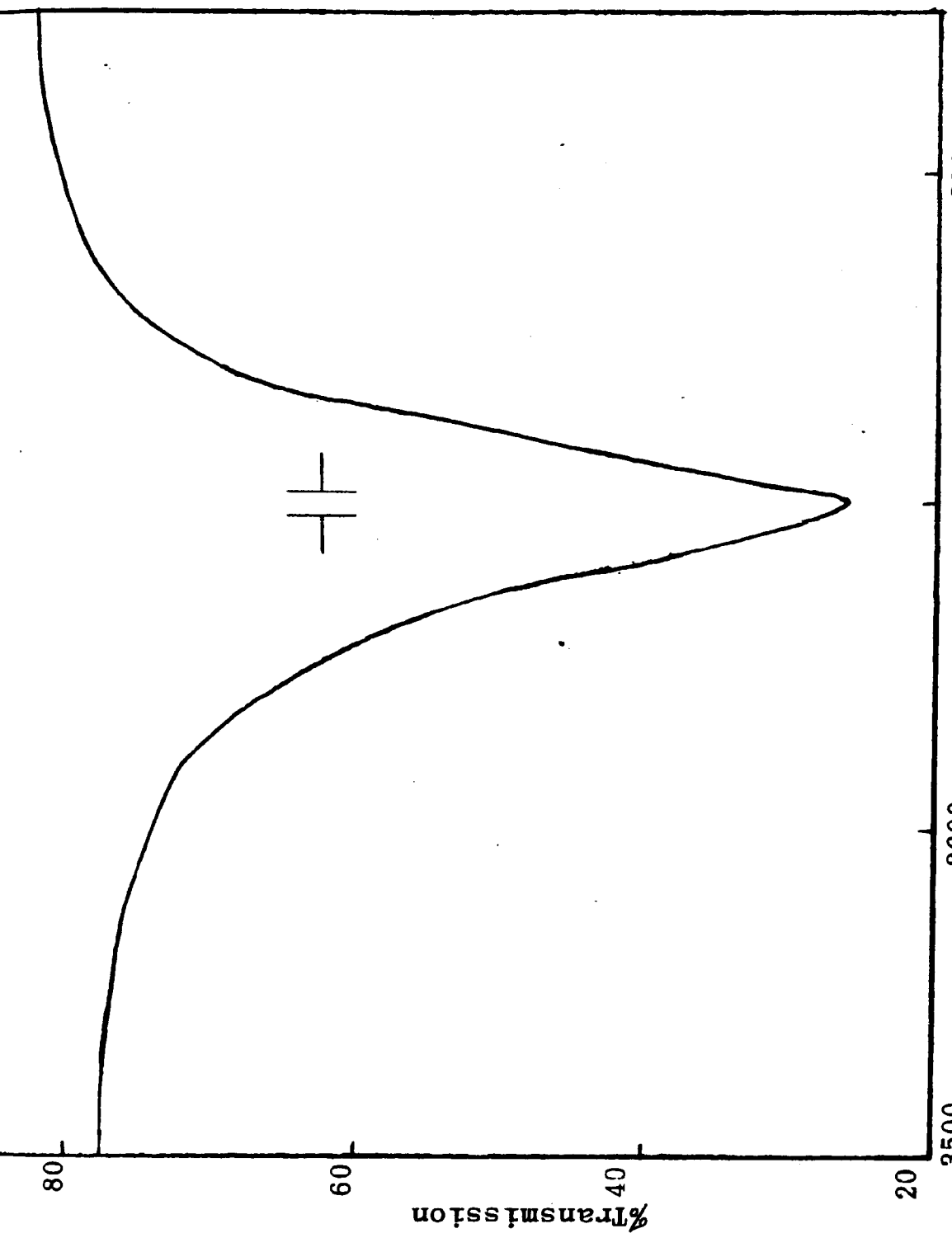


Figure 9. Transmission spectrum of Brucite powder, from 3500 cm^{-1} to 3850 cm^{-1}

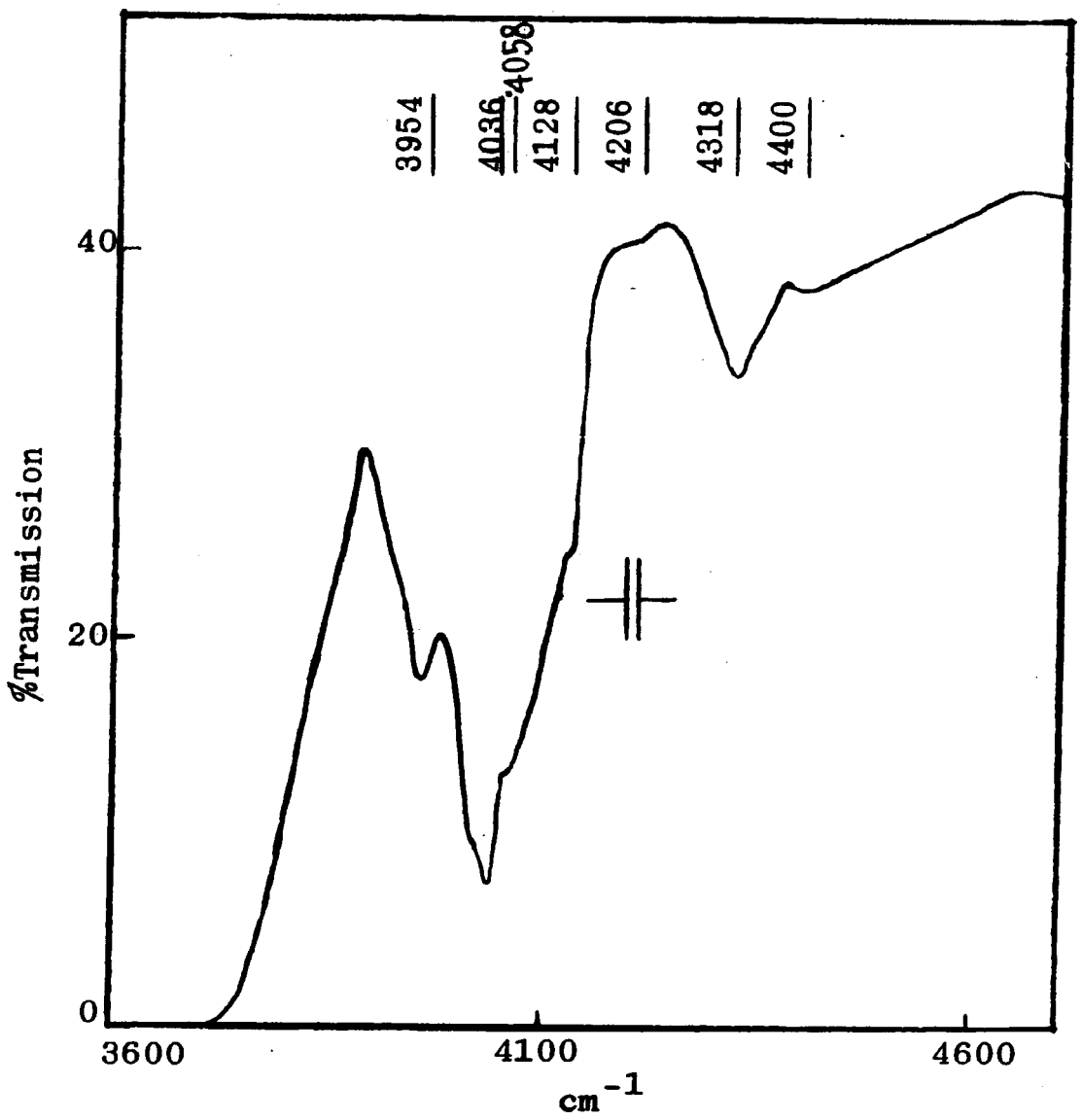


Figure 10. Transmission spectrum of Brucite powder, from 3600 cm^{-1} to 4700 cm^{-1}

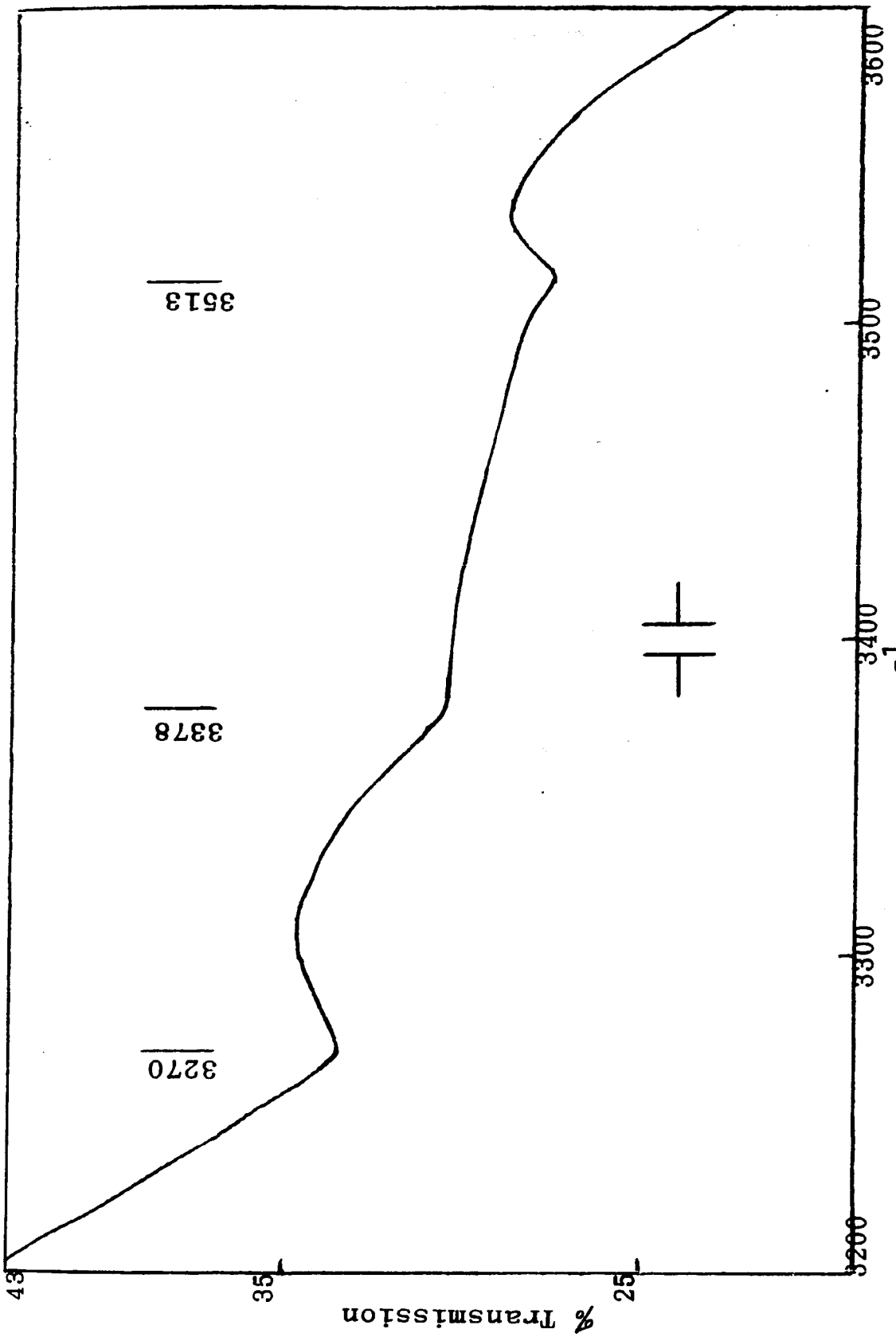


Figure 11. Transmission Powder Spectrum of Brucite (3200 cm^{-1} to 3600 cm^{-1})

spectra are usually a trifle large because of the effect of finite slit width on the asymmetric reflectivity curve.

4.4b Comparison of $Mg(OH)_2$ and $Mg(OD)_2$ Powder Spectra

It has been pointed out by Mara and Sutherland[11] that a comparison of the absorption frequencies in the OH and OD stretching regions can provide a valuable clue to the structure of brucite. A detailed powder spectrum of brucite was taken with a LiF prism to compare it with the corresponding region of the spectrum of chemically prepared $Mg(OD)_2$ obtainable only in a finely pulverized form. The brucite spectra are presented in Figures 10 and 11. Sample thicknesses were adjusted so as to give maximum contrast. As expected, the scattering loss was very high. On the high frequency side of 3700 cm^{-1} there occur two clusters of bands around 4030 cm^{-1} and 4330 cm^{-1}. They correspond to Mara's values of 4032 cm^{-1} and 4348 cm^{-1}. But in the present case, the resolution being better, at least seven bands are observed. On the low frequency side two more bands are observed in addition to the relatively strong one at 3270 cm^{-1} already reported by Mara. The positions and relative intensities of the bands are listed in Table 4.

The spectra of chemically prepared $Mg(OD)_2$ are reproduced in Figures 12, 13, and 14. The strongest band in this substance occurs at 2721 cm^{-1}. On the high frequency side of this one observes two clusters around 2956 cm^{-1} and 3117 cm^{-1} very similar to those observed in brucite. These correspond

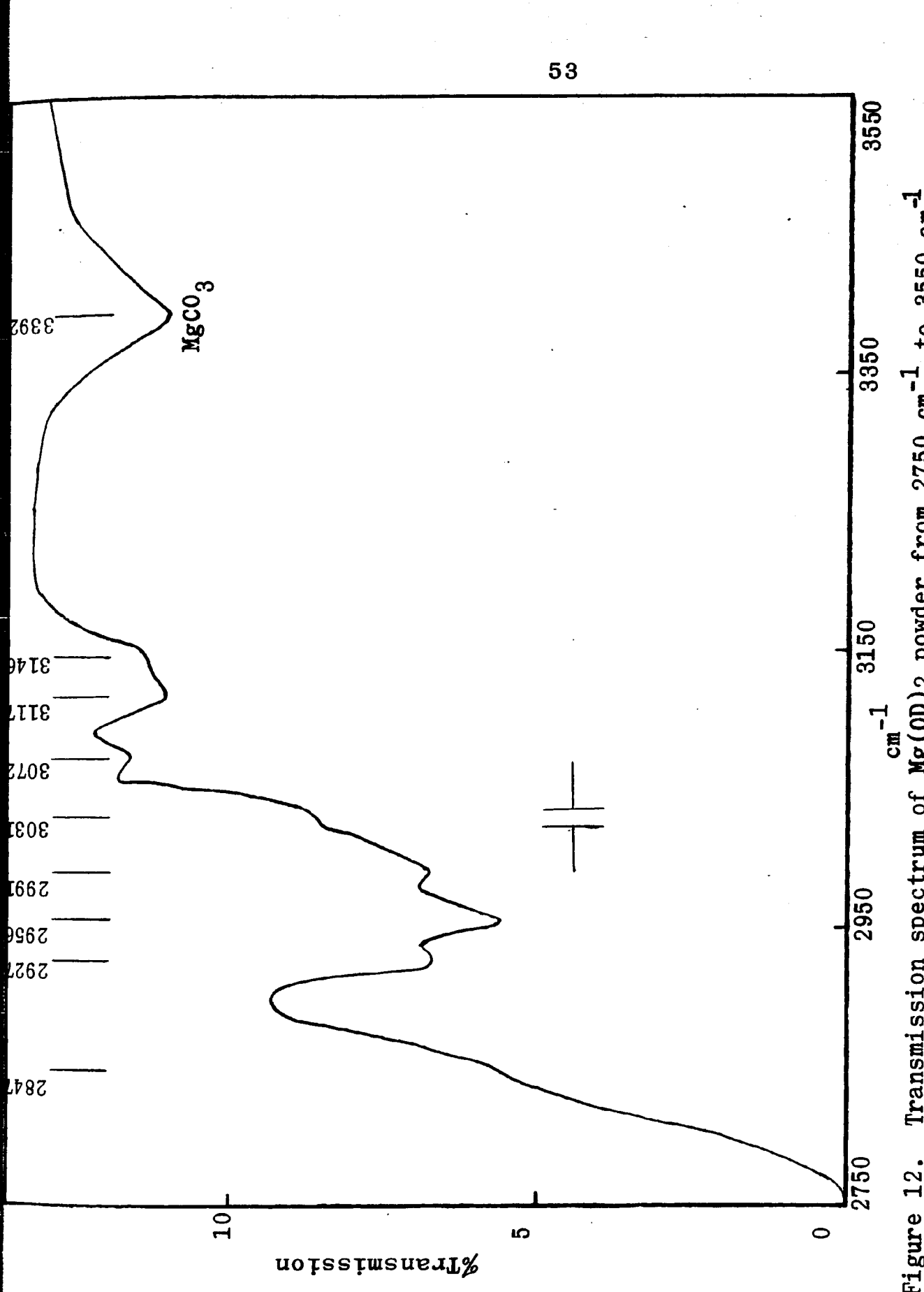


Figure 12. Transmission spectrum of $Mg(OD)_2$ powder, from 2750 cm^{-1} to 3550 cm^{-1}

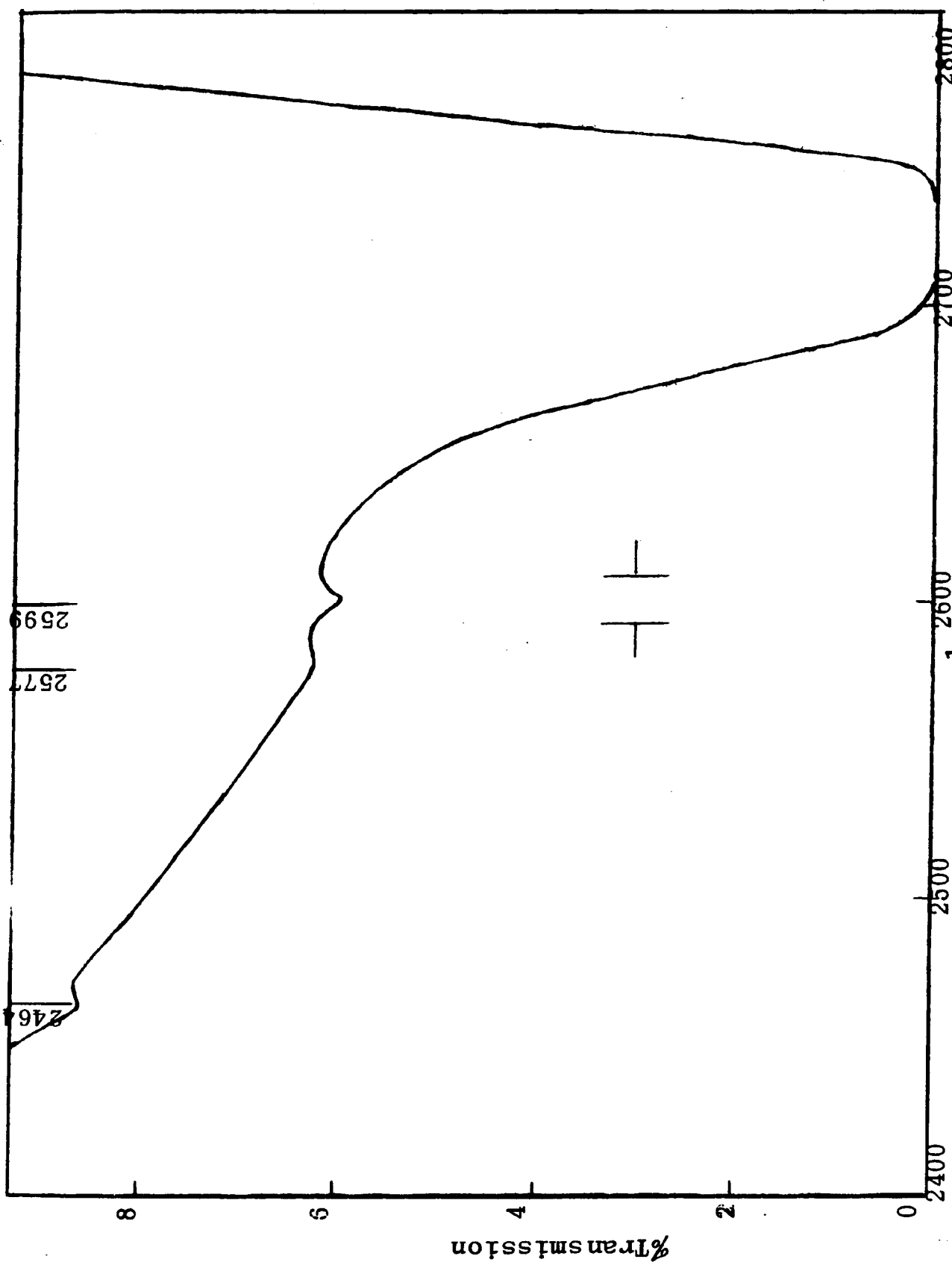


Figure 13. Transmission spectrum of $Mg(OD)_2$ powder, from 2400 cm^{-1} to 2800 cm^{-1}

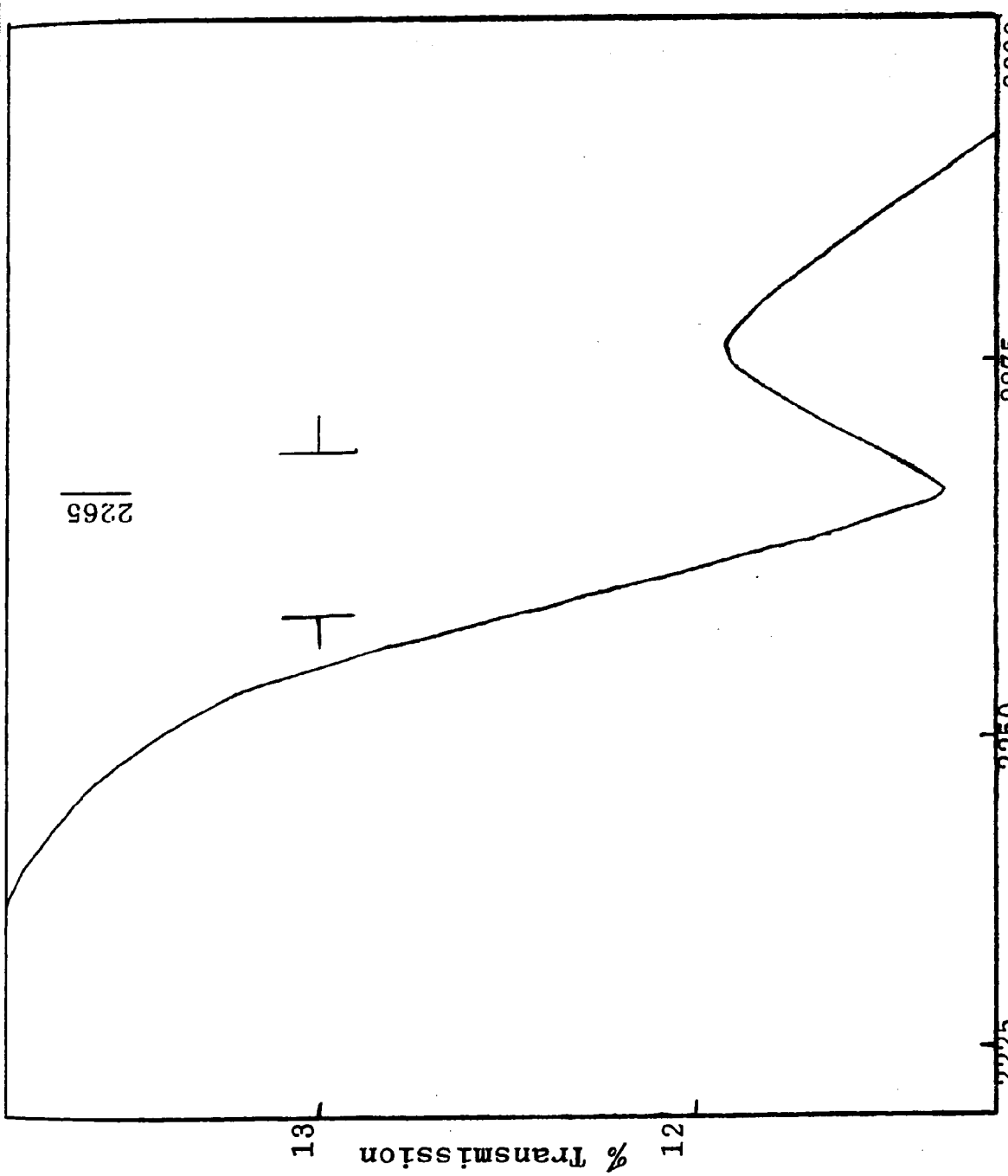


Figure 14. $Mg(OD)_2$ Transmission Powder Spectrum (2225 cm^{-1} to 2300 cm^{-1})

to the bands at 2915 cm^{-1} and 3077 cm^{-1} observed by Mara with a NaCl prism. The better resolution of the present work enables one to distinguish seven bands. Four bands are observed on the low frequency side of the main band. The strongest one of these is situated at 2265 cm^{-1}. In the spectra of both the substances the bands on the high frequency side of the strongest one are much stronger than those on the low frequency side.

An attempt was made to study the fundamental OD stretching at 2721 cm^{-1} with a grating spectrometer to look for possible fine structure. A shoulder on the absorption curve appeared at 2737 cm^{-1}, and two very weak lines at 2760 cm^{-1} and 2781 cm^{-1}. No comparison could be made with the corresponding OH band which was obscured by atmospheric water vapor absorption.

The frequencies of all the bands observed in the powder spectra of $Mg(OH)_2$ and $Mg(OD)_2$ are listed in Table 4 along with their ratios, which are always near 1.37. The relative intensities are also furnished to indicate the correspondence of the bands in the two substances.

4.5 Single Crystal Transmission Spectra

4.5a Transmission Spectra of Samples Cut Parallel to the Cleavage Plane at Room and Liquid Nitrogen Temperatures (2650 cm^{-1} to 5200 cm^{-1}).

Single crystal transmission spectra of brucite from 2650 cm^{-1} to 5200 cm^{-1} at both ambient and liquid nitrogen temperatures are reported in this section. Mara studied this region from 3125 cm^{-1} to 5000 cm^{-1} with a LiF prism, and

Table 4

Comparison of $Mg(OH)_2$ and $Mg(OD)_2$ Bands
(Powder)

$\nu Mg(OH)_2$ (cm^{-1})	$\nu Mg(OD)_2$ (cm^{-1})	Ratio
3270 W	2265 W	1.43
3378 V.W	2464 V.W	1.37
3513 W	2585 V.W	1.36
3700 V.V.S.	2721 V.V.S.	1.36
3954 M	2927 M	1.35
4036 S	2956 S	1.37
4058 W	2991 M	1.36
4128 W	3031 W	1.36
4206 W	3073 M	1.37
4318 S	3117 S	1.39
4400 W	3145 M	1.40

obtained low temperature spectra at low resolution with a NaCl prism.

A model 12C Perkin-Elmer spectrometer with a LiF prism has been used wherever possible to give more accurate frequency and intensity values. In the region of strong atmospheric water vapor absorption (3450 cm^{-1} to 3900 cm^{-1}) work at low temperatures could only be done with the model 21 Perkin-Elmer double beam spectrometer, for which a CaF_2 prism was available. It was impossible to prepare thin samples cut normal to the cleavage plane of sufficient area for use with the liquid air cell.

The spectra reported in Figure 15 from 2650 cm^{-1} to 3150 cm^{-1} were obtained with a relatively thick sample (750 μ) because the crystal is comparatively less absorbing in this region. At room temperature three bands are observed for the orientation used (parallel to the cleavage). The strongest band of the set is at 3025 cm^{-1}. Two relatively weak shoulders appear at 2923 cm^{-1} and 2764 cm^{-1}. The transparency of the sample in this region increases considerably at low temperature and all the bands almost completely vanish at the liquid nitrogen point. The sample showed its original absorption when brought back to room temperature.

The spectrum from 3125 cm^{-1} to 3450 cm^{-1} is presented in Figure 16. For a sample 300 μ thick two quite well resolved bands at 3272 cm^{-1} and 3368 cm^{-1} occur at room temperature, the former being much stronger than the latter. These bands are also extremely temperature dependent. At the liquid

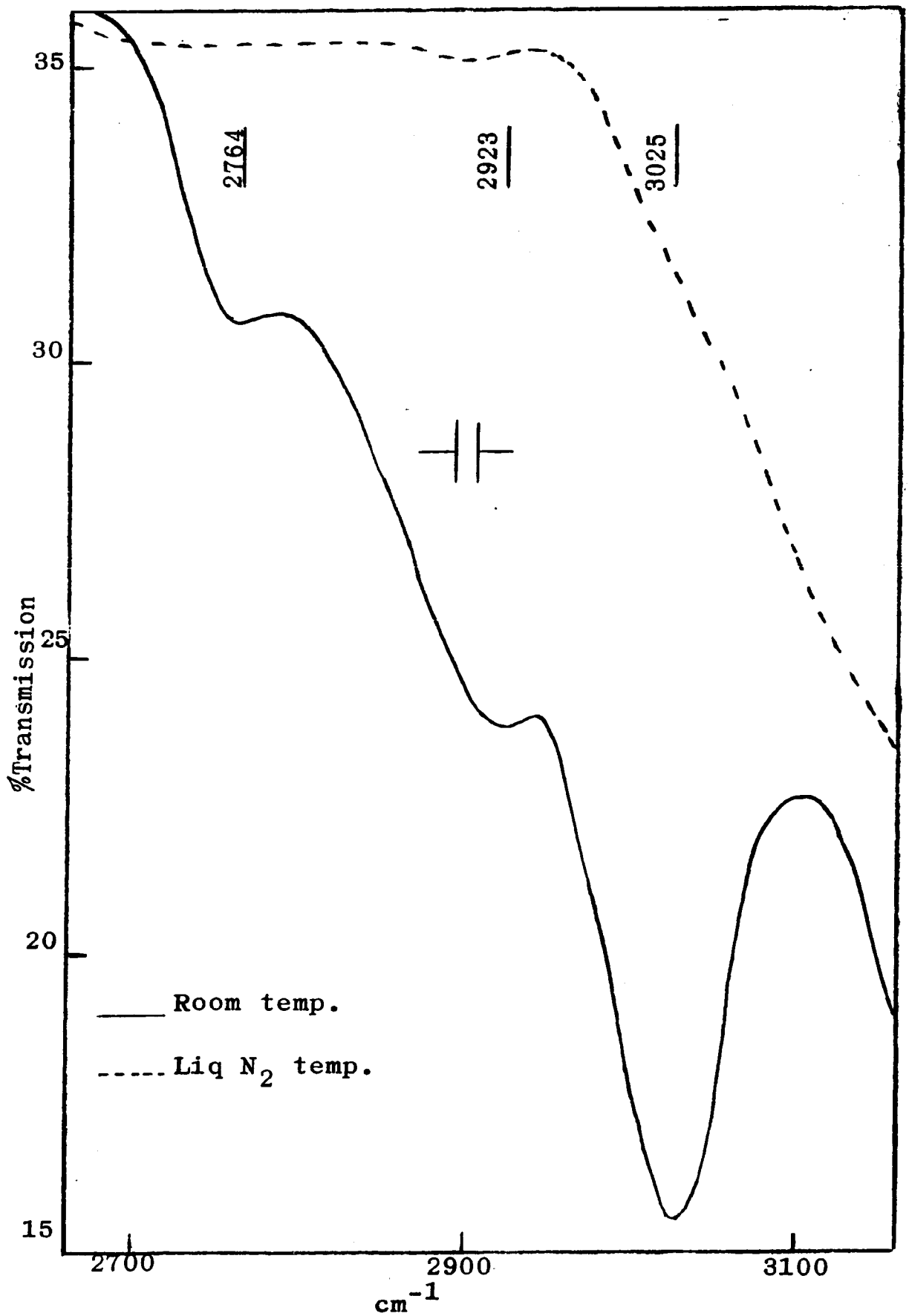


Figure 15. Transmission spectra of Brucite at two temperatures, from 2700 cm^{-1} to 3100 cm^{-1} (sample // to cleavage, 750 μ)

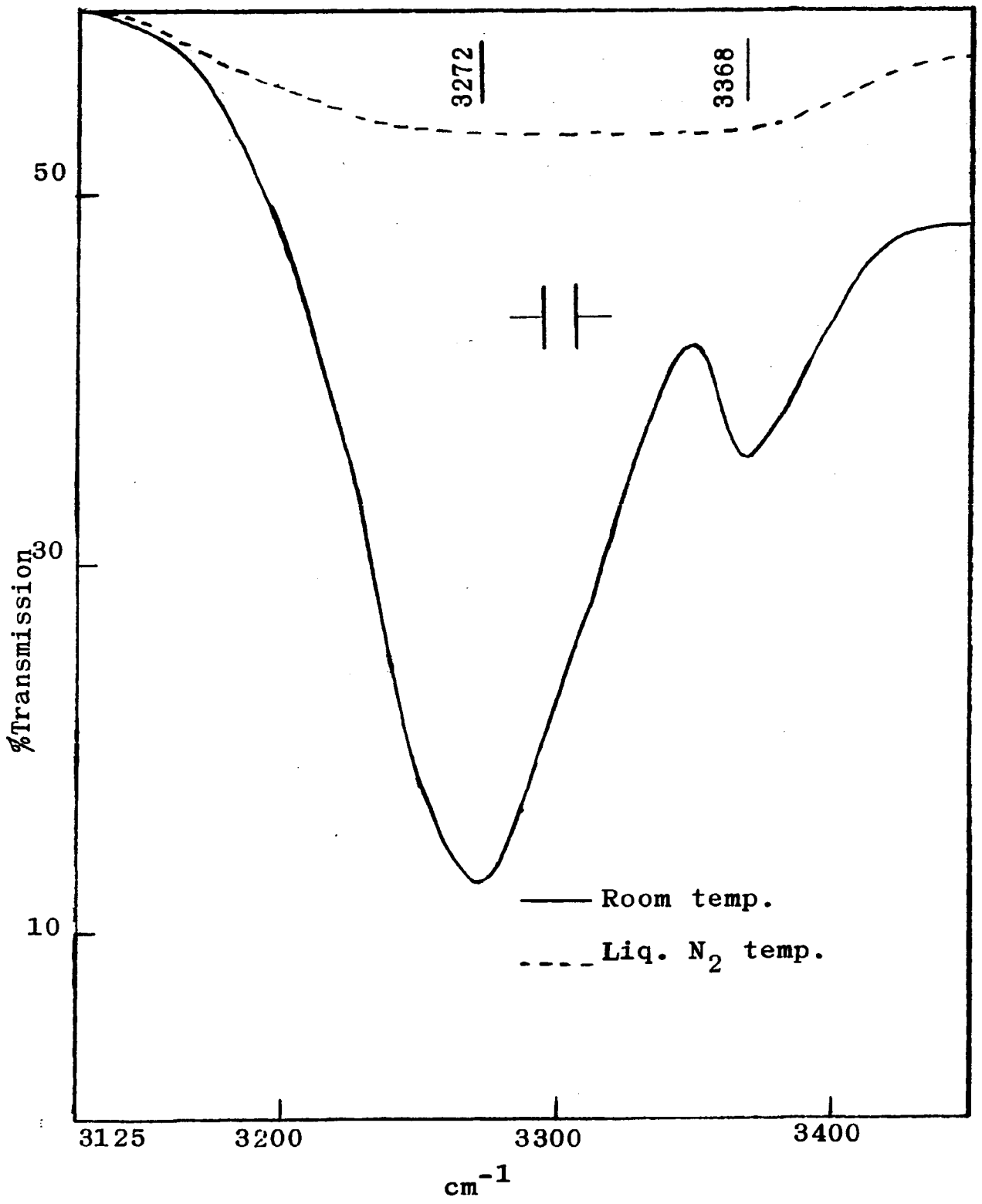


Figure 16. Transmission spectra of Brucite at two temperatures, from 3125 cm^{-1} to 3450 cm^{-1} (sample // cleavage, 300 μ)

nitrogen temperature both of them nearly vanish leaving only a very weak shallow dip.

The spectra from 3900 cm^{-1} to 4600 cm^{-1} are reported in Figures 17 and 18. Two samples, about 300μ and 100μ thick were used. Four well-resolved bands are observed. Their positions at room temperature are: 3956 cm^{-1}, 4042 cm^{-1}, 4316 cm^{-1} and 4440 cm^{-1}. A very weak band at 4550 cm^{-1} is also detectable. Actually these four bands may be considered as divided into two doublets, the one around 4000 cm^{-1} being much stronger than that around 4400 cm^{-1}. The second band of the first doublet and the first band of the second are the comparatively stronger ones. Their temperature dependence is not as prominent as in the previous cases. At the liquid air temperature the 3956 cm^{-1} band becomes a little bit weaker but relatively much sharper and shifts towards higher frequencies by about 10 cm^{-1}, the intensity of the strongest band at 4042 cm^{-1} increases a little and the shift is towards the lower frequency side by 16 cm^{-1}. Moreover, a small shoulder appears in the previous position. A thinner sample reveals all these features a little better.

The band at 4316 cm^{-1} sharpens and also increases slightly in intensity but no shift in frequency is recorded. The last band at 4440 cm^{-1} decreases very little in intensity but is sharper and shifts by about 20 cm^{-1} towards higher frequencies. The weakest band near 4550 cm^{-1} which can hardly be detected at room temperature becomes sharper and its position is also shifted to 4575 cm^{-1}.

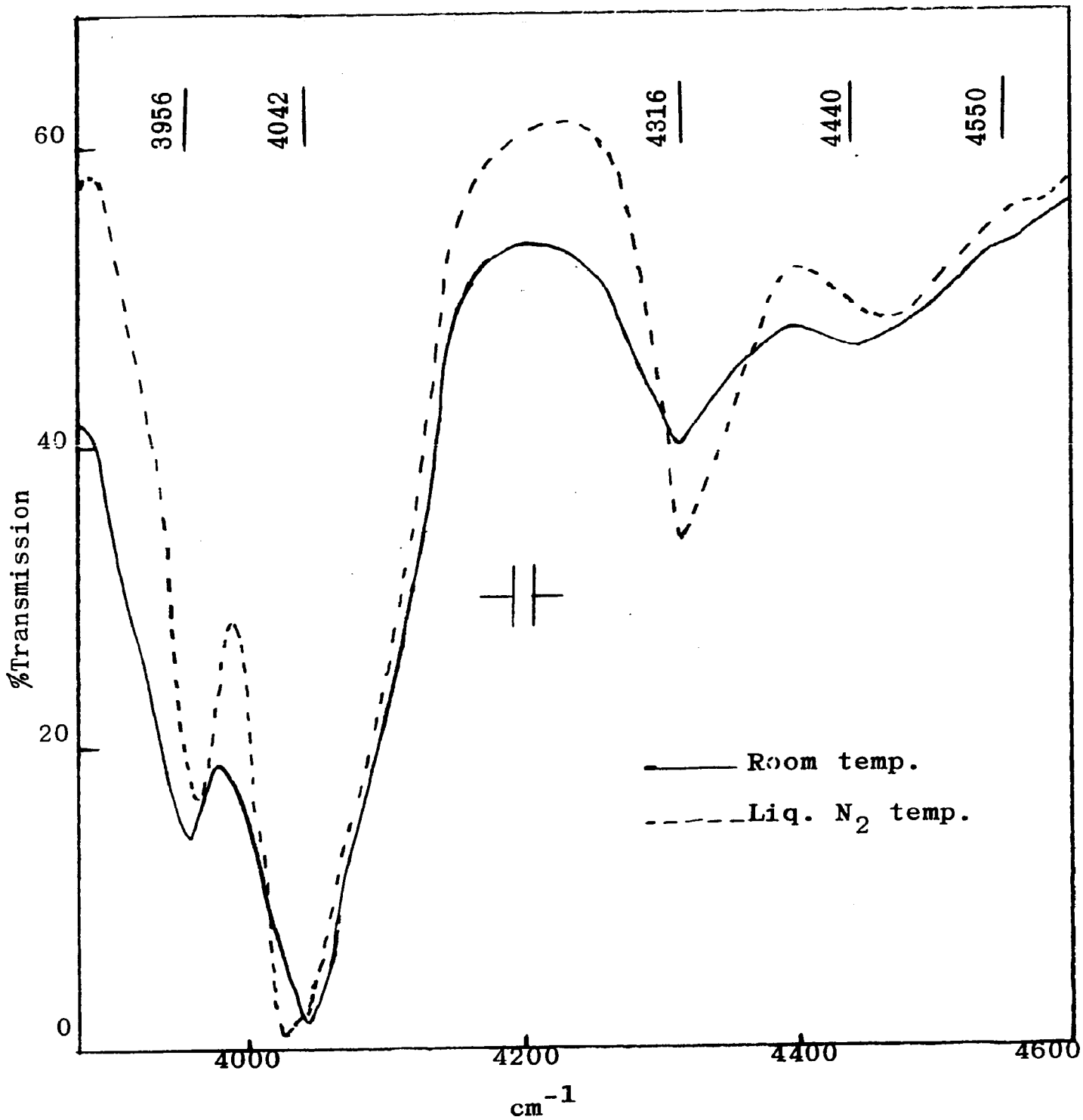


Figure 17. Transmission spectra of Brucite at two temperatures, from 3900 cm^{-1} to 4600 cm^{-1} (sample || to cleavage, 300μ)

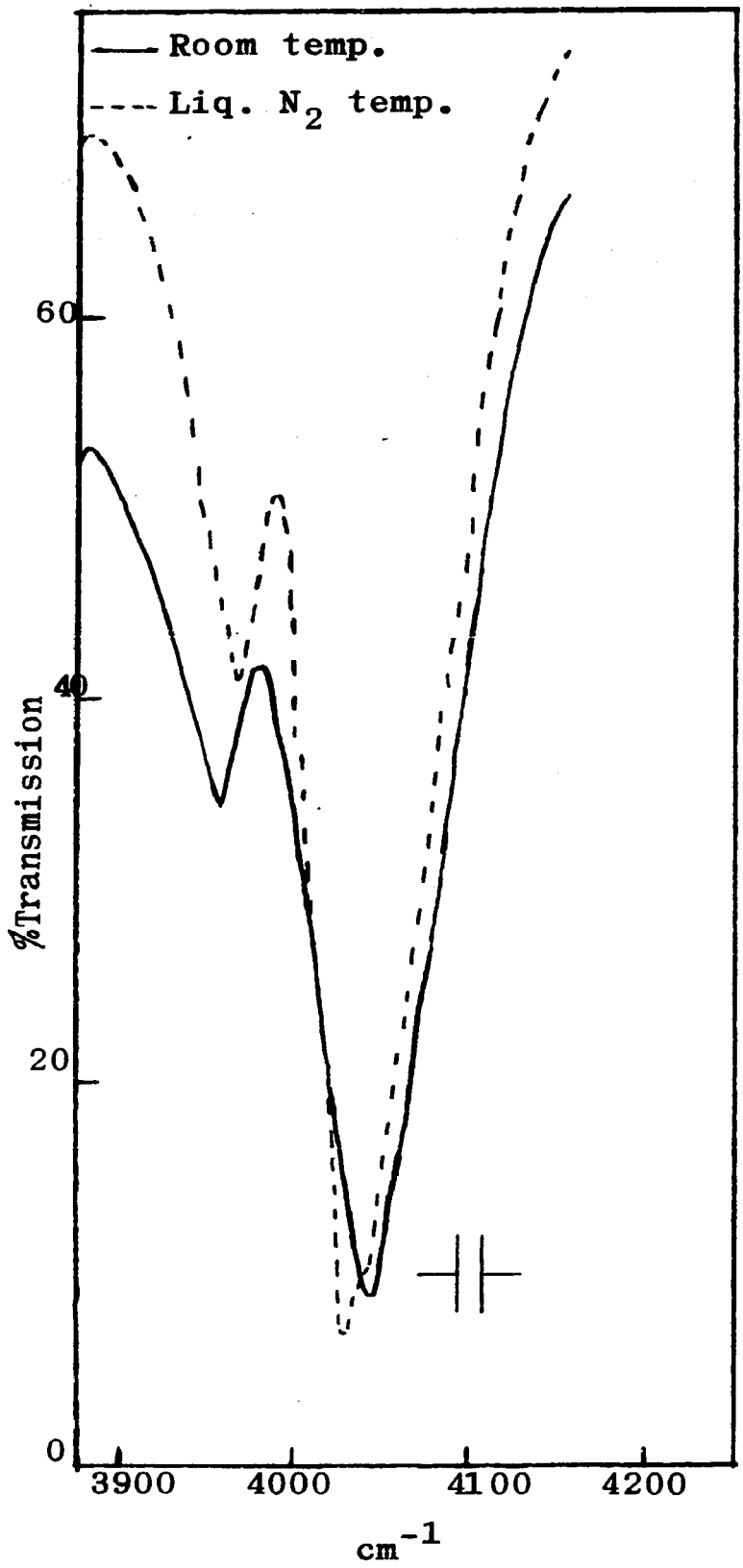


Figure 18. Transmission spectra of Brucite at two temperatures, from 3900 cm^{-1} to 4200 cm^{-1} (sample // to cleavage, 100 μ)

The spectra over the interval 4600 cm^{-1} to 5200 cm^{-1} at two temperatures are shown in Figure 19. A thick sample (750 μ) was used to obtain reasonable contrast in the region. A sharp band at 4710 cm^{-1} and a pair of shallow ones at 4865 cm^{-1} and 4985 cm^{-1} are observed. The low temperature sharpens all the bands, though the peak value of the intensity in the case of the strongest band has decreased very little. No shift in position of the bands could be detected.

As mentioned above, the interval from 3450 cm^{-1} to 3900 cm^{-1} has been scanned with a CaF_2 prism in a double beam spectrometer because this region is quite rich in atmospheric water vapor bands and the liquid air cell makes it difficult to pass dry nitrogen through the model 12C single beam spectrometer. A sample parallel to the cleavage and 100 μ thick was employed. The spectrum for this region is shown in Figure 20. Two almost equally strong and broad bands occur at 3530 cm^{-1} and 3790 cm^{-1}. A relatively weak band at 3703 cm^{-1} and an extremely weak band at 3655 cm^{-1} are also observed between the two strong ones. At liquid nitrogen temperature the 3530 cm^{-1} band almost disappears and the one at 3790 cm^{-1} is somewhat weakened. It is very difficult to determine the change in intensities of the weak bands at 3703 cm^{-1} and 3655 cm^{-1} because of the increase in general transparency of the crystal at low temperature. The best estimate appears to be that they are not altered appreciably. It should also be mentioned here that intensity measurements with the model 21 double beam spectrometer are not very

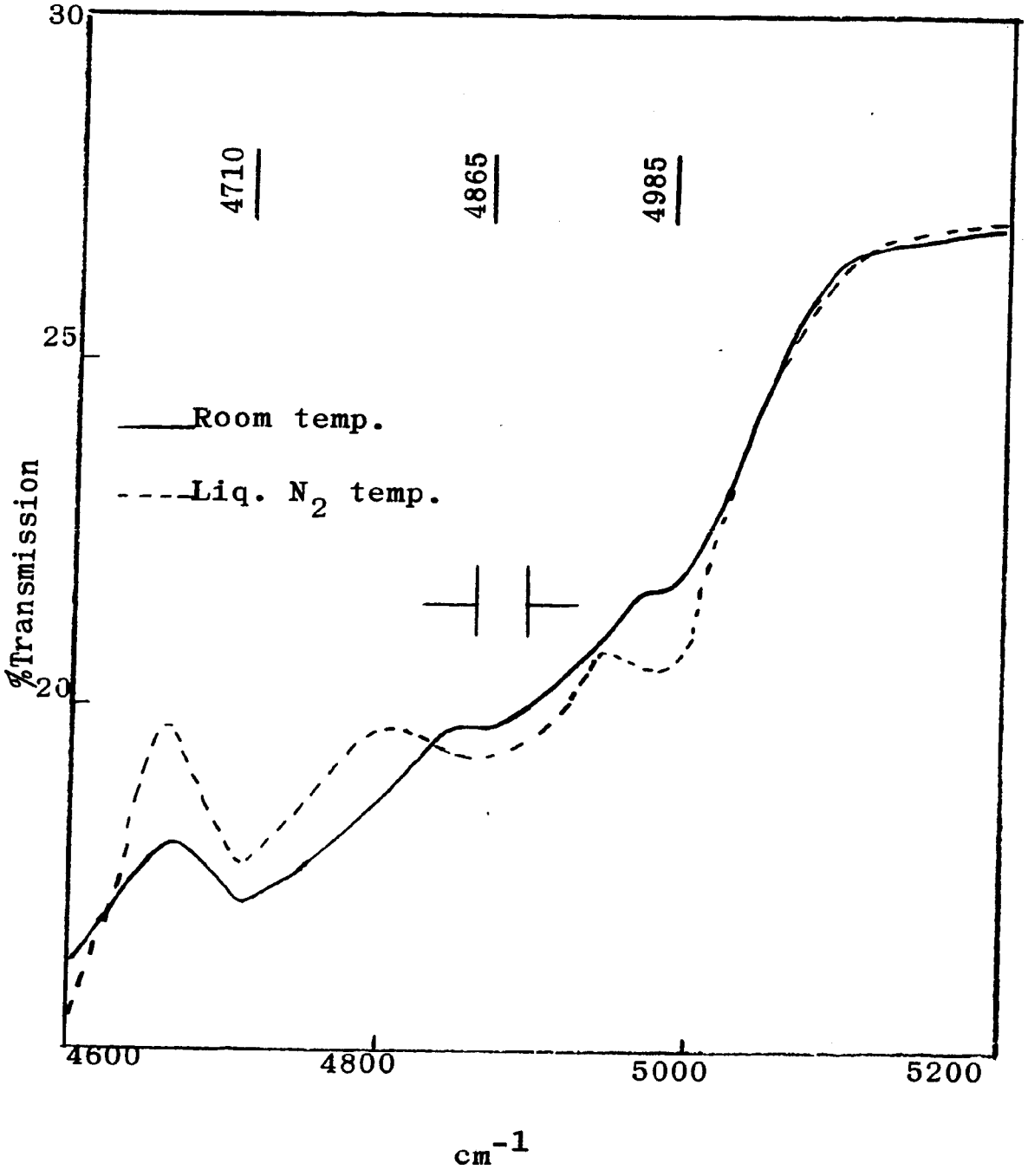


Figure 19. Transmission spectra of Brucite at two temperatures, from 4600 cm^{-1} to 5200 cm^{-1} (sample ∥ cleavage, 750 μ)

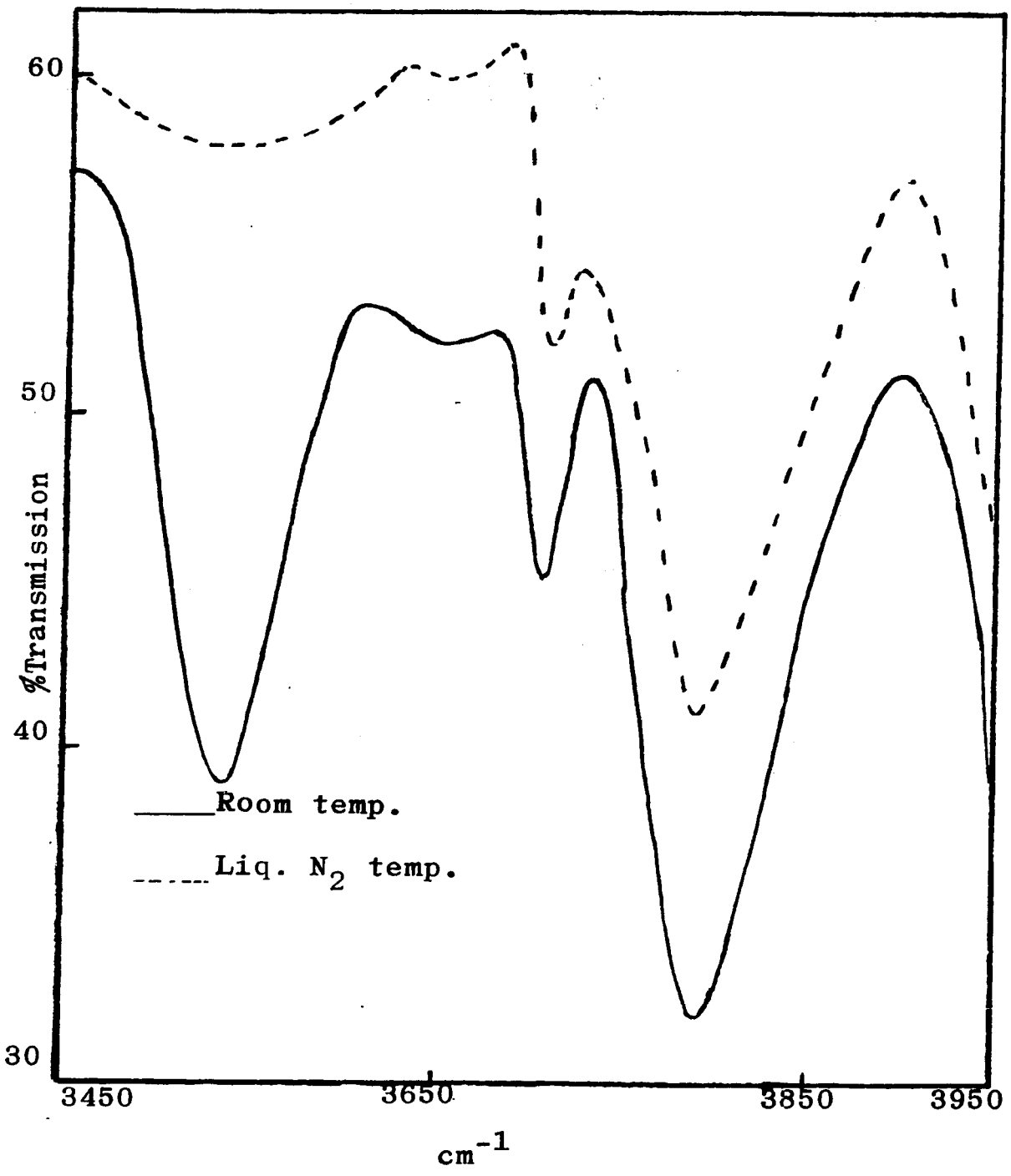


Figure 20. Transmission spectra of Brucite (sample ∥ to cleavage, 100μ) at two temperatures, from 3450 cm^{-1} to 3950 cm^{-1} (CaF_2)

accurate for very weak bands. A private communication from Mara and Sutherland shows that they also observed similar low temperature spectra in this region.

4.5b Polarized Transmission Spectra (2650 cm^{-1} to 5200 cm^{-1})

As expected, for a sample cut parallel to the (0001) plane, i.e., with the unique c-axis parallel to the incident beam, the spectrum was found to be independent of the direction of polarization of the electric field vector. However, the absorption of a section cut with its c-axis in the plane of the sample face was found to be extremely dependent upon the direction of polarization. In the interval between 1000 cm^{-1} and 2500 cm^{-1} no significant difference from Mara's data was detected. The frequencies of the several weak bands found there are given in Table 5 at the end of this chapter.

The polarized transmission spectra for a sample cut perpendicular to the cleavage plane are reported for the region from 2650 cm^{-1} to 5200 cm^{-1}. It should be recalled that the spectrum with the electric vector oriented perpendicular to the c-axis is equivalent to the unpolarized spectrum (section 4.5a) for a sample cut parallel to the cleavage plane (where the electric vectors are always normal to the c-axis).

The spectrum reported in Figure 21 covers the interval from 2650 cm^{-1} to 3150 cm^{-1} for a sample thickness of approximately 2 mm. The most notable feature of the spectrum is the complete dichroism of the two bands, one at 2700 cm^{-1} which is present only when the electric vector is parallel to the

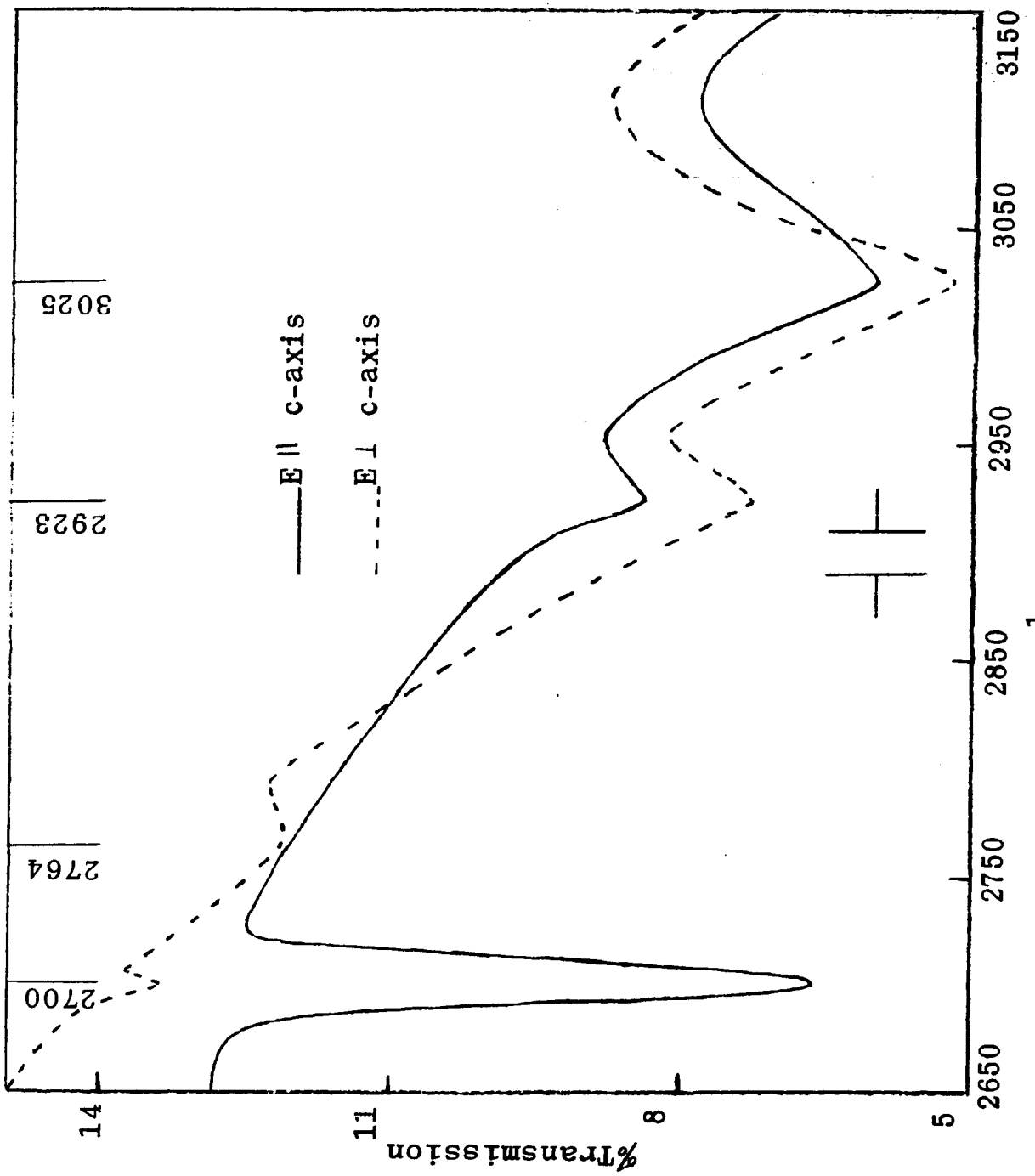


Figure 21. Polarized transmission spectra of Brucite, from 2650 cm^{-1} to 3150 cm-1 (sample 2mm)

c-axis of the crystal, whereas the other at 2764 cm^{-1} occur only with the field vector normal to the c-axis. The very weak peak at 2700 cm^{-1} remaining with the electric field perpendicular to the c-axis is probably due to the imperfections of the polarizer, since this peak is missing in the spectra in which the sample was cut parallel to the cleavage (Figure 15). The remaining two bands at 2923 cm^{-1} and 3025 cm^{-1} occur in both the polarizations.

In Figure 22 are shown the polarized spectra from 3150 cm^{-1} to 3900 cm^{-1} of a 300μ thick sample cut perpendicular to the cleavage plane. The band at 3220 cm^{-1} which is present only with the electric field parallel to the c-axis was not previously reported. The bands at 3249 cm^{-1} and 3330 cm^{-1} are also present only when the polarization is parallel, whereas the strong band at 3270 cm^{-1} is polarized normal to the c-axis. The 3368 cm^{-1} band is observed in both polarizations. As already mentioned in section 4.3, the crystal is completely opaque in the vicinity of 3650 cm^{-1} with light polarized parallel to the unique axis so that the dichroic property of the fairly strong band at 3534 cm^{-1} recorded with the electric vector set normal to the axis, could not be determined with certainity. In the same polarization a weak band occurs at 3650 cm^{-1} in agreement with the spectrum of the sample cut parallel to the cleavage. But no band is found at 3700 cm^{-1} in this polarization in contrast to the weak band observed here in the unpolarized spectrum with the c-axis parallel to the incident beam. The last band of this

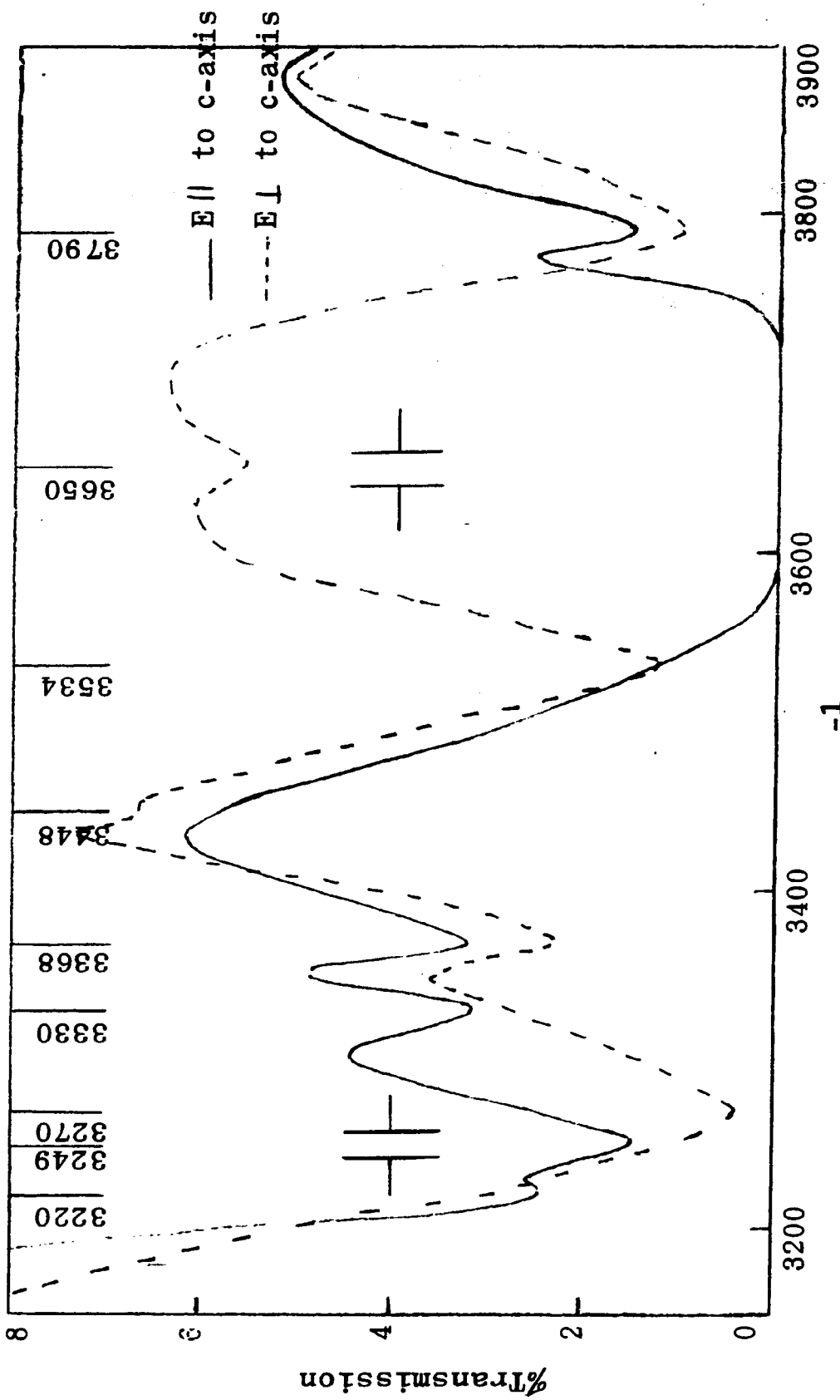


Figure 22. Polarized transmission spectra of Brucite, from 3150 cm^{-1} to 3900 cm^{-1} (sample 300 μ)

set at 3790 cm^{-1} is observed in both the polarizations, though it is stronger and broader with the electric vector perpendicular to the c-axis.

The transmission spectrum from 3900 cm^{-1} to 4600 cm^{-1} is presented in Figure 23. The strongest band in this region is at 4042 cm^{-1} and is polarized perpendicular to the c-axis. Two bands of about equal intensity at 4008 cm^{-1} and 4097 cm^{-1} observed with the electric field parallel to the c-axis are situated almost symmetrically around the strongest one. The band at 3956 cm^{-1} is observed in both the polarizations with equal intensity. The high frequency side of the spectrum consists of three bands present in both polarizations, at 4316 cm^{-1}, 4440 cm^{-1} and 4550 cm^{-1} with gradually diminishing absorption. But the first and last one of the triplet are stronger and the central one weaker in the parallel polarization than in the perpendicular.

The spectra of the same 300μ sample from 4600 cm^{-1} to 5200 cm^{-1} is shown in Figure 24. This region was not investigated previously with the higher resolution obtained with a LiF prism and therefore some finer details are evident in the present study. The parallel polarization give a single rather strong broad band at 4865 cm^{-1}, whereas three bands with gradually diminishing absorption are observed at 4710 cm^{-1}, 4865 cm^{-1} and 4985 cm^{-1} with the polarizer set normal to the c-axis. The last band is very shallow and its peak position is rather doubtful. As evident from the diagram, the central band at 4865 cm^{-1} is dichroic with stronger absorption

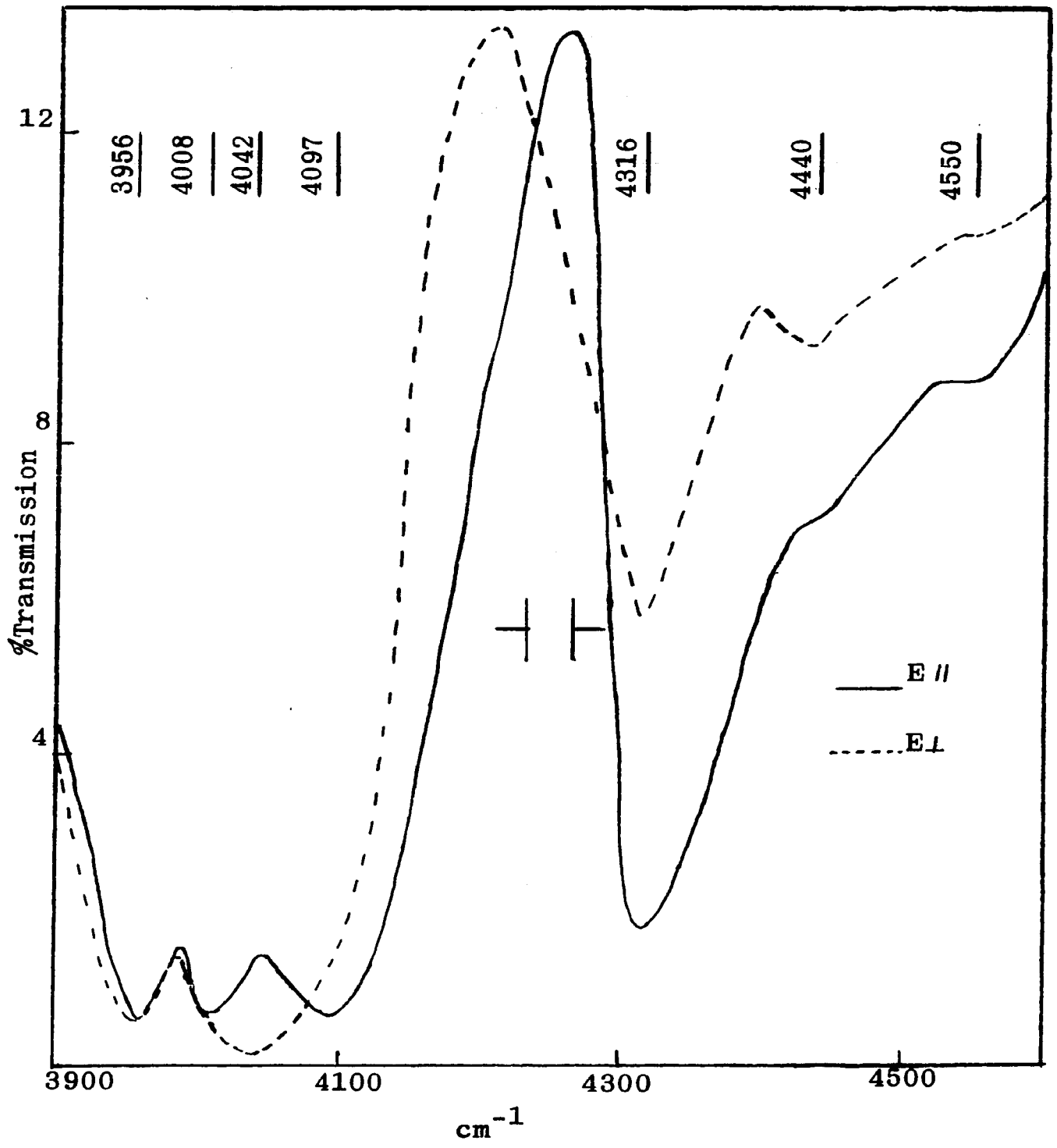


Figure 23. Polarized transmission spectra of Brucite, from 3900 cm^{-1} to 4600 cm^{-1} (sample 300μ)

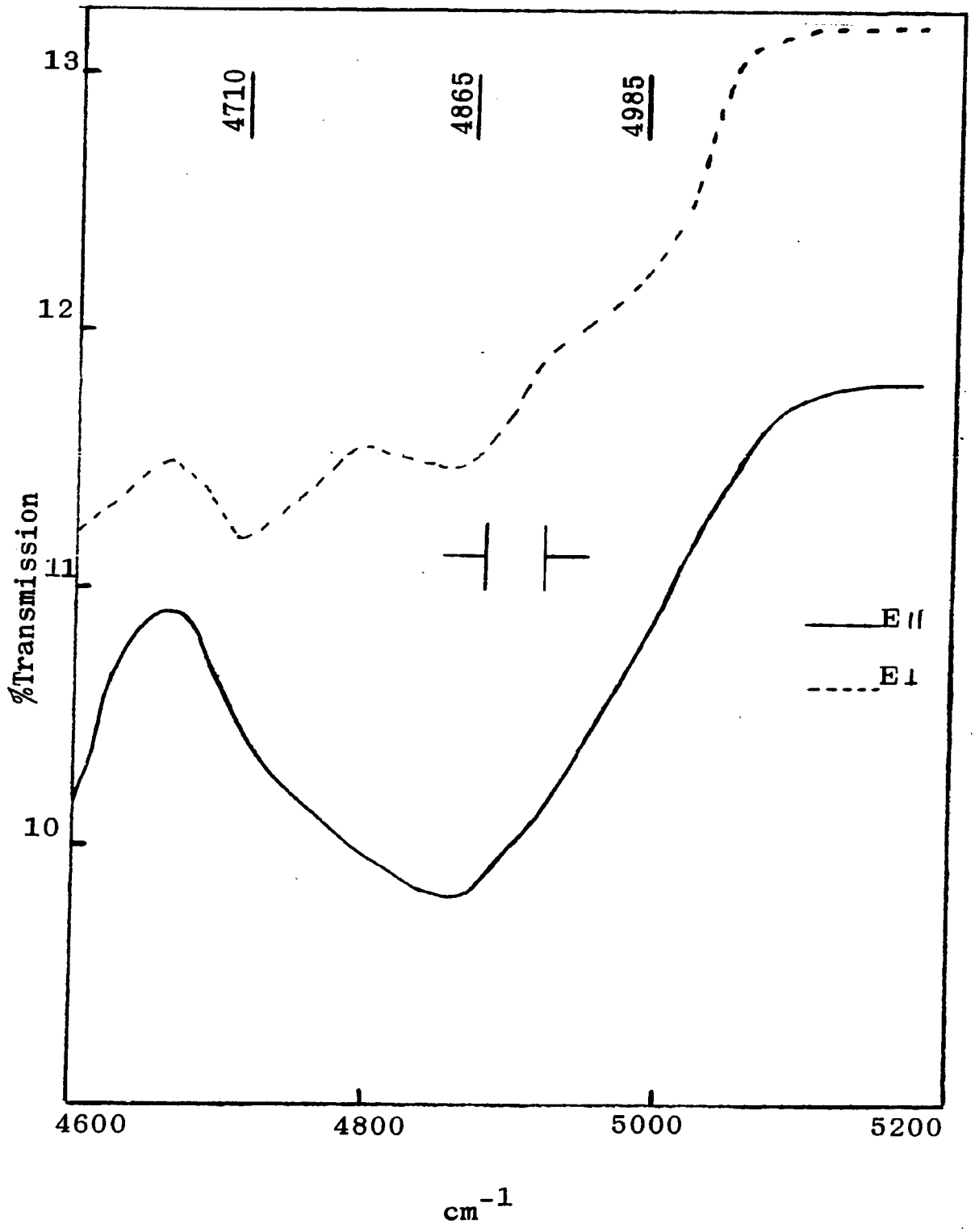


Figure 24. Polarized transmission spectra of Brucite, from 4600 cm-1 to 5200 cm-1 (sample 300 μ)

in the parallel polarization. It is the only band in this set that has been reported previously.

4.5c Transmission Spectra of Tilted Samples (3400 cm^{-1} to 3950 cm^{-1})

As reported in section 4.5b, for the region from 3550 cm^{-1} to 3750 cm^{-1} the thinnest available sample has satisfactory absorption values with the electric field perpendicular to the c-axis but is completely opaque for radiation polarized parallel to the c-axis. However, we know from the reflection and powder spectra that a very strong band occurs at 3700 cm^{-1} polarized parallel to the c-axis. No further information could be obtained from the data as to polarization and intensity of the relatively weak bands near 3700 cm^{-1}. But this information is available from transmission spectra of a thin sample cut parallel to the cleavage plane but tilted at an angle to the incident beam so that a component of the electric vector is parallel to the c-axis.

For a 100μ sample, such spectra are reported for three angles, 0°, 30° and 45° in Figure 25. At higher angles of incidence there is considerable reflection loss and the reported values of the optical density are not very accurate. The spectrum for 0°, i.e., for the c-axis parallel to the incident beam, is similar to the one reported in Figure 20. But as the tilting angle is increased the band at 3700 cm^{-1} becomes progressively more prominent — confirming our previous conclusion that this band is primarily polarized parallel to the c-axis. The small peak present at this position when the

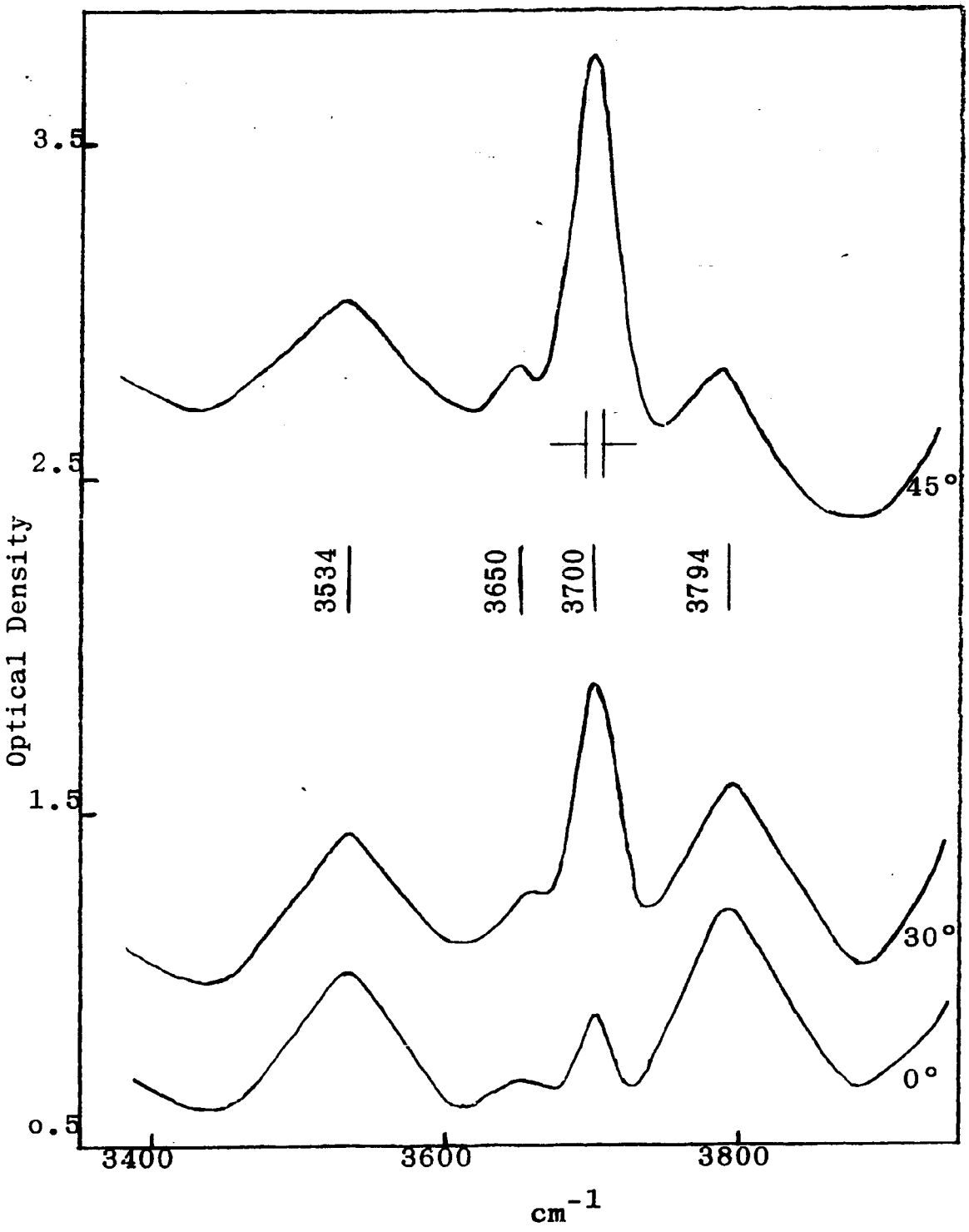


Figure 25. Transmission spectra of Brucite crystal with c-axis at 0°, 30° and 45° to incident beam, from 3400 cm^{-1} to 3900 cm^{-1} (100 μ thick)

c-axis is perpendicular to the incident electric vector may be attributed to the convergence of the incident beam and will be discussed in the next chapter. The two strong bands at 3534 cm^{-1} and 3794 cm^{-1} become progressively weaker with the increasing tilt-angle and one can conclude that these are primarily dichroic perpendicular to the c-axis. The very weak band near 3650 cm^{-1} does not change much with tilting.

The behavior of the 3700 cm^{-1} band at low temperature is presented in Figure 26. The same 100 μ sample cut parallel to the cleavage was used, and the liquid air cell was placed in such a way that the c-axis of the crystal made approximately an angle of 30° with the incident beam. Perkin-Elmer model 21 spectrometer with a CaF_2 prism was used. The tilted cell considerably reduced the available slit area. As compensation a partial obstruction was placed in the balancing path of the double beam instrument. For this reason no percent transmission values can be given in the figure. At room temperature the tilted sample presents a sharp strong band at 3702 cm^{-1} along with the very, very weak band at 3653 cm^{-1} and two moderately strong (though reduced in intensity due to the tilt) bands at 3530 cm^{-1} and 3790 cm^{-1}. The low temperature behavior of these three bands is reported in section 4.5a. The new strong band at 3702 cm^{-1}, however, remains at practically the same relative intensity at low temperature, though it is sharpened a little and shifted to 3707 cm^{-1}. The general background transparency of the crystal increases considerably as the temperature falls and thereby influences the

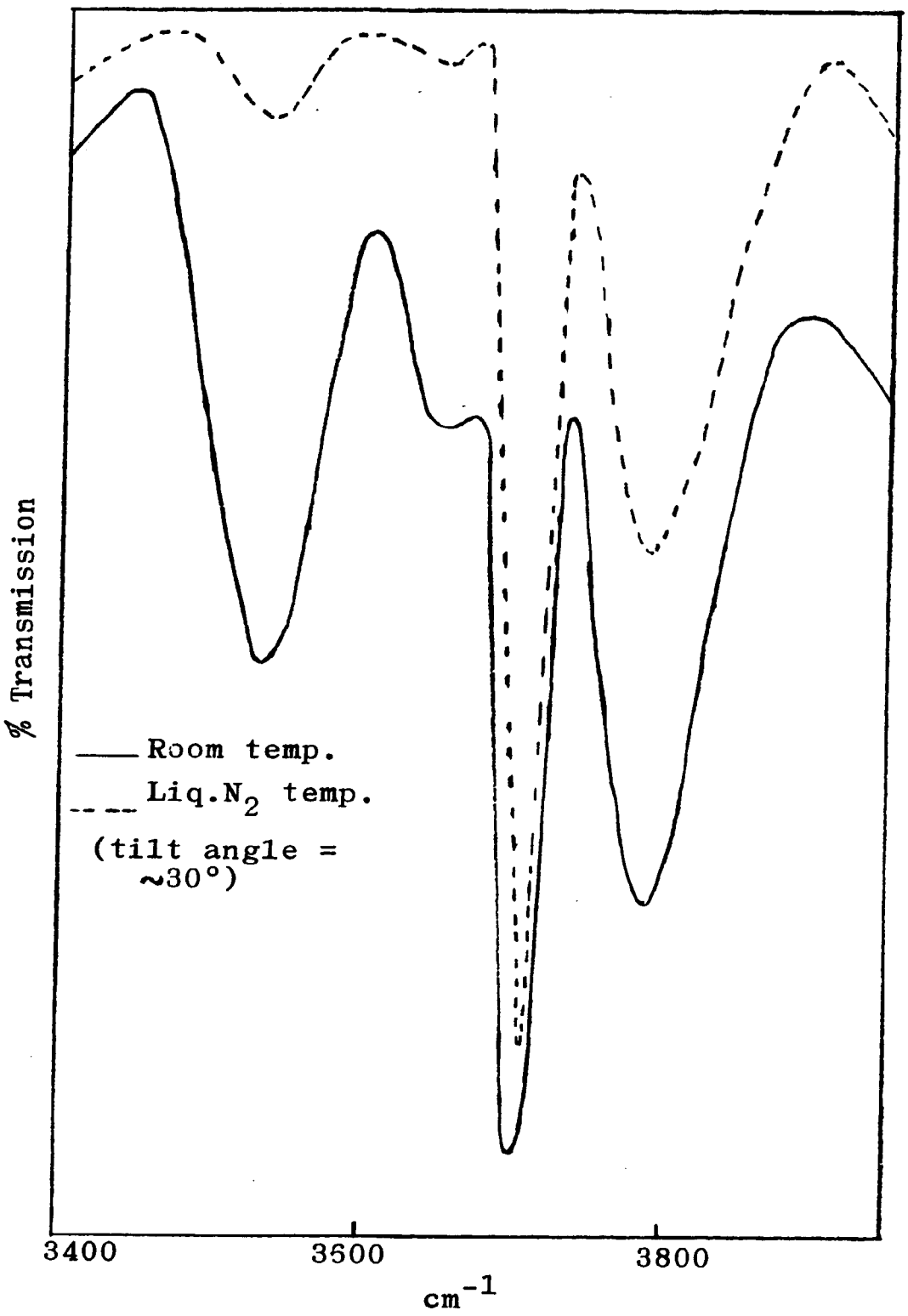


Figure 26. Spectra of a tilted sample (parallel to cleavage, 100 μ thick) at two temperatures from 3400 cm-1 to 3900 cm-1 (CaF_2)

peak value of the absorption.

4.5d Overtone Regions (6000 cm^{-1} to 11000 cm^{-1})

We have noticed that the strongest band in the OH stretching region of brucite occurs at 3700 cm^{-1}, along with a complex of weaker bands. The first overtone is expected around 7400 cm^{-1}. Yeou Ta[22] reported only one band in this region at 7142 cm^{-1} which appeared only when there was a component of the electric vector of the incident radiation parallel to the c-axis. Mara reported two bands, at 7520 cm^{-1} and 7300 cm^{-1}, both polarized parallel to the c-axis. In the present study an interval from 6000 cm^{-1} to 11000 cm^{-1} is covered, and in addition to an extensive group of bands in the first overtone region, a band has also been found in the second overtone region.

Because of the weak intensity of the overtone transitions, thick samples had to be used to record some of the bands. Figure 27 is a reproduction of the spectra in two orientations. Sample thicknesses were approximately 1.5 mm and 2.25 mm for faces parallel and perpendicualr to the cleavage plane, respectively. With the c-axis parallel to the incident beam one notices only a weak band at 7730 cm^{-1}. But with the c-axis normal to the incident beam one observes a cluster of bands in this vicinity with the strongest one at 7180 cm^{-1} and a single band at 10600 cm^{-1} in the second overtone region. On the low frequency side of the 7180 cm^{-1} band, only one weak band occurs at 6710 cm^{-1}. On the high frequency side,

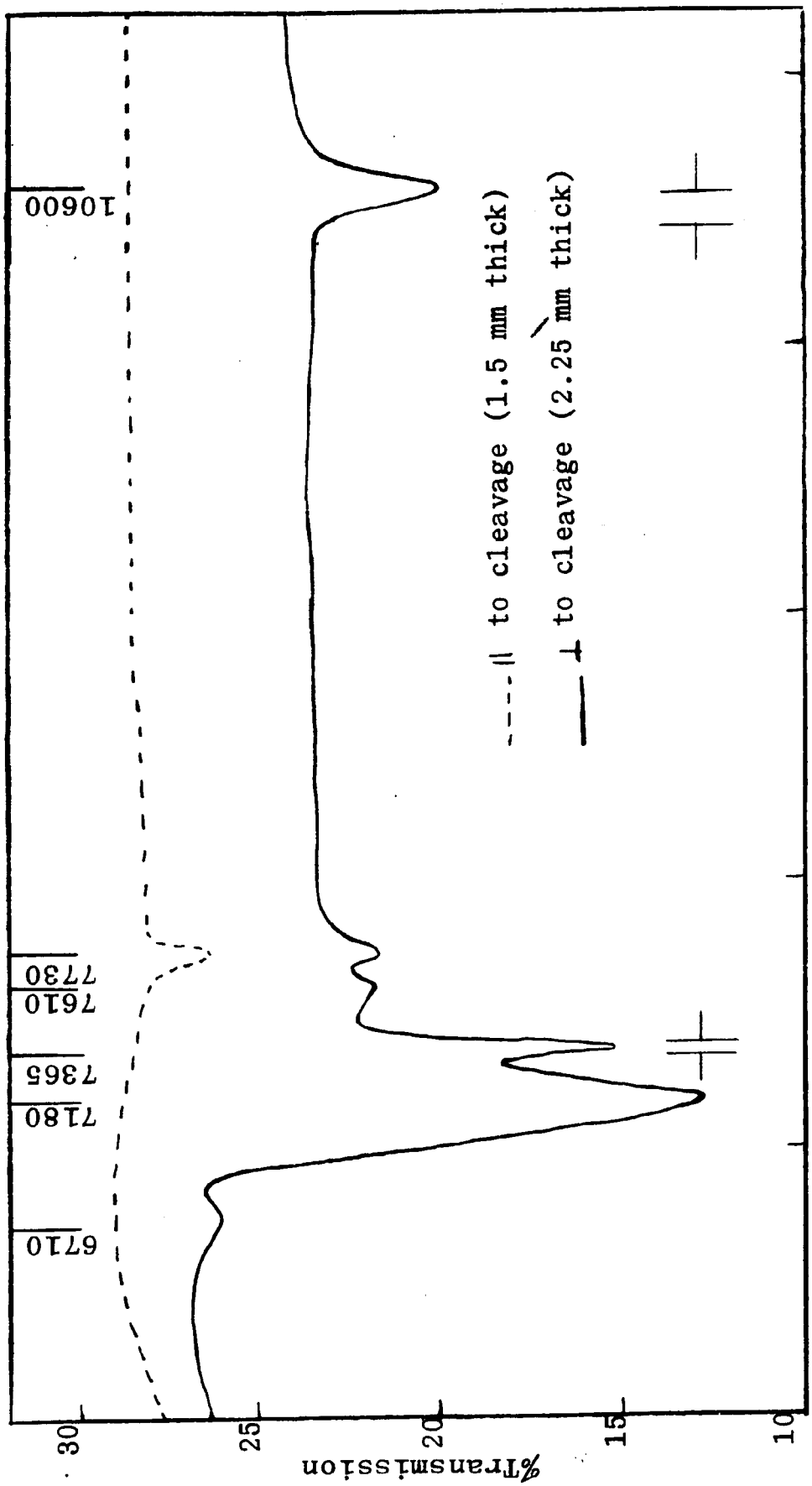


Figure 27. Transmission spectra of Brucite for two crystal orientations, from 6000 cm-1 to 11000 cm-1

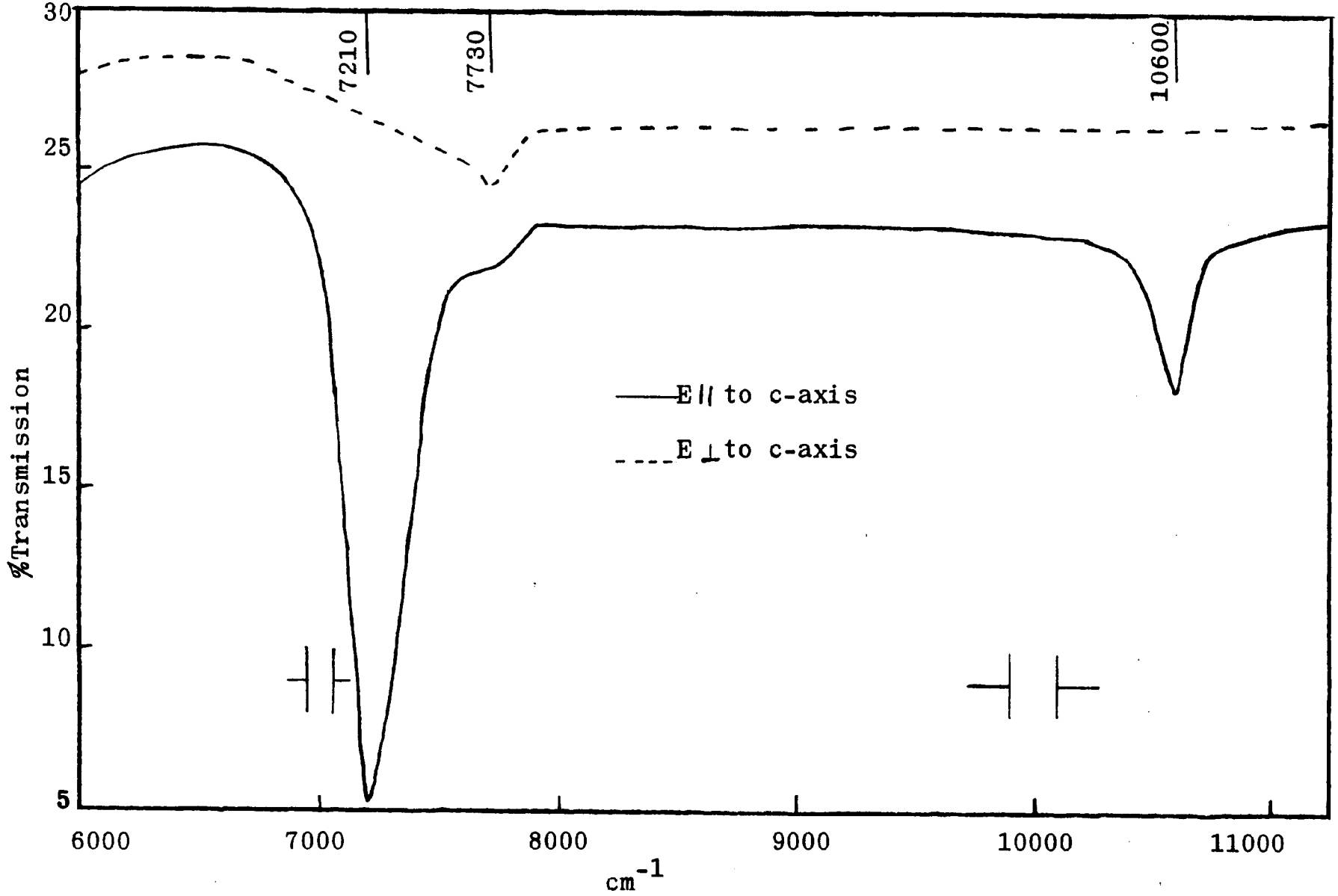


Figure 28. Polarized transmission spectra of Brucite, from 6000 cm^{-1} to 11000 cm^{-1} (sample 2.25 mm thick)

however, one well resolved band of medium intensity at 7365 cm^{-1} and two weaker ones at 7610 cm^{-1} and 7730 cm^{-1} are observed, the last one being common to both orientations.

A polarized spectrum is shown in Figure 28 for a sample cut perpendicular to the cleavage plane. The reduced resolution is a consequence of the wider slit necessary to compensate for the energy loss of the polarizer. The observed dichroism is consistent with the unpolarized spectra of the two crystal orientations of the previous figure, i.e., all of the bands except that at 7730 cm^{-1} are completely polarized parallel to the c-axis.

4.6 Summary

The spectrum of brucite has been reported over the entire region from 350 cm^{-1} to 11000 cm^{-1}. Since the thinnest available crystal samples cut both parallel and perpendicular to the (0001) plane are opaque in the interval 350 cm^{-1} to 800 cm^{-1}, that region has been investigated in reflection. A number of bands including a very broad, intense one at 515 cm^{-1} were found and their dichroic properties determined.

No new information has been gathered in the interval from 1000 cm^{-1} to 2600 cm^{-1}.

The region 2650 cm^{-1} to 5200 cm^{-1} has been studied in great detail and twenty-four bands resolved. The strongest band in this region occurs at 3700 cm^{-1} polarized parallel to the c-axis. The strength of the band renders the thinnest crystal specimen opaque, but its position has been evaluated from reflectivity measurements, from which the extinction

coefficient was also calculated. The frequency of this band was confirmed from an absorption spectrum of a thinly spread powder. A crystal sample parallel to the cleavage plane, but tilted so that its c-axis is inclined at an angle to the incident beam, shows the same absorption frequency.

Detailed powder spectra of chemically prepared $Mg(OH)_2$ and $Mg(OD)_2$ have also been obtained. Frequencies and relative intensities of the absorption bands are given in Table 4. Ratios of the frequencies of corresponding $Mg(OH)_2$ and $Mg(OD)_2$ bands are also given there, and the values are close to 1.37.

Low temperature spectra at the liquid nitrogen point have been obtained for the entire region using the relatively high resolution available with LiF and CaF_2 prisms for the orientation parallel to the cleavage plane. The temperature dependence of the strong 3700 cm^{-1} band has also been studied by the tilt method. It has been observed that almost all the bands on the low frequency side of the 3700 cm^{-1} band decrease considerably in intensity at the liquid nitrogen point. On the other hand, the 3700 cm^{-1} band and most of the bands on its high frequency side either gain strength or remain unchanged. The dichroism of all twenty-four bands has also been studied using samples of different thickness cut normal to the cleavage plane.

In the overtone region (6000 cm^{-1} to 11000 cm^{-1}), a number of bands have been located: a group of them around 7200 cm^{-1} and a single one at 10600 cm^{-1}. The strongest one of the first overtone group and the single line in the second

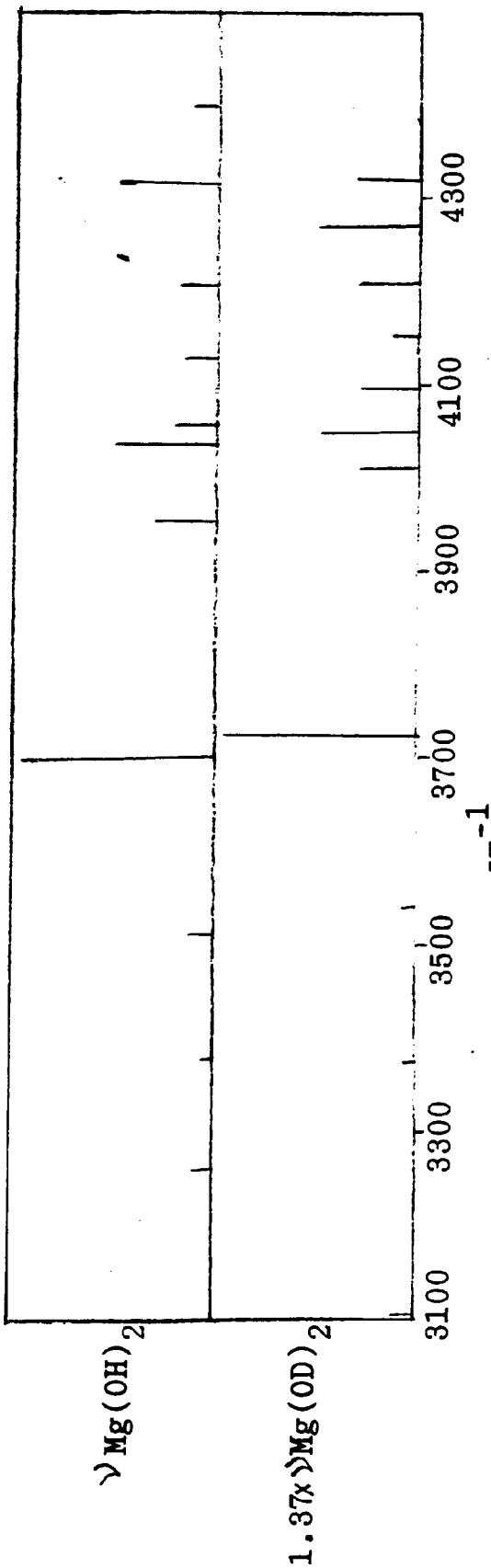


Figure 29a. Powder spectra of Brucite and $Mg(OD)_2$

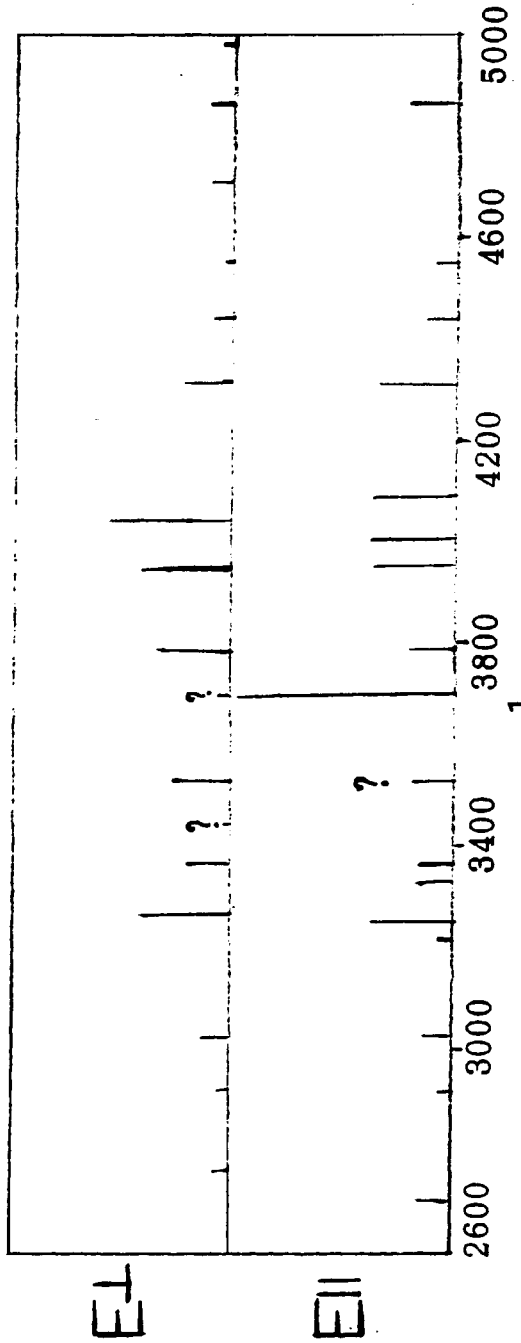


Figure 29b. Polarized transmission spectra of Brucite (2600 cm^{-1} to 5000 cm-1)

overtone region are both polarized parallel to the c-axis.

The Raman spectrum of brucite was taken and lines were observed with frequency shifts of 445 cm^{-1} and 3655 cm^{-1}.

All the infrared and Raman bands of brucite thus far observed are listed in Table 5 and some are shown in Figure 29. The relative intensities, polarizations and temperature effects are also included for the infrared bands.

TABLE 5

LIST OF INFRARED AND RAMAN BANDS OF BRUCITE

Infrared						
E‖		E⊥				
$\nu(cm^{-1})$	Int.	$\nu(cm^{-1})$	Int.	temp. effect	$\Delta\nu cm^{-1}$	Remarks
		*415N	W			
*515	V.S.	*515	V.S.			In reflection
*640P	M.W.					
		*700N	M			
1010		1010				
1205		1205				
1385		1385				
1412		1412				
1600P		1600				
2000		2000				

In transmission. Mostly very weak bands but hard to distinguish because of the high background opacity continued beyond 800 cm^{-1}.

TABLE 5 (con't)

E∥ ν (cm^{-1})	Int.	E⊥ ν (cm^{-1})	Int.	temp. effect	$\Delta\nu$ cm^{-1}	Remarks
2700P	S					
		*2764N	W	vanish		In transmission
2923	W	2923	W	D		
3025	M	3025	M	vanish		
*3220P	V.W.					
3249P	M.S.					
		3270N	S	vanish		
3330P	M					In transmission
3368	M	3368	M	vanish		
		*3448(?)N	V.V.W.	vanish		
3534(?)		3534N	M.S.	D		In transmission
		*3650 (?)	V.W.	Nil		
*3700P	V.V.S.	3700 (?)				

TABLE 5 (con't)

E‖ ν (cm^{-1})	Int.	E⊥ ν (cm^{-1})	Int.	temp. effect	$\Delta\nu$ cm^{-1}	Remarks
3790	M	3790N	M.S.	D		
3956	M.S.	3956	M.S.	I	-10	
4008P	M.S.					
		4042N	S	I	16	
4097P	M.S.					
4316P	M.S.	4316	M	I		
4440	V.W.	4440N	M.W.	I	-20	In transmission
4550P	V.W.	4550	V.V.W.	I	-25(?)	
		*4710	W	I		
4865P	M.W.	4865	W	I		
		*4985N	V.W.	I		

*6710P	W
*7180P	S
*7365P	M
*7610P	W

TABLE 5 (con't)

E∥ $\nu(cm^{-1})$	Int.	$\nu(cm^{-1})$	Int.	temp. effect	E⊥ $\Delta\nu cm^{-1}$	Remarks
*7730	W	*7730N	M.W.			
*10600P	M					In transmission

Raman νcm^{-1}
*3655
*445

Symbols:--

* = Bands discovered in the present investigation

P = Parallel dichroism

N = Perpendicular dichroism

$\Delta\nu$ = ν(Room temp.) - ν(Liquid N_2 temp.)

I = Increases in relative intensity at low temperature

D = Decreases in relative intensity at low temperature

Vanish = Band vanishes at liquid nitrogen point

Nil = No change in relative intensity at low temperature.
Relative intensities are for the bands of a particular group.

CHAPTER 5

ASSIGNMENTS AND DISCUSSION

5.1 OH Stretching Modes

The diatomic hydroxyl ion has only one stretching mode, but since two OH ions are in each unit cell of brucite, there exist two OH stretching fundamentals in the crystal. This was pointed out in Chapter 2 where the symmetry classification of the normal modes of vibration and the selection rules for the fundamentals were worked out. Since the unit cell contains a center of symmetry, the symmetric stretching mode (A_{1g}) is Raman active and forbidden in infrared, while the antisymmetric stretching mode (A_{2u}) is infrared active, polarized parallel to the c-axis of the crystal, and is not permitted in Raman scattering.

The vibration frequency (ω_o) of a free OH radical[15] is 3652.4 cm^{-1}. If there is no hydrogen bonding in the crystal both the symmetric and antisymmetric vibration frequencies are expected to occur at nearly the same value, namely, 3652 cm^{-1}, as is the case in the vapor spectra of all molecules containing OH groups. The structural evidence on brucite (Chapter 1) indicates the absence of any appreciable hydrogen

bonding. In the OH stretching region the observed Raman spectrum shows only one line at 3655 cm^{-1}, and this must be assigned to the A_{1g} mode.

In the infrared spectrum the assignment of the A_{2u} mode in the OH stretching region is hampered by the multitude of absorption bands there. However, one expects the A_{2u} mode to give rise to very strong absorption. The reflection spectrum of brucite shows that one band, at 3700 cm^{-1}, overwhelmingly dominates the others in strength. Furthermore, the polarization of the band is parallel to the c-axis. Hence, this band may be assigned to the A_{2u} mode with assurance. The powder spectra and the spectra of tilted samples have all confirmed this view. In the powder spectra of $Mg(OD)_2$ the corresponding band at 2721 cm^{-1} is also much stronger than the rest.

The assignment of the 3655 cm^{-1} and 3700 cm^{-1} bands as the symmetric and antisymmetric OH stretching modes rules out the possibility of the existence of any hydrogen bonding among the hydroxyl ions because in hydrogen bonded crystals these vibrations occur at much lower frequencies. Moreover, it is known that the OH stretching frequencies of hydrogen bonded substances are temperature dependent and shift considerably towards lower frequencies at the liquid nitrogen temperature. The spectrum of ordinary ice[40] is an example. In the present case the frequency and the intensity of the 3700 cm^{-1} band are not temperature dependent. If there is any shift at all at low temperature, it seems to be rather towards

higher frequencies. Hence it can be concluded that the present spectroscopic evidence is in complete agreement with other crystallographic evidence regarding the absence of any hydrogen bonding among the OH radicals.

There are two small discrepancies with the assignment of A_{2u}. These are: 1) the weak peak observed at 3700 cm^{-1} with a sample cut parallel to the cleavage plane and 2) the very weak band at 3650 cm^{-1} observed in infrared. We have seen from the factor group analysis that the OH stretching vibration should be completely dichroic, polarized parallel to the c-axis. For a sample cut parallel to the cleavage plane with the c-axis in the direction of the incident beam the electric field vector is always normal to the c-axis, and hence the band should not have been observed at all in this orientation. The most plausible explanation for its occurrence seems to be the effect of convergence of the incident beam. For very strongly absorbing modes with their changing dipole moment vectors oriented normal to the crystal face the otherwise forbidden vibrations might become active in convergent radiation, as has been shown by Wood and Mitra[44]. For microspectroscopic investigations, where the marginal rays are generally at an angle of 45° (N.A. 0.71) to the central one, this effect is quite pronounced. But even for ordinary commercial macro-spectrometers where the semi-angle of convergence never exceeds 7°, this effect might be large enough to make this band weakly observable in this orientation. For the allowed absorption (E parallel to the c-axis) a sample of brucite, 100μ thick, will transmit

only 10^{-100}% of the incident radiation at the frequency of maximum absorption. The band is indeed very very strong. As a confirmation of this view another piece of experimental evidence may be cited. Though this band occurs in the unpolarized spectrum of the (0001) face (c-axis parallel to the incident beam), it is completely absent in the polarized spectrum with the electric vector perpendicular to the c-axis, in accordance with the fact that the convergence should not have any effect in this case because even for the marginal rays the electric vector is still normal to the c-axis.

The low temperature spectrum of the face parallel to the cleavage plane in this region (Figure 20) gives the impression that the weak band at 3700 cm^{-1} has become even weaker at the liquid nitrogen temperature. However, if the occurrence of this forbidden band is explained by convergence of the incident beam its intensity should increase or remain unchanged as it does in the allowed orientation. But as already mentioned (Section 4.5a) the tremendous increase in background transparency at the liquid nitrogen point, and the abrupt change in intensity due to the beginning of the strong band at 3790 cm^{-1} may be responsible for this apparent weakening of the band and the relative intensity has probably remained stationary or even increased.

Since the crystal has a center of symmetry it is expected that the symmetric (g) OH stretching vibration should be completely forbidden in the infrared. Therefore even the very very low intensity in the infrared of the 3655 cm^{-1} band

(which is relatively quite strong in Raman and has been assigned as the A_{1g} mode) is rather embarrassing. However. this is the region very rich in atmospheric water vapor bands and although these have been reduced by passing dry nitrogen through the single beam spectrometer, it was not possible to suppress them completely. The compensation in the double beam spectrometer was not complete either. Hence small variations in the sample and background runs occurred, so that this very weak band at 3650 cm^{-1} in the infrared probably is due to the 3651 cm^{-1} band of water vapor.

5.2 Overtones of the OH Fundamentals

It has been found that the factor group selection rules are generally obeyed by combination and overtone transitions also, and they provide a successful guide for their classification.

The pure overtones of the OH fundamentals will be discussed in this section. They are fortunately non-degenerate vibrations (A_{1g} and A_{2u} only). The selction rules for combination and overtones of these modes for the factor group of brucite, D_{3d}, can be readily obtained from the character table (Table 3). The results for binary and ternary combinations are given below:

$$A_{1g} \cdot A_{1g} = A_{1g}$$
$$A_{1g} \cdot A_{2u} = A_{2u}$$
$$A_{2u} \cdot A_{2u} = A_{1g}$$

$$A_{1g} \cdot A_{1g} \cdot A_{1g} = A_{1g}$$
$$A_{1g} \cdot A_{1g} \cdot A_{2u} = A_{2u}$$
$$A_{1g} \cdot A_{2u} \cdot A_{2u} = A_{1g}$$
$$A_{2u} \cdot A_{2u} \cdot A_{2u} = A_{2u}$$

Since no Raman line has been observed in the overtone regions the present discussion is confined to the infrared bands. In the first overtone, i.e., in binary combination, only one band (A_{2u}) is allowed in the infrared and should be polarized parallel to the c-axis. But as in the fundamental OH stretching region, here also, quite a number of bands are observed. The strongest band occurs at 7180 cm^{-1} and is completely dichroic, with polarization parallel to the c-axis. This band can be assigned to $\nu_g(A_{1g}) + \nu_u(A_{2u})$.

In the second overtone region two combinations are infrared active. These are $2\ \nu_g(A_{1g}) + \nu_u(A_{2u})$ and $3\ \nu_u(A_{2u})$, both polarized parallel to the c-axis. Only one band has been observed, at 10600 cm^{-1}, with the electric vector oriented parallel to the c-axis. Since the extent of anharmonicity is not known, the band can be assigned to either of the two possibilities. From the frequencies of the fundamentals the former seems to be a little more probable. It is also quite possible that both of them are present and the resolution in the region is insufficient to separate them.

5.3 External (Lattice) Fundamentals

The frequencies of the external modes of oscillation, i.e., those arising from the vibration of hydroxyl radicals

as composite units against the magnesium ions and also the restricted rotations of the OH ions around their respective centers of gravities, will be much lower than those of the OH stretching vibrations previously discussed. Since the unit cell of brucite contains only two OH ions and one Mg ion there are only a few external modes, and the spectrum is expected to be quite simple. From the factor group analysis presented in Chapter 2, it is known that among the rotatory lattice modes there are two doubly degenerate vibrations. The symmetric mode (E_g) is permitted only in the Raman effect while the antisymmetric (E_u) mode is permitted only in the infrared. The latter should be polarized perpendicular to the c-axis. The translatory lattice modes are distributed among two non-degenerate vibrations (A_{1g} and A_{2u}) along the c-axis and two doubly degenerate (E_g and E_u) ones perpendicular to it. A_{1g} and E_g are only allowed in Raman scattering, while A_{2u} and E_u are only allowed in infrared. These vibrations are shown schematically in Figure 2.

In ionic crystals the translatory lattice vibrations are so strong that, except for extremely thin samples (tenths of a micron), they are practically opaque. Correspondingly, their reflectivity is very large (up to 95%) at such frequencies[45], and leads to reststrahlen phenomenon. It has been observed in Section 4.3a that the thinnest available samples of brucite are opaque below 1000 cm^{-1} so that they were examined by the reflection method. Since bructie is a semi-ionic crystal, we expect quite a strong reflection band, though not

as strong as in the alkali halides. The maximum reflective power goes up to 75%, and the band is quite broad and is typical of a reststrahlen band. The band occurs at about 515 cm^{-1} and is present in both polarizations. Therefore, it seems most probable that both the A_{2u} and E_u translatory lattice modes are excited at nearly the same frequency. It may be mentioned here that in MgO crystals[46] the reststrahlen frequency occurs near 570 cm^{-1}.

A completely dichroic, weak band, polarized perpendicular to the c-axis, occurs at 415 cm^{-1} on the low frequency side of this high reflectivity region. In the Raman spectrum only one line has been recorded in this region at 445 cm^{-1}. And, if we remember the general empirical rule[29] that rotatory lattice vibrations give rise to very strong Raman lines while the traslatory type gives rise to weak ones, one may tentatively assign this 445 cm^{-1} Raman band to the E_g OH libration mode. The infrared band, at 415 cm^{-1}, may be assigned to the E_u mode, since it has the correct polarization and also a frequency near to that of the E_g mode. It should be borne in mind that these assignments for the rotatory type of external oscillations are somewhat speculative. For a sound assignment one needs additional data. Spectra of $Mg(OD)_2$ would be especially useful; but are unfortunately quite difficult to obtain from the powder samples in this region. It may not be out of place to mention that Hexter and Dows[26] in their discussion of low frequency librations in vibration spectra of molecular crystals have predicted a frequency of 400 cm^{-1} for the doubly

degenerate libration frequency of the OH ions in brucite.

Since all of the external modes, expected from a unit cell group analysis, have been tentatively assigned, the other two bands at 640 cm^{-1} and 700 cm^{-1} observed in the reflection spectra must arise from combinations of the factor group lattice fundamentals described above with some inter-unit cell modes.

The weak bands between 1000 cm^{-1} and 2000 cm^{-1} could be assigned as combinations of the lattice modes as far as the numerical values of the frequencies are concerned, but since accurate polarization properties could not be obtained for these, no specific assignment has been made.

The frequencies reported in this section have all, save the Raman line, been obtained from the peak values of reflection measurement, and no attempt has been made to transform them to extinction coefficient values, because it was feared that while doing so some of the finer details of the spectra might have been lost. However, it is known empirically that the difference in the positions of the reflection maximum and the extinction coefficient maxiumum decreases with the frequency and increases with the intensity of the band; but even in the most severe cases it has been observed[47] that this difference has always been within 10 cm^{-1} to 25 cm^{-1}. In the present case the reflection maxima are quite strong, but as they are in the low frequency region of the spectrum, it is expected that the positions reported here are not far from the maxima of the extinction coefficient.

5.4 Complex Structure of the Absorption Spectra in the OH Stretching Region

5.4a Introduction

A factor group analysis based on the known structure of brucite has provided the symmetry classification and selection rules for the fundamental modes of vibration. Of the two OH stretching fundamentals predicted, only one is infrared active and must be assigned to the strongest band in the near infrared, at 3700 cm^{-1}. The numerous other absorption bands near 3700 cm^{-1} must therefore be due to some sort of combination spectrum since no other fundamentals should lie in the OH stretching region. Because of their relatively weak intensities, it seems reasonable that these frequencies become active only through some higher order effect. For example, if a sample of suitable thickness (0.5 μ) were available for satisfactory transmission spectra of the 3700 cm^{-1} fundamental, the complex series of lines near 3700 cm^{-1} would be too weak to be observed.

If the complex structure in the OH stretching region is owed to some sort of combination with the stretching fundamental, the combining frequencies (ν_L) must be either translatory lattice modes or librations (hindered rotation of the hydroxyl ion about its center of gravity). The notion that these bands are due to such combinations is also indicated by the temperature dependence of their intensities. All bands with frequencies smaller than 3700 cm^{-1} decrease markedly in intensity as the temperature is reduced, indicating

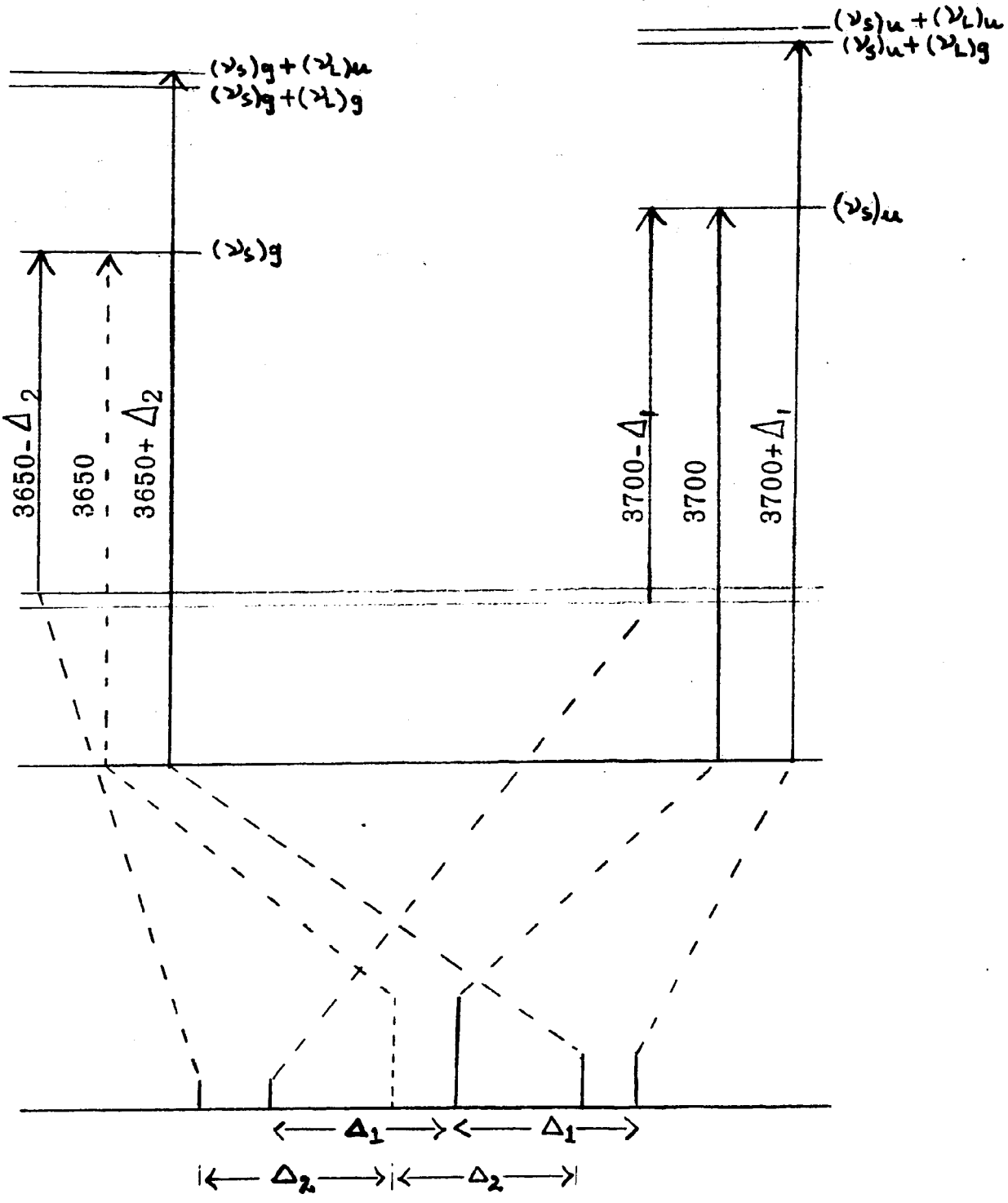


Figure 30. Infrared active sum and difference bands

that they originate from excited states and therefore are difference bands. On the other hand, bands lying above 3700 cm^{-1} change very little with temperature as would be expected for sum bands having the ground state as their origin.

The complex structure near 3700 cm^{-1} can be explained as combination spectrum, only if there corresponds to each difference band a sum band of like polarization, though the total number of sum bands may be larger than the number of difference bands because the latter die out rapidly in intensity. However, in forming the sums and differences it must be remembered that there are two OH stretching modes, at 3700 cm^{-1} (A_{2u}) and 3655 cm^{-1} (A_{1g}), and even though only one of these is infrared active by itself, both of them can give rise to infrared active bands in combination with lattice or librational modes, as indicated in Figure 30*. Table 6 shows the separation of the difference and sum bands from 3700 cm^{-1} and 3655 cm^{-1} fundamentals. To within the range of experimental error, there is a sum band for every difference band (letters a, b, c etc. show the presumed correspondence). Because of stretching — L (libration or lattice) interactions the spacing of the L levels above the first excited state of either the 3655 cm^{-1} or 3700 cm^{-1} vibration will be slightly

---

*There are in the crystal really an infinite number of OH stretching modes for which the vibrations of OH ions in successive unit cells are out of phase by a certain amount. Each one of these becomes active in combination with a librational mode with a corresponding compensating phase difference. But generally it is sufficient to consider a single unit cell because the interaction between two OH ions within a unit cell is much greater than that between the OH ions in neighboring unit cells.

TABLE 6

CORRESPONDENCE OF THE SUM AND DIFFERENCE BANDS

	sum bands			difference bands	
ν	ν-3655	ν-3700	ν	3655-ν	3700-ν
$\vec{E}$ parallel to c-axis					
3790	135a	90	3534	121a	166
3956	301b	256	3368	287b	332
4008P	353c	308	3330P	325c	370g
4097P	442d	397g	3249P	406d	451
4316P	661e	616	3220P	435d(?)	480
4440	785	740h	3025	630e	675
4550P	895f	850	2923	732	777h
			2700P	955f(?)	1000
$\vec{E}$ perpendicular to c-axis					
3790N	135i	90	3534N	121i	166
3956	301j	256	3368	287j	332n
4042N	387k	342n	3270N	385k	430
4316	661ℓ	616	3025	630ℓ	675
4440N	785	740o	2923	732	777o
4550	895m	850	2764N	891m	936

different from the spacing of these levels above the ground state. Consequently a difference of some tens of cm^{-1} between the separations of the sum and difference bands from the fundamentals would not be surprising.

5.4b The Model of Hexter and Dows

Hexter and Dows[26] in a recent communication proposed that this complex structure could be explained as a combination spectrum of the OH stretching mode with the OH librational mode, that is motions involving OH ions only.

A comparison of the powder spectra of $Mg(OH)_2$ and $Mg(OD)_2$ (Section 4.4) shows that the ratio of the corresponding frequencies in the two substances is always nearly equal to 1.37, the theoretical value of the isotopic ratio if the bands did arise purely through motions of the OH ions. The observed values for the ratio indicate that much of the spectrum must arise through OH motions only; but since not all the single crystal bands are resolved in the powder spectrum, and since the OH stretching frequency is much larger than the low lying frequency combining with it, it can not be definitely established that all of the bands near 3700 cm^{-1} are due to purely OH motions.

In the simple picture of Hexter and Dows it is assumed that the OH radical is free of interactions with neighboring ions, but its rotation is restricted by a force field which represents the combined effect of all the other ions. A simple harmonic potential function in the librational angle, θ,

is assumed:

$$V = \tfrac{1}{2}\, k\theta^2 \qquad (5\text{-}1)$$

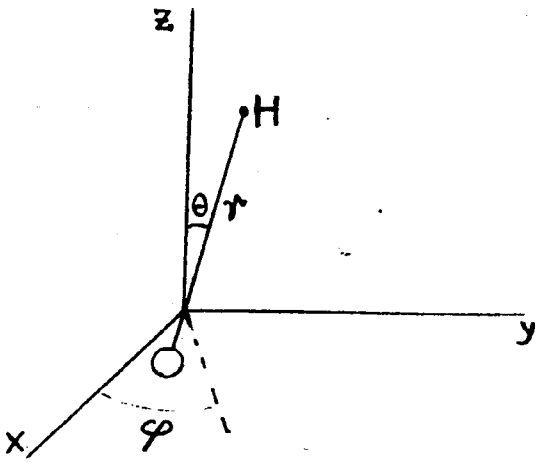


Figure 31. A Single Librator

The C_{3V} site symmetry of an OH ion requires axial symmetry about the equilibrium configuration in first approximation.

The Hamiltonian is given by

$$H\Psi = \tfrac{1}{2}k\theta^2\Psi - \frac{\hbar^2}{2\mu}\left[\frac{1}{r^2\sin\theta}\frac{\partial}{\partial\theta}\left(\sin\theta\frac{\partial\Psi}{\partial\theta}\right) + \frac{1}{r^2\sin^2\theta}\frac{\partial^2\Psi}{\partial\varphi^2}\right] \qquad (5\text{-}2)$$

Since interactions between stretching and librational modes are neglected, r is considered constant in first approximation. φ is an ignorable coördinate, so that $\Psi = e^{im\varphi}\,\Theta(\theta)$. The wave equation thus becomes

$$\left[\tfrac{1}{2}k\theta^2 - \frac{\hbar^2}{2I\sin\theta}\frac{d}{d\theta}\left(\sin\theta\frac{d}{d\theta}\right) + \frac{\hbar^2 m^2}{2I\sin^2\theta}\right]\Theta = E\,\Theta \qquad (5\text{-}3)$$

Making the substitution:

$$\Theta = \sqrt{\frac{\theta}{\sin\theta}}\,\chi \qquad (5\text{-}4)$$

and expanding the trigonometric functions of θ, the wave

equation is simplified to

$$\frac{d^2\psi}{d\theta^2} + \frac{1}{\theta}\frac{d\psi}{d\theta} - \frac{m^2}{\theta^2}\psi + \left[\left\{\frac{2I}{\hbar^2}E - \frac{1}{3}(m^2-1)\right\} - \left(\frac{Ik}{\hbar^2} + \frac{m^2}{15} - \frac{1}{60}\right)\theta^2\right]\psi = 0 \qquad (5\text{-}5)$$

where terms of the order θ^3 and higher have been neglected. The wave equation is essentially that of a two dimensional harmonic oscillator, and the energy levels are given by:

$$E = (n+1)\left[\hbar\omega + \frac{2B^2}{\hbar\omega}\left(\frac{m^2}{15} - \frac{1}{60}\right) - \frac{2B^4}{\hbar^3\omega^3}\left(\frac{m^2}{15} - \frac{1}{60}\right)^2 + \frac{4B^6}{\hbar^5\omega^5}\left(\frac{m^2}{15} - \frac{1}{60}\right)^3 + \ldots\right] + \frac{B}{3}(m^2-1) \qquad (5\text{-}6)$$

where n is the librational quantum number, $B = \frac{\hbar^2}{2I}$ (approximately 15 cm^{-1}) and $\omega = \sqrt{\frac{k}{I}}$ (Hexter and Dows suggest a value of about 400 cm^{-1}). The quantum numbers n and m are restricted to values

$$n = 0, 1, 2, 3.....$$

$$|m| = n, (n-2), (n-4).....$$

The intrinsic m-dependence of the energy is very small but splits the levels as shown in Figure 32. If the substitution $\theta = \alpha\theta'$ is made, the wave equation becomes:

$$\frac{d^2\psi}{d\theta'^2} + \frac{1}{\theta'}\frac{d\psi}{d\theta'} - \frac{m^2}{\theta'}\psi + [\varepsilon - \theta'^2]\psi = 0 \qquad (5\text{-}7)$$

where $$\alpha = \left(\frac{Ik}{\hbar^2} + \frac{m^2}{15} - \frac{1}{60}\right)^{-1/4} \approx \left(\frac{2B}{\hbar\omega}\right)^{1/2} \qquad (5\text{-}8)$$

and $$\varepsilon = \left\{\frac{2I}{\hbar^2}E - \frac{1}{2}(m^2-1)\right\}\left\{\frac{Ik}{\hbar^2} + \frac{m^2}{15} - \frac{1}{60}\right\}^{-1/2} \qquad (5\text{-}9)$$

Matrix elements for certain functions of θ' are given by

Nielsen[48], and others can be derived from these.

The selection rules for the librating oscillator are less restricted than those for the ordinary two dimensional harmonic oscillator. Hexter and Dows have shown that the strongest band is still $[v,n] \rightarrow [(v+1),n]$, where v and n are the stretching and librational quantum numbers. However, $n' = n'' \pm 2, 4, 6, \ldots$ and $n' = n'' \pm 1, 3, 5, \ldots$ are also allowed, though weaker in progression. The m selection rules, like the n selection rules, follow from the expressions for the components of the dipole moment. The z-component (parallel to the c-axis) is given by

$$\mu_z = (\mu_0 + \mu' \delta r) \cos\theta \qquad (5\text{-}10)$$

and since $\cos\theta = 1 - \frac{\theta^2}{2!} + \ldots\ldots$, the matrix element vanishes unless

$$\Delta n = 0 \qquad \text{(strong)}$$

or $$\Delta n = \pm 2, 4, 6 \ldots\ldots \qquad \text{(weaker in progression)}$$

Also since μ_z is independent of φ, the m selection rule for the parallel band is

$$\Delta m = 0$$

The selection rules giving the doubly degenerate perpendicular bands follow from

$$\left.\begin{aligned} \mu_x &= (\mu_0 + \mu'\delta r)\sin\theta\cos\varphi \\ \mu_y &= (\mu_0 + \mu'\delta r)\sin\theta\sin\varphi \end{aligned}\right\} \qquad (5\text{-}11)$$

$$\sin\theta = \theta - \frac{\theta^3}{3!} + \cdots\cdots$$

the selection rules are

$$\Delta n = \pm 1,\ 3,\ 5\ldots\ldots\ldots \quad \text{(weaker in progression)}$$

and $$\Delta m = \pm 1.$$

The decreasing intensities, in the series of bands $\Delta n = \pm 1$, 2, 3, 4....., can therefore be obtained approximately from the relative values of the matrix elements $\langle n|\theta|n+1\rangle$, $\langle n|\theta^2|n+2\rangle$, $\langle n|\theta^3|n+3\rangle$ etc., i.e., they will decrease in intensity by the factor $\left(\frac{2B}{\nu}\right)^{\Delta n}$. Since B $\approx$ 15 cm^{-1} and ν may be taken roughly as 400 cm^{-1}, the successive combinations will decrease in intensity approximately by $\frac{1}{13}$, $\left(\frac{1}{13}\right)^2$, ... etc.. In addition, the difference bands at room temperature will be weaker than the corresponding sum bands by the order of $\frac{1}{7}$, $\left(\frac{1}{7}\right)^2$,..... etc. due to the Boltzmann factor. For the ideal harmonic case the spectrum will be very simple. It is shown in Figure 32, where the band intensities are plotted on a logarithmic scale.

The observed spectrum is clearly very different from this simple picture no matter what value is chosen for ω. It differs from this simple picture in two striking ways. First, the sum and difference bands do not occur as series

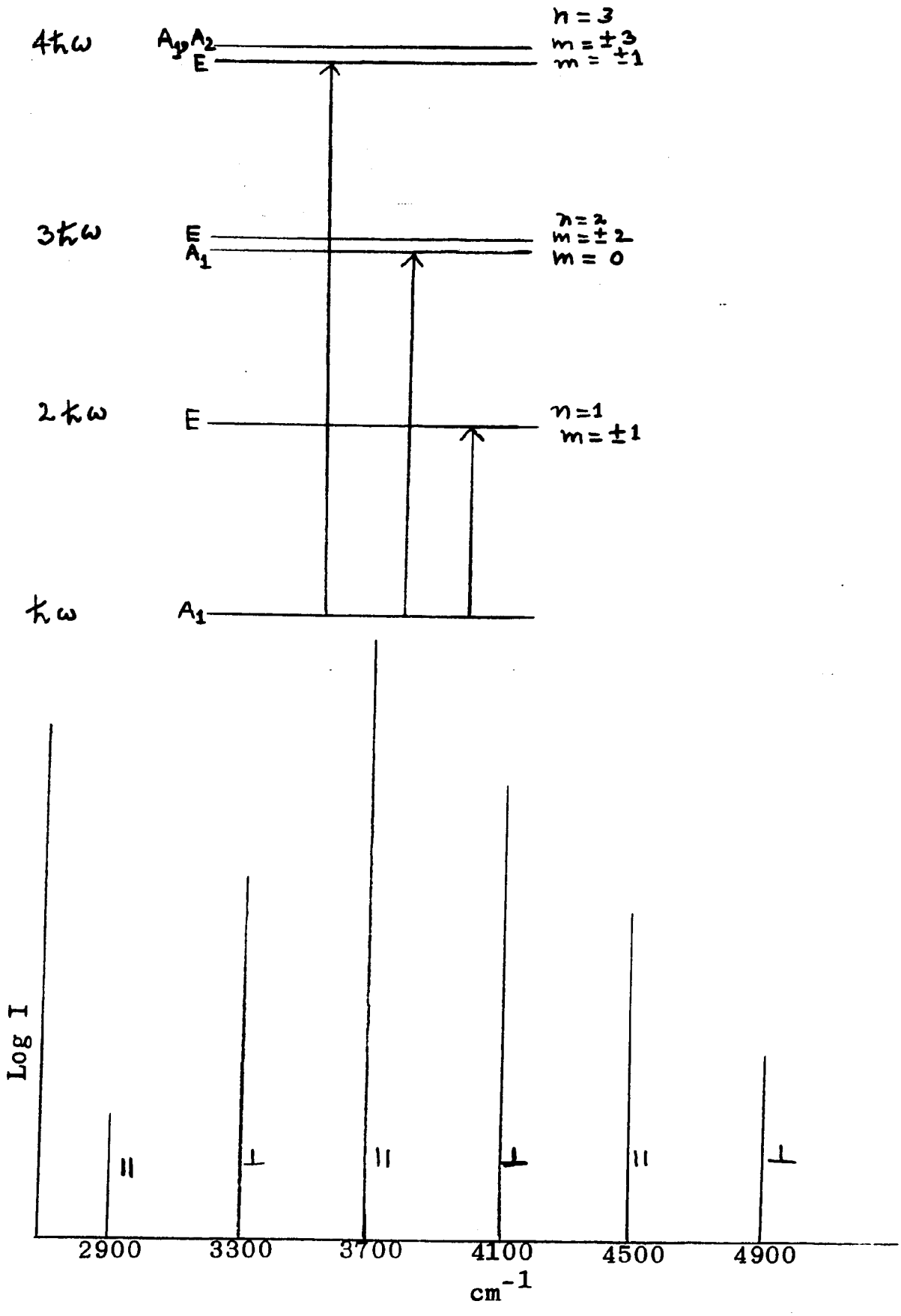


Figure 32. Spectrum of a single harmonic librator

of equally or even approximately equally spaced bands of decreasing intensity. Second, the sum and difference bands do not occur as alternately parallel and perpendicular bands. Both parallel and perpendicular polarizations of comparable strength are often observed at the same or very nearly the same frequencies. Hence, the observed complexity in the OH stretching region can not be explained by the model of a single librating oscillator, proposed by Hexter and Dows.

5.4c Two Weakly Interacting Coupled Librators

Since the unit cell of brucite contains two non-equivalent hydroxyl ions, a more realistic approach would be to consider a weak interaction between them. The infrared active combinations of the A_{1g} or A_{2u} stretching modes with one, two or three quanta of the Eg or Eu librational modes are given in Table 7. It is observed that combinations involving two or more quanta of the E modes may in principle give rise to absorption bands with both parallel and perpendicular components at the same or nearly the same frequencies. However, their exact positions, and the relative strengths of the two polarizations will depend on the extent and form of the interaction between the two librating oscillators.

The system of two coupled identical two dimensional harmonic oscillators is a highly degenerate one in zeroth order. Table 8 gives the degeneracies and the quantum numbers for the different excited states of the system. The quantum states of the system are expressed as $\{n_1 m_1 \quad n_2 m_2\}$,

TABLE 7
MULTIPLICATION TABLE FOR THE INFRARED ACTIVE STRETCHING LIBRATION COMBINATIONS

Librational Quanta	Combination	Polarization
E_g	$A_{2u} \cdot E_g = E_u$	$\perp$
E_u	$A_{1g} \cdot E_u = E_u$	$\perp$
$E_g^2 = A_{1g} + E_g$	$A_{2u} \cdot E_g^2 = A_{2u} + E_u$	$\parallel$ and $\perp$
$E_u^2 = A_{1g} + E_g$	$A_{2u} \cdot E_u^2 = A_{2u} + E_u$	$\parallel$ and $\perp$
$E_g \cdot E_u = A_{2u} + A_{1u} + E_u$	$A_{1g} \cdot E_g \cdot E_u = A_{2u} + A_{1u} + E_u$	$\parallel$ and $\perp$
$E_g^3 = A_{1g} + A_{2g} + E_g$	$A_{2u} E_g^3 = A_{2u} + A_{1u} + E_u$	$\parallel$ and $\perp$
$E_u^3 = A_{1u} + A_{2u} + E_u$	$A_{1g} E_u^3 = A_{1u} + A_{2u} + E_u$	$\parallel$ and $\perp$
$E_g^2 E_u = A_{1u} + A_{2u} + 2E_u$	$A_{1g} E_g^2 E_u = A_{1u} + A_{2u} + 2E_u$	$\parallel$ and $2\perp$
$E_g E_u^2 = A_{1g} + A_{2g} + 2E_g$	$A_{2u} E_g E_u^2 = A_{2u} + A_{1u} + 2E_u$	$\parallel$ and $2\perp$

TABLE 8
DEGENERACIES AND QUANTUM NUMBERS FOR TWO COUPLED LIBRATORS

Excited State	degeneracy	quantum nos.	$m_1 + m_2$	Species
First ($3\hbar\omega$)	4	$\{0_0 1_1\}, \{1_1 0_0\}$	1	E
		$\{0_0 1_{-1}\}, \{1_{-1} 0_0\}$	-1	E
		In u and g combinations:		
		$[0_0 1_{\pm 1}]_g$		E_g
		$[0_0 1_{\pm 1}]_u$		E_u
Second ($4\hbar\omega$)	10	$\{0_0 2_2\}, \{2_2, 0_0\}, \{1_1 1_1\}$	2	E
		$\{0_0 2_{-2}\}, \{2_{-2}, 0_0\}, \{1_{-1} 1_{-1}\}$	-2	E
		$\{0_0 2_0\}, \{2_0 0_0\}, \{1_1 1_{-1}\}, \{1_{-1} 1_1\}$	0	A
		In u and g combinations:		
		$[0_0 2_{\pm 2}]_g, [1_{\pm 1} 1_{\pm 1}]_g, [0_0 2_{\pm 2}]_u$		$2E_g, E_u$
		$[0_0 2_0]_g, [1_{+1} 1_{-1}]_g$		$2A_{1g}$
		$[0_0 2_0]_u, [1_{-1} 1_{+1}]_u$		A_{2u}, A_{1u}

where 1 and 2 denote the two librators, n, the librational quantum number, and m, its component. The levels have been grouped into u or g states. The symbol $[\ \ ]$ is explained by the following example:

$$[0_0 2_2]_g = \frac{1}{\sqrt{2}}\left[\psi_{\substack{n=0\\m=0}}(\theta_1\varphi_1)\psi_{\substack{n=2\\m=2}}(\theta_2\varphi_2) + \psi_{\substack{n=2\\m=2}}(\theta_1\varphi_1)\psi_{\substack{n=0\\m=0}}(\theta_2\varphi_2)\right]$$

$$= \frac{1}{\sqrt{2}}\left[\{0_0 2_2\} + \{2_2 0_0\}\right]$$

$$\text{and } [0_0 2_2]_u = \frac{1}{\sqrt{2}}\left[\{0_0 2_2\} - \{2_2 0_0\}\right]$$

The simplest possible form of the interaction energy, having the correct symmetry properties, gives rise to a perturbation term of the form:

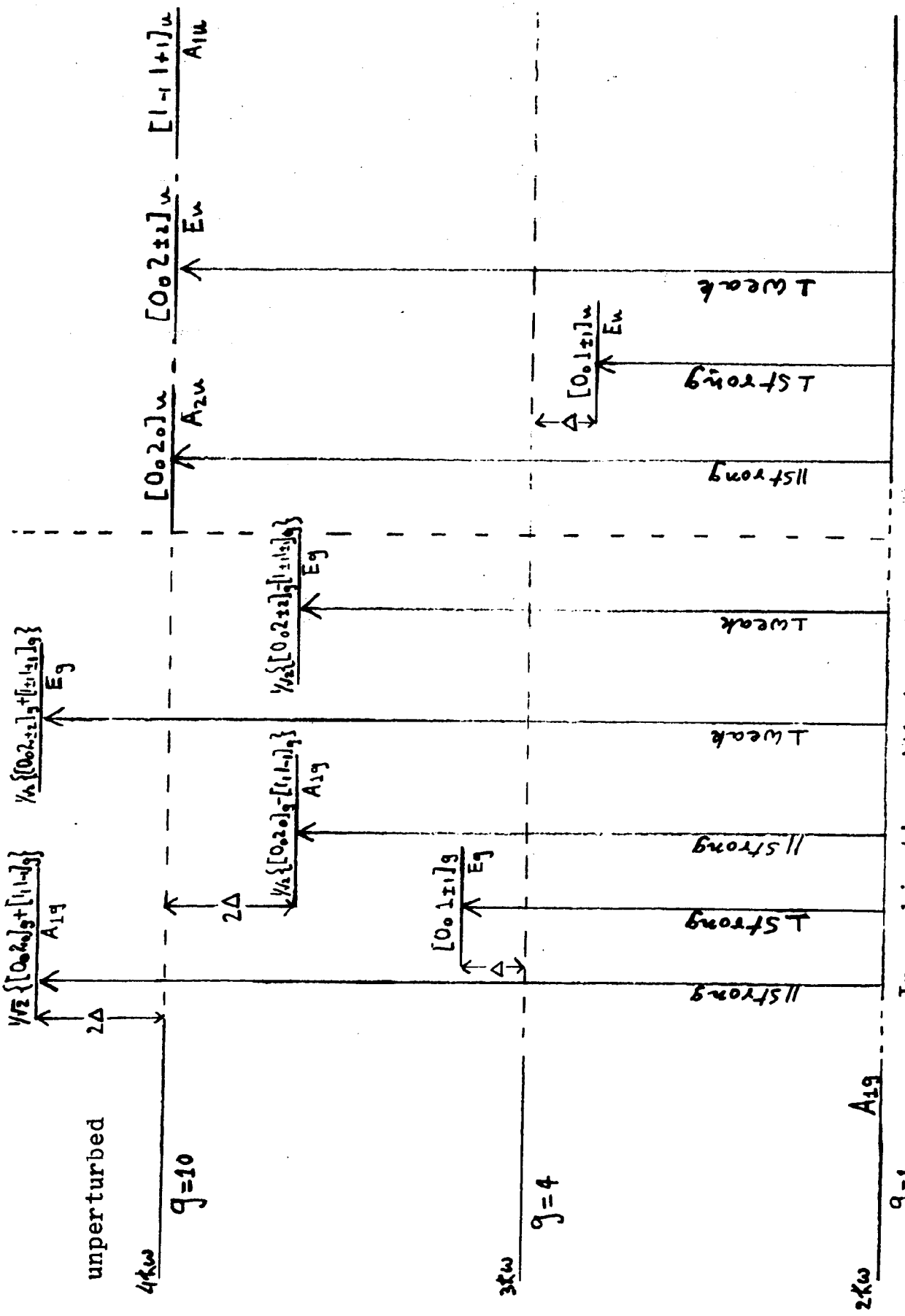
$$H^{(1)} = K\theta_1\theta_2\cos(\varphi_1 - \varphi_2)$$

$$= \frac{K}{2}\left(\frac{2B}{\hbar\omega}\right)\theta_1'\theta_2'\left\{e^{i(\varphi_1-\varphi_2)} + e^{-i(\varphi_1-\varphi_2)}\right\} \qquad (5\text{-}12)$$

The results of a perturbation calculation give the splittings of the excited states in terms of $\Delta = \frac{KB}{\hbar\omega}$. The energy level diagram is presented in Figure 33.

Transitions to the first group of excited states should give rise to two perpendicular bands of comparable intensity. These should be the strongest bands in the stretching-libration combination spectrum (excepting the fundamental itself).

Transitions from the ground state to the second group of excited states can in principle give rise to a whole series



In combination with A_{2u} stretch In combination with A_{1g} stretch

Figure 33. Energy levels of two coupled libators

of lines, but not all these transitions are equally probable. The strong lines are the parallel ones given by the selection rule $\Delta m_1 = 0, \Delta m_2 = 0$. Transitions with $\Delta m > 1$ or with Δm_1, $\Delta m_2 = \pm 1$ simultaneously should be very weak since these are forbidden in zeroth order (in the limiting case of no interactions). The x-component of the dipole moment, for example, is now given by

$$\mu_x = (\mu_0 + \mu' \delta r)(\sin\theta_1 \cos\varphi_1 - \sin\theta_2 \cos\varphi_2) \qquad (5\text{-}13)$$

and since the zeroth order wave functions consist of products of the form $\Theta e^{im_1\varphi_1} e^{im_2\varphi_2}$, the m selection rules for the perpendicular bands are in zeroth approximation

$$\Delta m_1 = \pm 1 \qquad \Delta m_2 = 0$$

or

$$\Delta m_1 = 0 \qquad \Delta m_2 = \pm 1$$

Hence there must be expected to be three strong parallel transitions to the second excited state. The three perpendicular ones must be expected to be very weak if the interaction energy is small.

Similarly it can be shown that among the group of transitions to the third set of excited levels the perpendicular bands will be stronger than the parallel ones. The spectrum predicted by the present model is shown in Figure 34.

In the observed spectrum there are two fairly strong perpendicular bands that could correspond to the predicted pair. But these are overlapped by the three strongest of the parallel combination bands, whereas the parallel bands should be well separated from the perpendicular ones according to

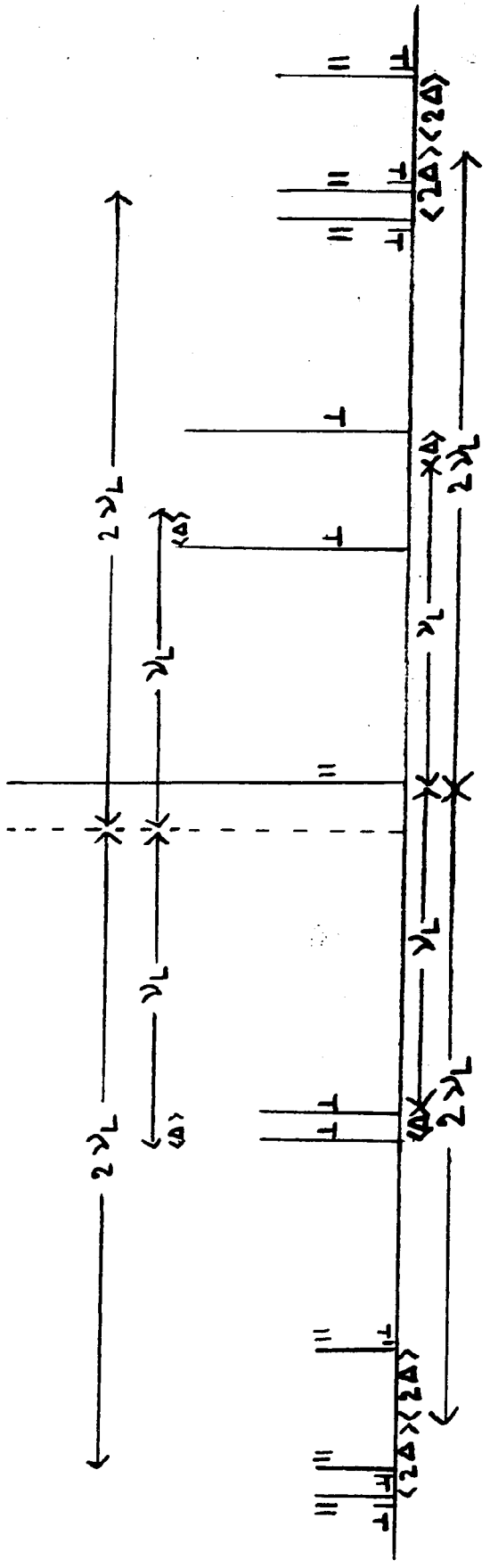


Figure 34. The spectrum of two coupled librators

the present model. The model also fails to account for the relatively weak bands close to the fundamental.

The introduction of a simple interaction term coupling the two identical librating oscillators is therefore still not enough to account for the observed spectrum, although such an interaction introduces some features which are qualitatively in line with some of the complexities of the observed spectrum.

5.4d Single Librator with 3-fold and 6-fold Restricting Potential

The interaction term introduced in the last section does not incorporate into the libration potential all the unique features of the structure of brucite. The hexagonal symmetry (D^3_{3d}) must be expected to introduce terms of a 3-fold and 6-fold nature into the potential. Even if there is no interaction between the two non-equivalent OH ions, the form of the libration potential may be altered appreciably by this symmetry of the crystalline force field. If the OH axis is tipped away from its equilibrium position through a large angle, the ion may experience strong 3-fold and 6-fold hindering potentials in its rotation on a cone about the equilibrium direction.

The potentials will be developed in power series in θ_1, and θ_2, the angles measuring the tipping from equilibrium of the two non-equibalent OH ions. The form of the complete potential function must be consistent with the symmetry of

the structure. The potential has been calculated for the electrostatic interactions arising from the first few neighboring ions, although no special significance can be ascribed to the relative magnitudes of the coefficients of the different terms derived in this way. Terms upto and including sixth power in the angles θ_1 and θ_2 may be significant. As a result the number of perturbation terms becomes huge if interactions between the two types of ions are taken into account. However, in the special case of a single librator with no interactions (or two librators always in phase) the potential is quite simple:

$$V = \frac{1}{2}k\theta^2 + \lambda_3\theta^3\cos 3\varphi + \lambda_4\theta^4 + \lambda_5\theta^5\cos 3\varphi + \lambda_6\theta^6\cos 6\varphi + \lambda_6'\theta^6 + \cdots \qquad (5\text{-}14)$$

If the 3-fold term is relatively important it may cause drastic changes in the shape of the libration potential, as illustrated for example in Figure 35. For such a librational

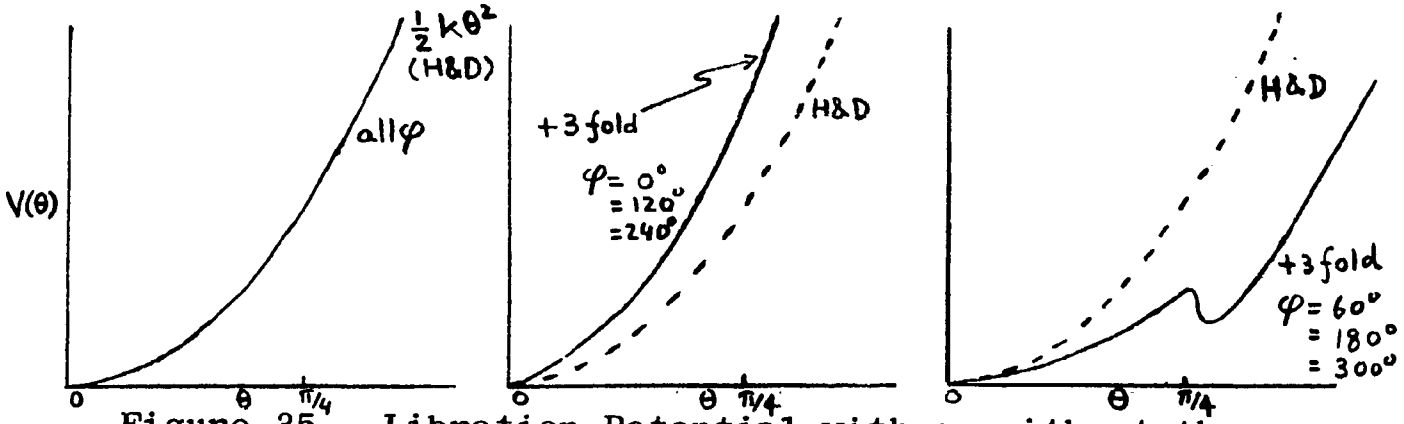


Figure 35. Libration Potential with or without the 3-fold term.

potential function, the levels near the dip in the potential curve must be expected to be strongly perturbed while those lying near the bottom of the well may not be affected much.

If the interactions between the two types of librators are included the leading term has the form:

$$K\theta_1\theta_2\cos(\varphi_1-\varphi_2)$$

which has been discussed in the previous section. The terms that are cubic in θ_1 and θ_2 have the form:

$$K_1\theta_1\theta_2^2\cos(\varphi_1+2\varphi_2)$$

$$K_2\theta_1^2\theta_2\cos(2\varphi_1+\varphi_2)$$

such complicated interaction terms will be neglected. The purpose of this section is to investigate the effect of the 3-fold and 6-fold terms in the potential energy of a single librator, (5-14).

In this case the first and second order Hamiltonians, expressed in terms of θ' (inclucing the terms left over from the θ expansions of the unpreturbed librating oscillator), are

$$H^{(1)} = \lambda_3\alpha^3\theta'^3\cos 3\varphi + \left\{\lambda_4 + B\left(\frac{2m^2}{189} - \frac{1}{378}\right)\right\}\alpha^4\theta'^4 \qquad (5\text{-}15)$$

and $$H^{(2)} = \lambda_5\alpha^5\theta'^5\cos 3\varphi + \lambda_6\alpha^6\theta'^6\cos 6\varphi + \left\{B\left(\frac{1349m^2}{907200} - \frac{641}{56700}\right) + \lambda_6'\right\}\alpha^6\theta'^6 \qquad (5\text{-}16)$$

or

$$H^{(1)} = A_1\theta'^3\cos 3\varphi + A_2\theta'^4 \qquad (5\text{-}15')$$

$$H^{(2)} = \Gamma\theta'^5\cos 3\varphi + \Delta\theta'^6\cos 6\varphi + \Omega\theta'^6 \qquad (5\text{-}16')$$

where,

$$\left.\begin{aligned} A_1 &\approx (2B\hbar\omega)^{1/2} x_3 \\ A_2 &\approx 2B\, x_4 \\ \Gamma &\approx \left(\frac{8B^3}{\hbar\omega}\right)^{1/2} x_5 \\ \Delta &\approx \frac{4B^2}{\hbar\omega} x_6 \\ \Omega &\approx \text{negligibly small} \end{aligned}\right\} \qquad (5\text{-}17)$$

The x's are dimensionless quantities related to the λ's by $\lambda = kx$.

The perturbation corrections are given in Table 9. In the second order calculation, terms smaller than $\frac{B^2}{\hbar\omega}$ have been neglected. The numerical values are in cm^{-1} where values of $\hbar\omega = 350\ cm^{-1}$ and $B = 15\ cm^{-1}$ have been assumed. The perturbed energy levels are compared with the unperturbed ones in Table 10 and Figure 36(where only transitions from the ground state are shown) for two sets of perturbation parameters. For the extreme case $\lambda_3 = 0.45$ k some levels are shifted by large amounts, but a perturbation calculation to within second order only is probably not justified for such a case.

The calculations do give an indication that certain levels are shifted much more than others and that the levels giving rise to parallel transitions from the ground state may not be separated much from levels giving rise to perpendicular transitions. If the 3-fold and 6-fold perturbation terms are

TABLE 9
PERTURBATION CORRECTIONS FOR A SINGLE LIBRATOR WITH 3-FOLD AND 6-FOLD RESTRICTING POTENTIAL

n	$\lvert m \rvert$	ΔE
0	0	$4Bx_4 - \frac{2B\hbar\omega}{\hbar\omega + B} x_3^2$
		$= 60x_4 - 28.77x_3^2$
1	1	$12Bx_4 - \left[\frac{3}{2(\hbar\omega+B)} + \frac{2}{(3\hbar\omega+5B)} + \frac{1}{2(3\hbar\omega+B)}\right] 6B\hbar\omega x_3^2$
		$= 180x_4 - 200.34x_3^2$
2	0	$28Bx_4 - \left[\frac{27}{\hbar\omega+3B} + \frac{4}{\hbar\omega+B}\right] 2B\hbar\omega x_3^2$
		$= 420x_4 - 831.92x_3^2$

TABLE 9 (con't)

n	$\lvert m \rvert$	ΔE
2	2	$24Bx_4 - \left[\frac{3}{\hbar\omega - B} + \frac{5}{3\hbar\omega + 7B} + \frac{1}{2(3\hbar\omega - B)} - \frac{3}{2(\hbar\omega + B)}\right] 6B\hbar\omega x_3^2$
		$= 360x_4 - 304.23x_3^2$
3	1	$48Bx_4 - \left[\frac{9}{\hbar\omega + 5B} + \frac{9}{\hbar\omega + B} + \frac{5}{3\hbar\omega + 5B} + \frac{2}{3\hbar\omega + B} - \frac{3}{\hbar\omega - B}\right] 6B\hbar\omega x_3^2$
		$= 720x_4 - 1360.98x_3^2$
3	$\cos 3\varphi$	$40Bx_4 - \left[\frac{27}{\hbar\omega - 3B} + \frac{1}{\hbar\omega - B} - \frac{17}{\hbar\omega + 3B} - \frac{1}{\hbar\omega + B}\right] 2B\hbar\omega x_3^2$
		$+ 240\frac{B^2}{\hbar\omega}x_6 = 600x_4 - 480.27x_3^2 + 154.29x_6$
3	$\sin 3\varphi$	$40Bx_4 - \frac{20B\hbar\omega x_3^2}{\hbar\omega + 3B} - 240\frac{B^2}{\hbar\omega}x_6$
		$= 600x_4 - 265.82x_3^2 - 154.29x_6$

TABLE 10

PERTURBATION CORRECTIONS FOR TWO SETS OF PARAMETERS (3-FOLD AND 6-FOLD RESTRICTING POTENTIAL).

n	|m|	$\Delta E \begin{cases} x_3 = 0.45 \\ x_4 = 0.033 \\ x_6 = -0.1 \end{cases}$	$\Delta E \begin{cases} x_3 = 0.25 \\ x_4 = 0.03 \\ x_6 = -0.05 \end{cases}$
0	0	$-4\ cm^{-1}$	$0\ cm^{-1}$
1	1	-34	-7
2	0	-152	-39
2	2	-49	-8
3	1	-248	-63
3	$\cos 3\varphi$	-91	-20
3	$\sin 3\varphi$	-18	+9

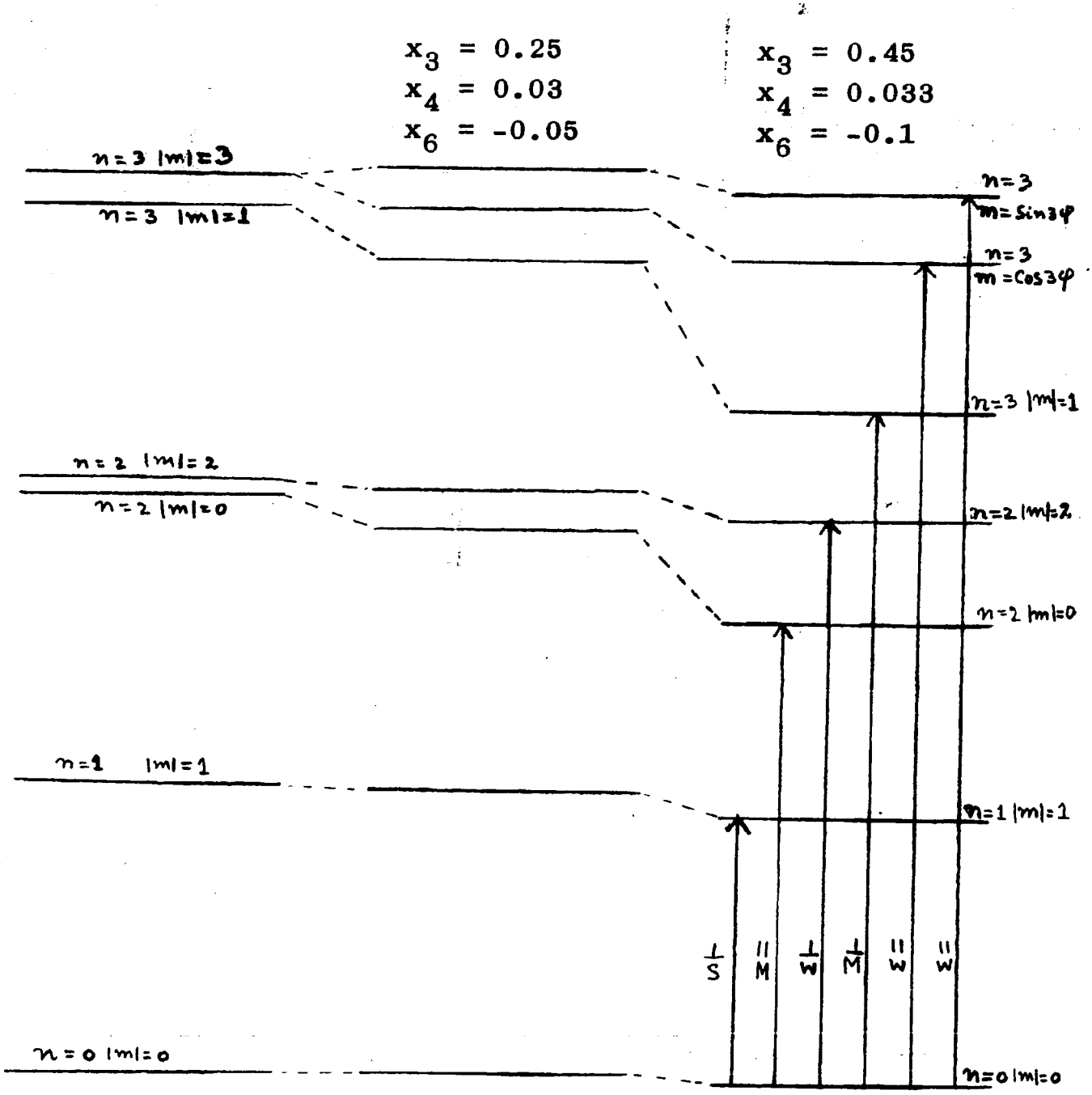


Figure 36. Energy levels of a single librator in a restricting potential with 3-fold and 6-fold terms

large the selection rule $\Delta m = \pm 1$ will break down and transitions for which $|\Delta m| = 2$ or 3 may give rise to observable lines.

However, it seems unlikely that the introduction of even a large 3-fold or 6-fold term in the potential can give rise to a spectrum in which the strongest perpendicular bands are overlapped by parallel bands of comparable intensity..

5.4e Discussion

From the last two sections it appears that neither the introduction of a small interaction between the two non-equivalent OH's nor the consideration of 3-fold and 6-fold terms in the potential for a single OH ion can individually explain all the features of the observed spectrum.

Since such modifications in the simple model of Hexter and Dows do give rise to complexities in the OH stretching region, the question arises whether a model incorporating both these aspects of the potential function can account for the observed spectrum; that is whether the picture of two interacting non-equivalent OH's librating in a complicated force field including major contributions from terms of 3-fold and 6-fold symmetry may be able to predict the observed complexities. However, calculations based on such a model have not been carried out, since it appears that the magnitude of the correction terms must be such that a perturbation calculation to second order is not justified. In addition, the near degeneracies of such a system depend on the magnitude

of the interaction terms relative to that of the 3-fold and 6-fold terms, so that the method of calculation will depend on the choice of parameters.

Even though a quantitative evaluation for such a model has not been made, it appears unlikely that the model can explain all the details of the observed spectrum. In particular, it must be expected that transitions to the lowest of the librational states should give rise to the strongest combination bands so that the relatively weak absorption near the fundamental, which seems to arise through transitions involving the ground state (as no significant decrease in intensity at the liquid nitrogen point is observed), can not be understood in terms of an OH stretching-librational model. Nevertheless, it must be expected that the gross features of the absorption in the near infrared are due to motions involving the OH ions only. However, combinations with other lattice modes can not be ruled out, particularly in the case of the two bands lying very near the fundamental. Even though the combinations of the OH stretching and librational motions can by themselves give rise to a complex spectrum, it appears that additional combinations with such lattice modes might be needed to account for the full complexity of the observed spectrum. These lattice modes must be low frequency ones (much less than 400 cm^{-1}) and must arise from motions involving more than one unit cell. They are not predicted to be active as fundamentals from a factor group analysis. It seems that the factor group selection rules are also violated for the

first overtone of the OH stretching vibration, which may account for additional complexity in the central strong parallel band in the region.

It should be borne in mind that combination and overtone spectra in crystals are essentially infinite body problems and may be immensely complicated through combinations of innumerable modes, which are inactive as fundamentals.

5.5 Summary

The fundamental modes of vibration in the brucite have been assigned according to their symmetry types obtained from a factor group analysis, and are presented in Table 11.

TABLE 11
ASSIGNMENT OF FUNDAMENTALS AND OH OVERTONES

Frequency cm-1	Symmetry type	Observed in	Description
415	E_u	IR	OH Libration (?)
445	E_g	Raman	OH Libration (?)
515	A_{2u}	IR	Mg-OH Lattice
515	E_u	IR	Mg-OH Lattice
3655 (ν_g)	A_{1g}	Raman	OH Stretching
3700 (ν_u)	A_{2u}	IR	OH Stretching
7180	$A_{1g} \cdot A_{2u}$	IR	$\nu_g + \nu_u$
10600	$A_{1g} \cdot A_{1g} \cdot A_{2u}$ or (and) $A_{2u} \cdot A_{2u} \cdot A_{2u}$	IR	$2\nu_g + \nu_u$ or (and) $3\nu_u$

Since the two possible OH stretching fundamentals are already assigned, the rest of the bands in the near infrared must arise from combinations involving the OH stretching frequencies. Their relatively weak intensity also supports this view. Moreover, the temperature dependence of these bands indicates that those below 3700 cm^{-1} are difference bands, whereas those above 3700 cm^{-1} sum bands. For every difference band a sum band of like polarization can be located at roughly the correct frequency. A comparison of the powder spectra of $Mg(OH)_2$ and $Mg(OD)_2$ indicates that most of these bands are excited through purely OH motions. But as all the bands observed in single crystal transmission spectra are not resolved in powder spectra,and as the OH stretching frequencies are much larger than the low-lying frequencies combining with them, one can not be certain whether all the fine structure of the bands is due to OH motions or not. Hexter and Dows suggested that the complex structure might be explained as arising from combinations of the OH stretching mode with the doubly degenerate libration mode, for which a restricting potential of simple harmonic form is assumed. A quantitative evaluation of the model reveals that such a simple picture is quite inadequate.

Two modifications of the model have been considered: 1) consideration of a weak interaction between the two non-equivalent OH ions in the unit cell of brucite, and 2) inclusion of terms of 3-fold and 6-fold nature, expected from the hexagonal symmetry of the crystal, in the restricting

potential for a single librator. Although similarities to certain features of the observed spectrum are exhibited by these models, major discrepancies exist. A treatment of the simultaneous action of both interactions might lead to an improvement, but it would be an extremely lengthy calculation.

The possibility of combinations with inter-unit cell lattice modes can not be ruled out, especially for the two lines occurring close to the fundamental, because they seem to defy explanation on the basis of OH stretching-libration combination. Even though the involved OH motions can by themselves give rise to a complex spectrum, it appears that additional combinations with such lattice modes are necessary to explain the observed spectrum.

BIBLIOGRAPHY

1. A.F. Rogers and P.F. Kerr, Optical Mineralogy, McGraw Hill, New York,(1942), p.205.

2. G. Aminoff, Geol. Foren. Forh. Stock., 41, 407 (1919).

3. G. Aminoff, Z. Krist., 56, 506 (1921).

4. G.R. Levi and A. Ferrari, Atti. Luic., 31, 397 (1924).

5. G. Natti and L. Passerini, Gazz., 58, 617 (1928).

6. L.R. Bury and E.R.H. Davies, J. Chem. Soc., 2013 (1932).

7. H.D. Megaw, Proc. Roy. Soc., A142, 207 (1933).

8. F. Trendelenburg and O. Wieland, Wiss. Veroffentl. Siemens-Konzern, 13, 37 (1924).

9. J. Garrido, Z. Krist., 95, 192 (1936).

10. J.D. Bernal and H.D. Megaw, Proc. Roy. Soc., A151, 384 (1935).

11. R.T. Mara and G.B.B.M. Sutherland, J. Opt. Soc. Amer., 43, 1100 (1953).

12. H.E.Petch and H.D. Megaw, J. Opt. Soc. Amer., 44, 744 (1954).

13. H.E. Petch, Phys. Rev., 99, 1635 (1955).

14. D.D. Elleman and D. Williams, J. Chem. Phys., 25, 742 (1956).

15. G. Herzberg, Molecular Spectra and Molecular Structure I and II, D. Van Nostrand, New York, (1950 and 1954 respectively).

16. W.R. Busing and H.A. Levy, J. Chem. Phys., 26, 563 (1957).

17. R.T. Mara and G.B.B.M. Sutherland, J. Opt. Soc. Amer., 46, 464 (1956).

18. W.W. Coblentz, Phys. Rev., 20, 252 (1905); Investigations of Infrared Spectra, Carnegie Institute of Washington, Washington, D.C. (1905-1908).

19. E.K. Plyler, Phys. Rev., 28, 284 (1926).

20. W.D. Keller and E.E. Pickett, Amer. J. Sci., 248, 264 (1950).

21. R.T. Mara, Thesis, University of Michigan, (1953).

22. M. Yeou Ta, Comptes Rendu, 211, 467 (1940).

23. J. Louisfert, J. Phys. et Rad., 8, 21 (1947).

24. C. Duval and J. Lecomte, Bull. Soc. Chim., 8, 713 (1941); Bull. Soc. Franc. Mineral, 66, 284 (1943).

25. J. Lecomte, Proc. Indian Acad. Sci., 28, 339 (1948).

26. R.M. Hexter and D.A. Dows, J. Chem. Phys., 25, 504 (1956).

27. E. Hasche, Ann. der Phys., 8, 59 (1931).

28. S. Bhagavantam and T. Venkatarayudu, Proc. Indian Acad. Sci., A9, 224 (1939).

29. S. Bhagavantam, Proc. Indian Acad. Sci., A13, 543 (1941).

30. R.S. Halford, J. Chem. Phys., 14, 8 (1946).

31. D.F. Hornig, J. Chem. Phys., 16, 1063 (1948).

32. S. Bhagavantam and T, Venkatarayudu, Theory of Groups and its Application to Physical Problems, Andhra University, Waltair, India (1951).

33. W.H. Shaffer, Notes on Application of Group Theory to Some Physical Problems, unpublished.

34. A.R. Downie, M.C. Magoon, T. Purcell and B. Crawford, Jr., J. Opt. Soc. Amer., 43, 941 (1953).

35. N. Acquista and E.K. Plyler, J. Research Nat. Bur. Standards, 49, 13 (1952).

36. Instruction Manual for Perkin -Elmer 12C Infrared Spectrometer, Appendix, Perkin-Elmer Corp., Glenbrook, Conn. (1950).

37. R.B. Barnes et al, J. Appl. Phys., 16, 77 (1945).

38. J.K. Hardy, Phys. Rev., 38, 2162 (1931).

39. R. Newman and R.S. Halford, Rev. Sci. Instr., 19, 270 (1948).

40. N. Ockman, Thesis, University of Michigan, (1957).

41. G. Vidale and R.C. Taylor, J. Am. Chem. Soc., 78, 294 (1956).

42. I. Šimon, J. Opt. Soc. Amer., 41, 336 (1951).

43. T.S. Robinson, Proc. Phys. Soc. (London), B65, 910 (1952); T.S. Robinson and W.C. Price, Proc. Phys. Soc. (London), B66, 969 (1953).

44. D.L. Wood and S.S. Mitra, J. Opt. Soc. Amer. (to be published).

45. M. Czerny, Zeit. f. Phys., 65, 600 (1930).

46. J.C. Willmott, Proc. Phys. Soc. (London), A63, 389 (1950).

47. M. Hass, Thesis, University of Michigan (1955).

48. H.H. Nielsen, Rev. Mod. Phys., 23, 90 (1951).